SOLUBILITY ENHANCEMENT OF POOR WATER-SOLUBLE ANTILIPEMIC DRUGS ATORVASTATIN AND FENOFIBRATE BY MICRONIZATION AND SOLID DISPERSION METHOD

Thesis Submitted for the Award of the Degree of

DOCTOR OF PHILOSOPHY

in

Pharmaceutical Chemistry

By

Ramesh Nawale

Registration Number: 42200094

Supervised By

Dr. Sanjeev Kumar Sahu [UID:24026]

Professor, Pharmaceutical Chemistry

LOVELY PROFESSIONAL UNIVERSITY

PUNJAB, India- 144411

LOVELY PROFESSIONAL UNIVERSITY, PUNJAB

2026

DECLARATION

I, Ramesh Nawale, bearing Registration No. 42200094, hereby declare that the research work embodied in the Ph.D. thesis titled "Solubility Enhancement of Poor Water-Soluble Antilipemic Drugs Atorvastatin and Fenofibrate by Micronization and Solid dispersion method" submitted to Lovely Professional University is the original and bonafide work carried out by me under the supervision of Dr. Sanjeev Kumar Sahu, Professor, School of Pharmaceutical Sciences, Lovely Professional University.

I further declare that:

a) The work presented in this thesis is a genuine contribution to the field of research and is a result of investigations carried out by me during the period of my doctoral study.

b) The research work has been conducted in accordance with the academic and ethical standards prescribed by the university.

c) Due acknowledgements and references have been duly given wherever the work of others has been cited or used.

d) The thesis has not been submitted either partly or fully to any other university or institution for the award of any degree or diploma.

I understand that any violation of the above declarations may lead to the cancellation of my degree by the university at any stage.

Signature of Scholar
Name : Ramesh Nawale
Registration Number: 42200094
Date

CERTIFICATE

This is to certify that the work reported in the Ph. D. thesis entitled "Solubility Enhancement of Poor Water-Soluble Antilipemic Drugs Atorvastatin and Fenofibrate by Micronization and Solid dispersion method" submitted in fulfillment of the requirement for the award of degree of **Doctor of Philosophy (Ph.D.)** in the Pharmaceutical Chemistry, is a research work carried out by Ramesh Nawale, 42200094, is bonafide record of his/her original work carried out under my supervision and that no part of thesis has been submitted for any other degree, diploma or equivalent course.

 **Signature of Supervisor** **Name: Dr. Sanjeev Kumar Sahu** **UID: 24026** **Date**	**Signature of Co-supervisor (if applicable)** **Name :** **UID (if applicable)** **Date**

ABSTRACT

Fixed-dose combinations (FDCs) are oral formulations containing two or more active agents designed to simplify dosing regimens, improve adherence, and enhance therapeutic outcomes in chronic conditions such as dyslipidemia and metabolic syndrome. In elderly populations, co-occurrence of type 2 diabetes, hypertriglyceridemia, and cholesterol imbalance is frequent, increasing the need for combination lipid-lowering therapies. Fenofibrate (FNF), a PPAR-α agonist, effectively decreases triglycerides and elevates HDL-C and is often administered alongside statins when monotherapy provides inadequate control. Clinical evidence, including the DIACOR and ACCORD trials, has shown superior lipid correction with fenofibrate–statin combinations relative to single-drug therapy. However, both Fenofibrate and Atorvastatin (ATR) exhibit extremely low aqueous solubility and consequently poor bioavailability, often necessitating higher doses and increasing the risk of adverse effects. While numerous solubility-enhancement approaches have been investigated for each drug individually, reports on combination nanosuspensions remain limited.

This research aimed to develop a nanosuspension of ATR and FNF to improve dissolution and oral absorption. Stabilizers were screened using an OFAT approach considering particle size (PS), polydispersity index (PDI), and zeta potential (ZP), followed by formulation optimization through a Box–Behnken Design (3 factors, 3 levels, 15 runs). A stabilizer blend of Poloxamer-407 and PVP produced an optimized formulation with nanoscale particle size (~183.9 nm) and ZP of −22.9 mV, exhibiting spherical morphology under SEM. FT-IR, DSC, and XRD confirmed drug–excipient compatibility and reduced crystallinity. The optimized nanosuspension demonstrated markedly enhanced solubility (ATR: 91.26 ± 8.24 µg/mL; FNF: 74.32 ± 9.11 µg/mL) with >90% drug release within 60 minutes, and significantly improved pharmacokinetic parameters (ATR: Cmax 2.97-fold, AUC0–24h 2.49-fold; FNF: Cmax 3.74-fold, AUC0–24h 3.17-fold) compared with pure drugs.

In the second phase, solid dispersion-based dispersible tablets (ATR 20 mg / FNF 145 mg) were developed using Soluplus and Kollidon for binary systems, while ternary dispersions offered the highest enhancement in solubility and dissolution. The

optimized tablets exhibited rapid disintegration (24 ± 2 s), >85% cumulative release within 30 minutes, uniform content, adequate hardness, and friability below acceptable limits. Pharmacokinetic evaluation further confirmed a notable increase in bioavailability compared with the untreated drug forms.

In conclusion, nanosuspension and solid dispersion approaches significantly improved the solubility, dissolution behavior, and bioavailability of ATR–FNF FDCs. These outcomes demonstrate the potential of advanced formulation strategies to develop an effective oral FDC platform with enhanced therapeutic efficiency and improved patient compliance.

Keywords: Fixed-Dose Combination, Nanosuspension, Solubility Enhancement, Atorvastatin, Fenofibrate, Bioavailability

ACKNOWLEDGEMENT

This dissertation is the outcome of the support and contributions of many individuals, and I express my sincere appreciation to all who played a role in its completion.

I extend my deep gratitude to my supervisor, **Dr. Sanjeev Kumar Sahu**, Professor, School of Pharmaceutical Sciences, Lovely Professional University, Phagwara, Punjab. His guidance, encouragement, and valuable insights have been fundamental to the development of this work.

I am also thankful to **Dr. D. V. R. N. Bhikshapathi**, Principal, Teegala Ram Reddy College of Pharmacy, Hyderabad, for providing the necessary facilities and continuous support that enabled this research.

I owe my deepest gratitude to my family my wife Dr. **Sneha,** my daughter **Tanishq**, and my son **Krishiv**. Their patience, sacrifices, and unwavering support have been the foundation that kept me moving forward. I also appreciate the encouragement and affection of all my near and dear ones.

Above all, I express my humble thanks to the Almighty for granting me the strength, perseverance, and opportunity to complete this work.

I remain grateful to everyone who, directly or indirectly, contributed to the successful completion of this dissertation.

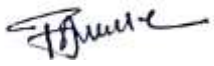

Ramesh Nawale

TABLE OF CONTENTS

LIST OF TABLES

LIST OF FIGURES

LIST OF ABBREVIATIONS

Abbreviation	Full form
ATR	Atorvastatin
FNF	Fenofibrate
NS	Nanosuspension
SD	Solid dispersion
BSD	Binary solid dispersion
TSD	Ternary solid dispersion
FTIR	Fourier transform infrared spectroscopy
DSC	Differential scanning calorimetry
SEM	Scanning electron microscopy
XRD	X-ray diffraction
HPLC	High performance liquid chromatography
UV	Ultraviolet
DAD	Diode array detector
PS	Particle size
PI	Polydispersity index
ZP	Zeta potential
QTPP	Quality target product profile
CQA	Critical quality attribute
DOE	Design of experiments
BBD	Box-behnken design
OFAT	One-factor-at-a-time
CMC	Carboxymethyl cellulose
IS	Internal standard
ACN	Acetonitrile
RPM	Revolutions per minute
Da	Damköhler number

Abbreviation	Full form
AUC_{0-24h}	Area under the Ccurve from 0 to 24 hr
CMAX	Maximum plasma concentration
PVP	Polyvinylpyrrolidone
QBD	Quality by design
SLS	Sodium lauryl sulphate
TPGS	d-α-tocopheryl polyethylene glycol 1000 succinate
HDL	High-density lipoprotein
LDL	Low-density lipoprotein
WHO	World health organization
IAEC	Institutional animal ethics committee
CPCSEA	Committee for the purpose of control and supervision of experiments on animals
NIN	National institute of nutrition

List of Units

Unit	Description
nm	Nanometer
mV	Millivolt
µg/mL	Micrograms per milliliter
mg	Milligram
g	Gram
mL	Milliliter
ºC	Degrees celsius
rpm	Revolutions per minute
%	Percent
min	Minutes
hr	Hour

Unit	Description
cm^{-1}	Wavenumber (used in spectroscopy)
µL	Microliter
ng/mL	Nanograms per milliliter
kV	Kilovolt

CHAPTER 1
INTRODUCTION

1. INTRODUCTION

1.1. Cardiovascular diseases and the burden of dyslipidemia

Cardiovascular diseases (CVDs) represent a global health crisis, accounting for a staggering proportion of deaths and disability worldwide. As per data published by world health organization, heart syndromes result in more or less 17.9 million demises per year, representing 31% of all world-wide deceases (WHO, 2021). This immense prevalence translates into a significant socioeconomic burden, encompassing direct healthcare costs, lost productivity due to illness and premature mortality, and the impact on families and communities (Mensah *et al.,* 2019). The substantial healthcare expenditure associated with these conditions highlights the urgency for efficient prevention and management approaches.

Atherosclerosis, a slow-progressing inflammatory pathology driven by lipid accumulation in arteries, plays a central role in the onset of cardiovascular diseases. This plaque accumulation leads to the narrowing and hardening of arteries, impeding blood flow and increasing the susceptibility of acute cardiovascular events specifically myocardial infarction and stroke (Libby, 2021). A primary driver of atherosclerosis is dyslipidemia, a condition marked by abnormal concentrations of lipids, including cholesterol and triglycerides, in the bloodstream (Packard & Chapman, 2021).

The link between specific lipid abnormalities and the progression of atherosclerosis is well-established. Elevated levels of low-density lipoprotein cholesterol (LDL-C) are particularly atherogenic, as LDL particles can infiltrate the arterial intima, undergo oxidation, and initiate the inflammatory cascade that leads to plaque formation (Borén *et al.,* 2020). HDL-C provides cardiovascular protection primarily through reverse cholesterol transport, wherein cholesterol is removed from arterial walls and returned to the liver for elimination (Tall & Bhatnagar, 2001). Elevated triglycerides (TGs), often associated with other lipid abnormalities and metabolic disturbances, are also increasingly recognized as a recognized a discrete risk determinant for CVD, particularly in women and individuals with diabetes (Miller *et al.,* 2011).

Risk stratification in hyperlipidemic patients is crucial for guiding therapeutic interventions. Clinical guidelines, such as those issued by the American Heart Association (AHA) and the European Society of Cardiology (ESC), utilize various risk assessment tools that incorporate lipid levels alongside other traditional cardiovascular susceptibility aspects and presence of diabetes (Arnett *et al.,* 2019; Mach *et al.,* 2020). These guidelines establish target levels for LDL-C, HDL-C, and TGs based on an individual's overall cardiac threat profile. Achieving these target lipid levels is paramount in preventing the initiation and progression of atherosclerotic disease and reducing the incidence of adverse cardiovascular events. For instance, individuals at very high risk, such as those with established CVD or diabetes with target organ damage, typically require more aggressive LDL-C lowering compared to those at lower risk. Similarly, managing elevated TGs is important, especially for individuals with triglyceride concentrations exceeding 500 mg/dL to avert the onset of pancreatitis, and in those with moderately elevated levels as part of overall cardiovascular risk reduction strategies (**Table 1. 1**).

Table 1. 1: Summary of target lipid levels according to major clinical guidelines

Lipid parameter	**AHA/ACC guidelines (example targets for high-risk individuals)**	**ESC/EAS guidelines (example targets for very high-risk individuals)**
LDL-C	< 70 mg/dL	< 55 mg/dL or ≥ 50% reduction
HDL-C	> 40 mg/dL (Desirable)	> 40 mg/dL (Desirable)
Triglycerides	< 150 mg/dL (Desirable)	< 150 mg/dL (Desirable)

1.2. Pathophysiology of dyslipidemia and mixed hyperlipidemia

Understanding the pathophysiology of dyslipidemia is fundamental to developing effective therapeutic strategies. Lipids, being hydrophobic molecules, are transported in the bloodstream within lipoprotein particles. Structurally, lipoproteins feature a non-polar core of triglycerides and cholesteryl esters, coated externally by phospholipids, free cholesterol, and apolipoproteins that stabilize the particle in

aqueous environments. These particles exist in five major classes: chylomicrons, VLDL, IDL, LDL, and HDL (Wen, 2019).

LDL: This lipoprotein mainly facilitates the movement of cholesterol from hepatic stores to peripheral cells. Elevated LDL levels lead to increased deposition of cholesterol in the arterial walls.

HDL: Mediates reverse cholesterol transport, delivering cholesterol collected from peripheral tissues to the liver for metabolic clearance or metabolism. Higher HDL profiles are generally attributed with a reduced threat of CVD.

VLDL: Primarily transports distributing endogenously synthesized triglycerides from the liver to various tissues for energy utilization or storage. The catabolism of VLDL by lipoprotein lipase (LPL) generates IDL and eventually LDL.

Triglycerides: The main form of stored energy in the body. Elevated triglyceride levels can be influenced by dietary intake, endogenous production in the liver, and impaired clearance.

The regulation of lipid metabolism is an interdependent genetic pathways, dietary, lifestyle, and comorbid aspects. Genetic predispositions can significantly influence an individual's baseline lipid levels and their response to dietary and pharmacological interventions (Do & Kathiresan, 2013). Dietary intake particularly saturated and trans fats and cholesterol, can impact LDL-C levels, while high carbohydrate and alcohol intake can contribute to elevated triglyceride levels (Willett, 2012). A sedentary lifestyle and obesity are accompanied with dyslipidemia, metabolic insulin dysfunction, and cardio-metabolic syndrome (Eckel *et al.,* 2010). Furthermore, various comorbid conditions, such as diabetes mellitus, hypothyroidism, and nephrotic syndrome, can contribute to secondary dyslipidemia (Brunzell & Deeb, 1999).

Clinically, dyslipidemia is distinguished as either primary or secondary in origin. Primary dyslipidemia often arises from genetic defects affecting lipoprotein synthesis, metabolism, or clearance. Examples include familial hypercholesterolemia (LDL receptor mutations) and familial hypertriglyceridemia (LPL deficiency). Secondary dyslipidemia results from underlying medical conditions or medications that affect lipid levels.

Mixed hyperlipidemia, associated with higher levels of both LDL-C and triglycerides, is a common and particularly challenging clinical scenario. It is frequently associated with cardio-metabolic syndrome, with multiple metabolic abnormalities, which considerably increases the threat of CVD and type 2 diabetes (Reaven, 2005). The interplay between insulin resistance and lipid metabolism is complex, with insulin resistance often leading to increased VLDL production, decreased LPL activity, and reduced HDL-C levels, contributing to both hypertriglyceridemia and elevated small, dense LDL particles, which are particularly atherogenic (**Figure 1.1**).

Cholesterol transport – central role of the liver

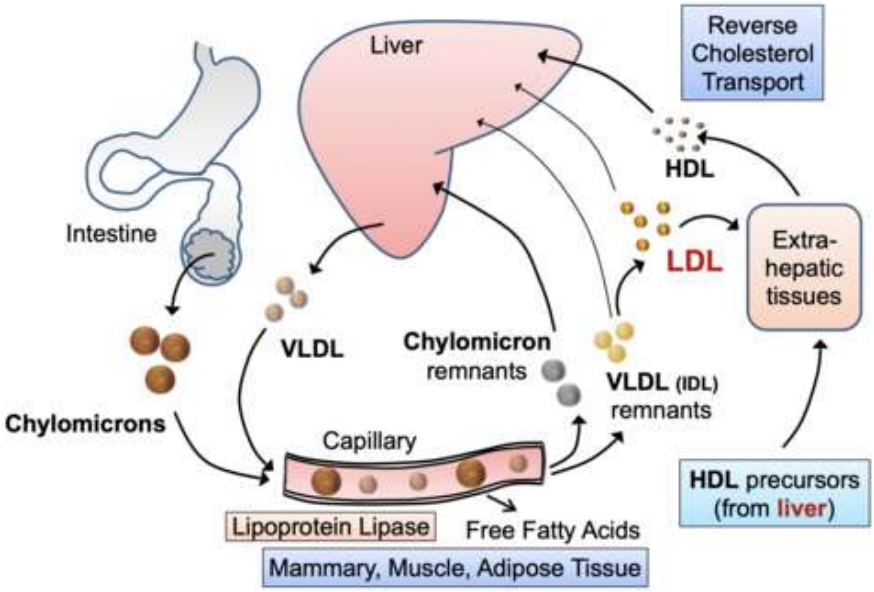

Figure 1. 1: Overview of lipoprotein metabolism and the development of atherosclerosis

(Source: https://o.quizlet.com/7OMhTu5Xt-zWpaa6MBapaw.png**)**

1.3. Limitations of current therapeutic approaches

The cornerstone of dyslipidemia management involves lifestyle modifications, including dietary changes (reduction in saturated and trans fats, cholesterol, and refined carbohydrates), regular physical activity, and weight management. While these interventions are crucial, they are often insufficient to achieve target lipid levels, particularly in high-risk individuals or those with significant genetic predispositions. Consequently, pharmacological interventions play a vital role in managing dyslipidemia and reducing cardiovascular risk.

Monotherapy with single lipid-regulating agents, such as competitive enzyme blockers- HMG-CoA reductase, fibrates (PPAR-α agonists), bile acid–binding resins, cholesterol uptake inhibitors (e.g., ezetimibe), and PCSK9 modulator, has been the traditional approach. Statins are the first-line therapy for lowering LDL-C and have demonstrated significant reductions in cardiovascular events (Baigent *et al.,* 2010). Fibrates are primarily used to lower triglycerides and raise HDL-C (Frick *et al.,* 1987). However, monotherapy often has limitations in achieving comprehensive lipid goals, especially in patients with mixed hyperlipidemia where both LDL-C and triglycerides are elevated.

Achieving optimal lipid control in high-risk patients frequently necessitates a multi-mechanism therapeutic approach targeting different aspects of lipid metabolism. Combining drugs with mechanisms of synergistic effects can lead to more significant reductions in LDL-C and triglycerides, alongside improvements in HDL-C. For instance, combining a statin with a fibrate can address both elevated LDL-C and triglycerides.

However, the use of multiple individual medications can lead to problems with patient compliance. The pill burden associated with taking several different drugs at varying times can be cumbersome, leading to missed doses and suboptimal therapeutic outcomes (Haynes *et al.,* 1996). Furthermore, polypharmacy intensifies the threat of adverse drug interactions and contribute to higher healthcare costs.

Adverse effects associated with lipid-lowering drugs also pose a significant challenge. Statins, while generally well-tolerated, can cause myalgia (muscle pain), and in rare cases, more severe myopathy and rhabdomyolysis (muscle breakdown). They can also lead to mild elevations in liver enzymes. Fibrates can cause gastrointestinal disturbances, and there is a concern for an increased risk of gallstones. The potential for overlapping or synergistic adverse effects when multiple lipid-lowering agents are used concurrently necessitates careful monitoring and dose adjustments.

1.4. Pharmacological profile of atorvastatin

Atorvastatin (ATR) is a synthetic 3-OH-3-CH_3-glutaryl coenzyme-A reductase inhibitor, categorized under statins. Chemical composition of ATR is $C_{33}H_{35}FN_2O_5$ with molecular-mass of 558.64 g/mol. ATR's mechanism implicates the competitive

blockade of HMG-CoA reductase, primary regulatory enzyme in liver cholesterol production (Istvan & Deisenhofer, 2001). By inhibiting this enzyme, ATR reduces the intracellular cholesterol levels in hepatocytes, leading to an up-regulation of LDL receptors on the liver cell surface. Augmented LDL cellular receptor expression improves the uptake of LDL particles from the circulation, resulting in a significant lessening in plasma LDL-C profile. ATR also exhibits modest effects on lowering triglycerides and increasing HDL-C.

ATR is administered orally and is rapidly bioavailable following intestinal absorption. However, it undergoes substantial metabolism during first-pass through the liver and intestines primarily via the cytochrome P450 (CYP) 3A4 enzyme. This pronounced pre-systemic clearance contributes to its considerably low systemic bioavailability, reported to be almost 12% (Lennernäs, 2003). Peak plasma concentrations (Cmax) are typically reached within 1-2 hours *p.o.* ATR is highly bound to plasma proteins (approximately 98%). It is metabolically processed in the liver to various metabolites (active and inactive), which primarily cleared via the bile and feces. The elimination half-life of ATR is around 14 hours, allowing for once-daily dosing. Its pharmacodynamic effect, the reduction in LDL-C, is dose-dependent.

ATR is recommended for the management of familial hyper-cholesterolemia, combined dyslipidemia, and hyper-triglyceridemia. It is also used for the primary prevention of cardiovascular disease in individuals at high risk. The typical starting dose ranges from 10 to 20 mg once daily, with the possibility of increasing the dose up to 80 mg once daily based on the patient's LDL-C response and tolerability. Clinical trials have demonstrated that ATR can pronouncedly reduction in LDL-C by 30-60% governed by the dosage (Jones *et al.,* 1998).

Poor aqueous solubility, high first-pass effect: A major limitation of ATR is its minimal solubility in aqueous media, characterized as a Biopharmaceutics Classification System (BCS) Class II drug. Limited solubilization can hinder its dissolution in the gastrointestinal fluids, leading to incomplete and variable absorption. The extensive first-pass metabolism further contributes to its low systemic bioavailability, meaning that only a small fraction of the administered dose reaching systemic circulation to mediate its clinical effect.

Low with variable bioavailability of ATR presents a significant challenge for achieving consistent and predictable therapeutic outcomes. Factors such as food intake, gastric pH, and individual differences in intestinal permeability and metabolic enzyme activity can influence its absorption and bioavailability, leading to inter-patient variability in drug response.

While generally well-tolerated, ATR can be associated with certain side effects. The most common is myalgia, characterized by muscle pain, tenderness, or weakness. In rare but serious cases, it can lead to myopathy and rhabdomyolysis, which involves severe muscle damage and can potentially, cause kidney failure. Regular monitoring of creatine kinase (CK) levels may be necessary in patients experiencing muscle symptoms. ATR can also cause mild and transient elevations in liver transaminases (ALT and AST). Regular monitoring of liver function tests is recommended, particularly during the initial stages of therapy and with dose increases.

1.5. Pharmacological profile of fenofibrate

Fenofibrate (FNF) is a fibric acid derivative, widely used to treat hypertriglyceridemia and mixed dyslipidemia. FNF is a pro-drug with molecular-mass of 360.83 g/mol and chemical composition $C_{20}H_{21}ClO_4$. Pro-drug (*p.o.*) is efficiently converted to fenofibric acid through esterase-mediated hydrolysis in plasma and peripheral tissues.

Fenofibric acid exerts its primary effects by exerting its action through stimulation of PPAR-α, a nuclear receptor that modulates gene expression involved in lipid homeostasis (Staels *et al.,* 1998). Activation of PPAR-α leads to several beneficial effects on lipid profiles, including:

Increased expression of lipoprotein lipase (LPL), which enhances the chemical break down of triglycerides in VLDL and chylomicrons, contributing to a reduction in plasma triglyceride levels. Decreased hepatic production of apolipoprotein C-III, an inhibitor of LPL activity, further contributing to triglyceride lowering. Increased hepatic uptake and beta-oxidation of fatty acids, reducing the availability of substrates for triglyceride synthesis. Increased synthesis of apolipoprotein A-I and ATP-binding cassette traNOPorter A1 (ABCA1), leading to increased HDL-C levels and enhanced reverse cholesterol traNOPort. Modest reductions in LDL-C, notably in patients with predominance of TG and a predominance of small, dense LDL.

FNF is primarily intended for treating severe hypertriglyceridemia to reduce the risk of pancreatitis. It is also used in the management of mixed dyslipidemia, often in combination with a statin, to address both elevated triglycerides and LDL-C. FNF has shown particular benefit with diabetic dyslipidemic patients, a common condition manifested by elevated TG, low HDL-C, and often increased LDL-C.

Similar to ATR, FNF exhibits poor aqueous dissolvability, categorizing it as a BCS Class II drug. This poor solubility hinders its solubility rate in the gastrointestinal fluids, leading to variable and often incomplete absorption. The bioavailability of conventional FNF formulations can be influenced by food intake, with absorption generally being enhanced when administered with meals (Martin *et al.,* 1993).

Undesirable effects if FNF include digestive discomfort such as nausea, abdominal discomfort, and diarrhoea. A potential concern associated with fibrate use is an increased risk of gallstone formation due to increased biliary cholesterol excretion. FNF can also cause mild and reversible elevations in liver transaminases. In rare cases, myopathy has been reported, and the risk may be increased when used in combination with statins.

1.6. Fixed-dose combinations in hyperlipidemia

Given the frequent co-existence of elevated LDL-C and triglycerides in many patients with dyslipidemia, particularly those with mixed hyperlipidemia and metabolic syndrome, there is a significant clinical need for therapeutic strategies that can effectively address both lipid abnormalities. Fixed-dose combinations (FDCs) of lipid-lowering agents, such as a statin and a fibrate, offer a potential solution to this challenge.

The synergistic effects of statins and fibrates on the lipid profile make their combination a rational approach for managing mixed hyperlipidemia. Statins primarily target LDL-C reduction by inhibiting cholesterol synthesis, while fibrates primarily lower triglycerides and raise HDL-C by activating PPAR-α. Combining these agents can lead to a more comprehensive improvement in the overall lipid profile compared to monotherapy with either drug alone.

Clinical studies have demonstrated that the co-administration of a statin and a fibrate can result in considerable decline in LDL-C, substantial lowering of triglycerides, and

a beneficial amplification of HDL-C levels (Jones *et al.,* 2011). This multi-pronged approach addresses the complex lipid abnormalities associated with increased cardiovascular risk.

FDCs offer several potential advantages over administering the individual components separately. Improved patient compliance is a key benefit, as taking a single pill can simplify the medication regimen, potentially leading to better adherence and improved therapeutic outcomes (Cramer *et al.,* 2008). By combining two medications into one tablet, FDCs can also be more cost-effective for both patients and healthcare systems compared to prescribing and dispensing two separate drugs. Furthermore, the potential for synergistic or additive efficacy in achieving lipid targets makes FDCs an attractive option for patients who do not reach their goals with monotherapy.

Regulatory agencies worldwide recognize the value of FDCs in improving patient care and have established guidelines for their development and approval. Several FDCs containing a statin and another lipid-lowering agent, such as ezetimibe (a cholesterol absorption inhibitor), are already available in the market. However, FDCs combining a statin and a fibrate have faced more complex regulatory considerations due to concerns about potential drug interactions and overlapping toxicities, particularly myopathy. Nevertheless, there is growing interest in developing safe and effective statin-fibrate FDCs for carefully selected patient populations with mixed hyperlipidemia who require this combination therapy.

The development of FDCs presents unique pharmaceutical challenges. The two active pharmaceutical ingredients (APIs) must be chemically and physically compatible within the same formulation to ensure stability, efficacy, and safety throughout the product's shelf life. Physicochemical incompatibilities between ATR and FNF, such as differences in solubility, stability under various conditions (temperature, humidity), and potential for interactions, need to be carefully addressed during the formulation development process.

1.7. Oral bioavailability and solubility challenges in BCS class II drugs

BCS serves as a scientific model for categorizing drugs based on dissolution potential and intestinal absorptivity. This system helps to estimate systemic uptake of drug

products and can guide formulation development strategies (Amidon *et al.,* 1995). BCS Class II drugs are characterized by high permeability but low aqueous solubility.

BCS classification and implications for drug development: For BCS Class II drugs, the rate-limiting step in their oral absorption are often their dissolution in the gastrointestinal fluids. Once dissolved, their high permeability allows for efficient transport across the intestinal membrane into the systemic circulation. Therefore, enhancement of aqueous solubility and dissolution rate is vital to achieve adequate systemic absorption for improving their oral bioavailability and achieving optimal therapeutic concentrations.

ATR and FNF: BCS Class II Drugs: As previously mentioned, both ATR and FNF fall under the BCS Class II category. Their poor aqueous solubility significantly limits their dissolution in the gastrointestinal tract, leading to incomplete and variable absorption, and consequently, low systemic bioavailability.

Solubility vs permeability and rate-limiting step in absorption: In the case of ATR and FNF, their high permeability potential is often not fully realized due to the bottleneck created by their poor solubility. Even if the chemical entity can readily pass the intestinal tissue once dissolved, the limited amount that dissolves in the first place restricts the overall extent of absorption. Therefore, strategies aimed at increasing their solubility and dissolution rate are paramount for improving their oral bioavailability.

Gastrointestinal pH, solubilization, and pre-systemic metabolism: The solubility behavior of weakly ionisable drugs (acid and base) like ATR and FNF can be influenced by the pH of the gastrointestinal fluids, which varies along the digestive tract. In the milieu pertaining to phospholipids and bile salts in the small bowel can aid in the solubilization of lipophilic drugs by forming micelles. However, for poorly soluble drugs, this endogenous solubilization may not be sufficient for optimal absorption. Additionally, both ATR and FNF undergo significant pre-systemic metabolism in the gut wall and liver, further reducing the amount of drug that reaches the systemic circulation intact. Enhancing dissolution can potentially lead to a faster rate of absorption, which might partially saturate the metabolic enzymes in the gut

wall, thereby increasing the fraction of the administered dose that escapes first-pass metabolism.

Necessity of solubility enhancement for effective therapy: To overcome the limitations associated with the poor aqueous solubility of ATR and FNF and to improve their oral bioavailability, various solubility enhancement strategies are necessary to ensure consistent and effective therapeutic outcomes, particularly when aiming for a fixed-dose combination where achieving adequate and predictable absorption of both drugs is critical.

1.8. Solubility enhancement strategies

Numerous approaches have been assessed to optimize solubility and dissolution rate of drugs with limited solubility in water like ATR and FNF. These strategies may be outlined as:

Micronization: Reducing the particle size of chemical entity increases its surface area, contributing to a faster solubilization rate according to the Noyes-Whitney equation. However, micronization alone may not be sufficient for highly lipophilic drugs, and the increased surface area can also lead to aggregation and poor wettability (Ainurofiq *et al.,* 2021).

Lipid-based systems: Self-emulsifying (SEDDS) and self-microemulsifying (SMEDDS) drug delivery systems utilize lipids, surfactants, and co-solvents to enhance drug solubilization in the gastrointestinal tract, promoting absorption.

Cyclodextrins: These cyclic oligosaccharides can form inclusion complexes with hydrophobic drug molecules, increasing their apparent solubility in aqueous media.

Solid Dispersions: This technique involves dispersing the poorly soluble drug in a hydrophilic carrier matrix in a solid state. The drug can be present in an amorphous form or as microcrystals within the carrier, leading to enhanced wettability and dissolution.

Nanosuspensions: These are dispersed colloidal systems of nanosized drug particles (typically < 1000 nm) maintained by surfactant or polymers. Minimization of particle size dramatically enlarges the available surface and solubilization of the drug.

Other techniques: These include salt formation, co-crystallization, and the use of amorphous solid dispersions (Jagtap M, 2025).

While these solubility enhancement techniques offer promising solutions, they also come with their own set of regulatory and manufacturing challenges. Issues such as scalability, cost-effectiveness, long-term stability of the enhanced formulations, and the need for specialized equipment and processing conditions need careful consideration during drug development (Kumari *et al*., 2023). For successful clinical translation and widespread patient access, the chosen solubility enhancement technology should be amenable to large-scale manufacturing and should be economically viable. Simpler and more robust techniques are often preferred for industrial application. Both solid dispersions and nano-suspensions have been planned as particularly formulation strategies to enhance solubilization and systemic availability of BCS Class II drugs. They offer distinct advantages in terms of increasing the dissolution rate and potentially improving drug absorption. Solid dispersions can improve wettability and reduce drug crystallinity, while nanosuspensions provide a significant increase in surface area for dissolution (Abhijeet *et al.,* 2025).

1.9. Solid dispersions: theory, carriers, and techniques

Solid dispersions (SDs) represent a promising approach to overcome the poor aqueous solubility of drugs by dispersing them in a solid, inert, and usually hydrophilic matrix. The drug in the SD can exist in various states, including eutectic mixtures, solid solutions (molecular dispersions), and amorphous dispersions (Tristiyanti *et al.,* 2026).

Eutectic mixtures: These are intimate mixtures of two or more components that solidify simultaneously at a temperature lower than the melting point of the individual components. The drug is typically present in a crystalline form, but the presence of the carrier can improve its wettability and dissolution.

Solid solutions (molecular dispersions): In this type, the drug molecules are incorporated into the matrix at the molecular level, forming a single-component phase system. This intimate mixing can significantly enhance the drug's apparent solubility and dissolution rate due to the absence of crystal lattice energy.

Amorphous dispersions: Here, chemical entity is dispersed amorphously entrapped within the carrier (non-crystalline). Amorphous forms, characterized by greater

molecular mobility and thermodynamic instability, usually exhibit increased solubility and rapid dissolution than their crystalline equivalents.

Mechanisms: Improved Wettability, Reduced Crystallinity: The enhancement in solubilization perceived with solid dispersions is associated with diverse mechanisms:

Improved wettability: Hydrophilic carrier can improve the wettability of the hydrophobic drug particles, allowing for better contact with the dissolution medium.

Reduced Drug Crystallinity: By dispersing the drug in an non-crystalline form or reducing its crystal size, the energy required for dissolution (lattice energy) is reduced, leading to faster dissolution.

Formation of metastable forms: Solid dispersion techniques can stabilize the drug in a higher energy, metastable form, which generally exhibits higher solubility.

Localized solubilization: The hydrophilic carrier can create a microenvironment with a higher drug concentration at the solid-liquid interface, facilitating dissolution.

Role of polymers: PVP, HPMC, PEG, Soluplus: Various hydrophilic polymers are commonly used as carriers in solid dispersions, including:

Polyvinylpyrrolidone (PVP): A water-soluble polymer known for its good drug solubilizing properties and ability to inhibit drug crystallization.

Hydroxypropyl methylcellulose (HPMC): A cellulose derivative with varying viscosity grades, widely used for its biocompatibility and ability to form stable dispersions.

Polyethylene glycol (PEG): A water-soluble polyether compound available in various molecular weights, often used as a carrier due to its good solubility and ability to improve drug wettability.

Soluplus: A graft copolymer consisting of polyvinyl caprolactam-polyvinyl acetate-polyethylene glycol, known for its excellent solubilizing properties and ability to prevent drug recrystallization (Rocha *et al.,* 2023).

Techniques: Solvent Evaporation, Melt Extrusion, Spray Drying: Several methods are employed to prepare solid dispersions:

Solvent evaporation: This involves dissolving both chemical entity and carrier inside common low-boiling solvent, followed by volatilizing solvent under reduced pressure or by heating. The resulting solid dispersion is then collected and further processed.

Melt extrusion: This technique implicates thermal fusion of the components (drug and carrier) and then extruding the molten mass through an orifice. The extrudate is then cooled and milled to obtain the solid dispersion. This practice stays particularly apt for heat-labile drugs.

Spray drying: In this process, a solution of the drug and carrier in a volatile solvent is aerosolized into a heated gas, causing rapid drying of the solvent and development of ultrafine, solid dispersion.

Solvent evaporation method: Process Parameters, Advantages: The solvent evaporation method is a relatively simple and widely used technique used for preparing solid drug–polymer dispersion. Key practice parameters include the choice of solvent (which should dissolve both the drug and the carrier), the active-to-carrier ratio, rate of solvent evaporation, the temperature, and the mixing speed. Advantages of this method include its simplicity, versatility in handling various drugs and carriers, and the potential for achieving good drug dispersion within the matrix (Deshmukh *et al.,* 2025).

Characterization: DSC, PXRD, FTIR, SEM: Solid dispersions are typically characterized using a variety of techniques to assess the physical state of the drug and its interaction with the carrier:

Differential Scanning Calorimetry (DSC): Used to determine the thermal behavior of the drug and the solid dispersion, identifying changes in melting point, glass transition temperature, and crystallinity.

Powder X-ray Diffraction (PXRD): Provides information about the crystalline or amorphous nature of the drug in the solid dispersion. A reduction or disappearance of characteristic drug peaks suggests lowering crystallinity or formation of a non-crystalline dispersion.

Fourier Transform Infrared Spectroscopy (FTIR): Used to investigate potential interactions between the drug and the carrier at the molecular level.

Scanning Electron Microscopy (SEM): Provides Visual assessment of solid dispersion morphology and particle size (Rocha *et al.,* 2023).

1.10. Nanosuspensions principles and applications

Nanosuspensions are defined as colloidal dispersions of limitedly water-soluble dispersed drug particulates within a water-based or organic medium with droplet size typically covering from 1 to 1000 nm. Drug particles are formulated with surfactants or polymers to retain particle dispersion and Ostwald ripening (Jacob S *et al.,* 2025).

The significant enhancement in dissolution rate observed with nanosuspensions is primarily endorsed to the dramatic enhancement in particle surface of the drug. According to the Noyes-Whitney equation:

dC/ dt: dissolution rate

D: diffusion coefficient-drug

A: Drug particle surface area

Cs: Drug's saturation solubility

C: Drug's concentration at time t in the dissolution medium

h: Diffusion layer thickness

Surfactants, polymers: Due to their high surface energy, nanoparticles tend to aggregate to minimize their surface area, leading to Ostwald ripening (growth of larger particles at the expense of smaller ones) and sedimentation. Therefore, the stabilization of nanosuspensions is crucial for maintaining their long-term physical stability and ensuring consistent dissolution behaviour. Surfactants (surface-active agents) and polymers are commonly used as stabilizers. Surfactants minimize interfacial forces between the dispersed drug and solvent while polymers can provide steric or electrostatic stabilization by a surface layer that shields the nanoparticles (Sarkar C *et al.,* 2023).

Top-down vs bottom-up approaches: Nanosuspensions can be prepared using two main approaches:

Top-down techniques: These involve reducing the size of larger drug particles to the nanometer range using mechanical forces. Examples include media milling (nanomilling) and high-pressure homogenization.

Bottom-up techniques: These involve building up nanosized particles from molecular solutions through precipitation or crystallization processes. Sonoprecipitation is an example of a bottom-up technique (Subbaiah M A M, *et al.,* 2024).

Sonoprecipitation involves the precipitation of nanosized drug particles from a solution using ultrasonic irradiation. Typically, the drug is solubilized in an appropriate solvent, and resultant mixture is then rapidly homogenized with a non-solvent in association with stabilizers under the influence of ultrasound. The high-intensity ultrasound generates cavitation bubbles, which collapse violently, leading to rapid nucleation and growth of drug nanoparticles with controlled size and morphology (Tsiaxerli A *et al.,* 2024). Advantages of sonoprecipitation include its potential for producing narrow particle size distributions, the possibility of continuous processing, and the avoidance of harsh mechanical forces or high temperatures. Scalability can be achieved by optimizing the reactor design and ultrasonic power (Aldeeb M. M. E *et al.,* 2024).

By significantly enhancing the dissolution rate and potentially the saturation solubility of poorly soluble drugs, nanosuspensions can lead to faster and more complete absorption of the drug via the digestive tract. This can result in a higher peak serum value (C_{max}), a shorter time to attain peak systemic (T_{max}), and an increased overall drug exposure, as reflected by the area under the plasma concentration-time curve (AUC).

1.11. Analytical and *in vivo* evaluation of formulations

The successful formulation of enhanced drug release systems like solid dispersions and nanosuspensions requires thorough *in vitro* and *in vivo* evaluation to assess their performance and predict their clinical behavior (Aldeeb, M. M. E *et al.,* 2024).

Establishing an *in vitro–in vivo* correlation (IVIVC) is highly desirable in pharmaceutical development. An IVIVC constitutes a predictive tool connecting *in vitro* release (e.g., dissolution rate) characteristics of a pharmaceutical formulation to its *in vivo* behavior (e.g., plasma drug concentration or bioavailability). An established IVIVC delivers a modelling approach for formulation optimization and predicting *in vivo* pharmacokinetics from laboratory-based data, potentially limiting the need for extensive *in vivo* experimentation (Sarkar C *et al.,* 2023).

In vitro dissolution profiling is crucial for evaluating the diffusion rate of the drug from the formulated systems. Standard USP (United States Pharmacopeia) dissolution apparatuses (basket and paddle type) are regularly adopted. However, to better mimic the physiological conditions of the gastrointestinal tract, biorelevant dissolution media, which simulate the pH, osmolality, and presence of surfactants (e.g., bile salts, phospholipids) found in the stomach and intestine, are increasingly employed.

Animal models (e.g., rats): Pharmacokinetic studies *in vivo* are essential to characterize the drug's ADME properties from the novel formulations. Animal models, such as rats, are often used as a preliminary step before human studies; consist of delivering the formulations to the animals and then collecting blood samples at various time points to measure the plasma drug concentration.

T_{max} (Time to Maximum Concentration): The time at which the peak plasma drug concentration is reached. A shorter T_{max} indicates faster absorption.

C_{max} (Maximum Concentration): Highest systemic drug concentration post-dosing a higher C_{max} suggests greater extent of absorption.

AUC (Area under the Plasma Concentration-Time Curve): Represents cumulative plasma concentration over time, quantifying absorption (bioavailability).

MRT (Mean Residence Time): Mean systemic retention time of the drug.

Bioavailability index (Relative Bioavailability): Compares the bioavailability of an assessment of the test formulation relative to the reference product (e.g., a marketed product or a conventional formulation). It is often calculated as Percentage AUC of test versus reference formulation (Aldeeb, M. M. E *et al.,* 2024).

Statistical analysis and interpretation of pharmacokinetic data: The pharmacokinetic data obtained from *in vivo* studies are subjected to statistical analysis to identify; there are substantial variances in the absorption parameters amongst the different formulations. Data are analyzed with suitable statistical methods, such as ANOVA and post-hoc procedures to compare the means of pharmacokinetic parameters. The interpretation of these data is crucial for determining the impact of the formulation strategies (nanosuspension vs. solid dispersion) on the oral bioavailability of ATR and FNF. Significant improvements in C_{max} and AUC for the novel formulations

compared to conventional formulations would indicate enhanced drug absorption (Subbaiah M A M, *et al.,* 2024).

1.12. Rationale of the study

The rationale for this study stems from the significant clinical need for effective therapeutic strategies to manage mixed hyperlipidemia, associated with raised levels of both LDL-C and triglycerides. Current approaches often involve monotherapy, which may not adequately address both lipid abnormalities, and the use of multiple medications, contributes to poor patient compliance and enhance the probability of adverse effects. Fixed-dose combinations (FDCs) of a statin (like ATR) and a fibrate (like FNF) offer a promising approach to address this challenge by providing synergistic lipid-lowering effects in a single dosage form (Tristiyanti D *et al.,* 2026).

Nevertheless, ATR and FNF suffer from poor water solubility (BCS Class II), which significantly limits their bioavailability *p.o.* and contributes to variable therapeutic responses. Enhancing the dissolution behaviour and solubility characteristics of the drugs is crucial for improving their absorption and achieving consistent and predictable therapeutic outcomes, especially in an FDC formulation.

This study proposes a novel approach by exploring two advanced drug delivery systems – nanosuspensions and solid dispersions – to overcome the solubility limitations of ATR and FNF, independently and concurrently. Nanosuspensions, with their nanosized drug particles, offer a substantial increase in particle's surface for solubilization, while solid polymer-dispersions, by incorporating the drug molecularly into a hydrophilic excipient, can enhance wettability and reduce crystallinity (Roche B *et al.,* 2023).

The novelty of this research lies in the comparative evaluation of these two distinct yet powerful formulation strategies for a fixed-dose co-formulation of ATR and FNF. By formulating both drugs as nanosuspensions and as solid dispersions, and then comparing their physicochemical features, *in vitro* solubilizing behavior, and *in vivo* pharmacokinetic profiles, this study focuses on identifying the formulation with the highest potential to improve bioavailability of this important drug combination. The ultimate goal is to develop a formulation that can improve patient outcomes and therapeutic consistency in the management of mixed hyperlipidemia.

1.13. Significance and scope of the research

This research holds significant potential for advancing the management of dyslipidemia, particularly mixed hyperlipidemia. By addressing the major limitation of poor oral bioavailability of ATR and FNF through the application of nanotechnology (nanosuspensions) and polymer science (solid dispersions), this study can contribute to the development of more effective and reliable lipid-lowering therapies.

The study demonstrates the integration of cutting-edge formulation technologies to enhance the delivery of a challenging drug combination. The comparative evaluation of nanosuspensions and solid dispersions will provide valuable perceptions into the benefits and weaknesses of respective methodology for this specific drug combination, contributing to the broader knowledge in the field of pharmaceutical formulation.

The potential for industrial-scale production of stable and bioavailable FDCs based on the findings of this research could lead to more convenient and cost-effective treatment options for patients, ultimately improving medication adherence and therapeutic outcomes. This research aligns with the growing need for patient-centric drug delivery systems that simplify treatment regimens and enhance the quality of life for individuals managing chronic conditions like dyslipidemia.

The comprehensive comparative analysis between two advanced formulation systems for this specific FDC will provide a strong foundation for future research and development in the area of lipid-lowering therapies and combination drug products.

These drugs exhibit high permeability but limited solubility, which significantly restricts their dissolution rate and, consequently, their absorption following oral administration. To address these challenges, dispersible tablet formulations have gained considerable attention as an effective drug delivery strategy (Alshehri *et al.,* 2015. Dispersible tablets are designed to disintegrate rapidly in water, developing a uniform dispersion easy to administer, thereby improving patient compliance especially in geriatric populations. In the present investigation, solid dispersion strategy was employed to release ATR and FNF by embedding them in hydrophilic carriers, which increased their surface area and wettability. These solid dispersions

were subsequently formulated into dispersible tablets, combining the solubility enhancement benefits of solid dispersion with the ease of administration characteristic of dispersible dosage forms (Kukulka *et al.,* 2016). This dual approach not only aims facilitate rapid dissolution rate and *in vivo* availability of the drugs but also offers a patient-friendly formulation that addresses limitations associated with conventional oral solid dosage forms.

CHAPTER 2
LITERATURE REVIEW

2. LITERATURE REVIEW

2.1 Clinical studies on combination therapies

Table 2.1 presents a summary of published clinical studies investigating various combination therapies, highlighting their therapeutic efficacy, safety profiles, clinical outcomes, and comparative advantages over monotherapy.

Table 2. 1: Clinical studies on combination therapies

Title & Reference	Main findings / conclusion	Remarks
Cardiology and Therapy (Francisco G. Padilla-Padilla *et al.,* 2025)	In a randomized, multicenter, double-blind study involving 76 diabetic patients with mixed dyslipidemia, a fixed-dose combination of ATR 20 mg and FNF 160 mg produced a significantly greater reduction in triglycerides compared to ATR monotherapy (–144.3 vs –64.0 mg/dL at 4 months, p = 0.004). Improvements were also observed in LDL-C, total cholesterol, and non-HDL cholesterol, with a comparable safety profile between the two groups.	The study shows that ATR 20 mg + FNF 160 mg FDC achieves greater triglyceride reduction and improved lipid profile in mixed dyslipidemia compared to ATR alone, without added safety risks.
Cardiovascular Diabetology. (Sangmo Hong *et al.,*	In a large real-world cohort of 110,723 diabetic patients with triglycerides ≥150 mg/dL, adding FNF to statin therapy	This real-world study demonstrates that adding FNF to statins in diabetic patients with hypertriglyceridemia

2024)	was associated with a significantly lower risk of myocardial infarction (HR 0.878), stroke (HR 0.901), the composite of MI/stroke (HR 0.897), and all-cause mortality (HR 0.716) over a mean follow-up of approximately 4 years.	significantly lowers the risk of myocardial infarction, stroke, and all-cause mortality.
Cardiovascular diabetology, (Ku *et al.,* 2024)	In a retrospective cohort of 114,920 type-2 diabetic patients on statin therapy, concurrent FNF use was associated with a lower risk of the composite outcome of lower extremity amputation (LEA) and peripheral arterial disease (PAD) (HR 0.81), as well as reduced risk of LEA alone (HR 0.76) and PAD alone (HR 0.81) over a median follow-up of ~7.6 years. Importantly, no significant increase in acute kidney injury, rhabdomyolysis, or hospitalizations was observed.	FNF-PREVENT study demonstrates that FNF added to statin therapy in diabetic patients lowers the risk of lower-extremity amputation and peripheral arterial disease, without increasing rhabdomyolysis or acute kidney injury.
Patent WO2023152138A1-Extended-Release	Patent describes biodegradable microspheres composed of a polylactic-co-glycolic acid	Patent describes a PLGA-based sustained-release microsphere system for FNF,

Fenofibrate Microspheres (2023)	polymer matrix encapsulating FNF, engineered for controlled, sustained drug release over at least one month, and potentially up to two to three months. These microspheres, with a mean diameter of approximately 55–65 µm, are suitable for injectable formulations, such as intra-articular administration.	offering 1–3 months of controlled release and potential for alternative delivery and reduced dosing, though not commercialized.
Drug Design, Development and Therapy, (Chilbert, Maya R *et al.,* 2022)	The study discusses the Dual-drug therapy with ezetimibe and rosuvastatin for lipid management. It concludes that this combination significantly improves LDL-C reduction compared to monotherapy, with a similar safety profile. The combination therapy also shows benefits in patients with statin intolerance and provides a synergistic effect in lipid-lowering.	Supports the use of combination therapy in lipid management, especially in patients not achieving targets with statin monotherapy.
Annals of Internal Medicine, (Zhou, Shiyu *et al.,* 2024)	This multi-database cohort study comparing ATR and rosuvastatin found that rosuvastatin is linked to lower	Provides a balanced evaluation of rosuvastatin's efficacy and safety, highlighting the importance of individualized

	mortality and cardiovascular events but a higher risk of diabetes, highlighting the importance of individualized therapy balancing efficacy and safety.	treatment plans.
Herz, (Zhang, L *et al.*, 2020)	This meta-analysis focuses on East Asian populations, comparing Rosuvastatin versus ATR: effects on LDL cholesterol and safety profile. The results indicate that rosuvastatin has a superior LDL-C lowering effect and a comparable safety profile to ATR in this population group.	Highlights the potential preference for rosuvastatin in East Asian populations due to its enhanced efficacy.

2.2 Nanotechnology-based drug delivery systems

Table 2.2 summarizes the published literature on nanotechnology-based drug delivery systems, emphasizing their role in enhancing drug solubility, stability, bioavailability, targeted delivery, and therapeutic efficacy.

Table 2. 2: Nanotechnology-based drug delivery systems

Title & Reference	Main findings / conclusion	Remarks
Current Pharmaceutical Design, (Elsebay,	The article reviews nanosuspension technology as a formulation strategy to tackle poor	Suggests nanosuspension as a promising approach for improving the delivery of lipid-

Mohamed T *et al.,* 2023)	aqueous solubility and bioavailability of poorly soluble drugs. It concludes that nanosuspensions enhance dissolution rate, stability, and bioavailability, making them suitable for various routes of administration.	lowering drugs; however, limited studies are available on the development of dual-drug nanosuspension systems containing ATR and FNF for simultaneous enhancement of solubility and therapeutic efficacy.
International Journal of Nanomedicine, (Liang, You *et al.,* 2025)	This study evaluates the pharmacokinetics of ATR when co-administered with luteolin nanosuspensions in rat models. The findings reveal significant drug-drug interactions, affecting the absorption and metabolism of ATR, which underscores the importance of considering such interactions in combination therapies.	Highlights the need for careful assessment of pharmacokinetic interactions in nanotechnology-based combination therapies; however, there is insufficient information regarding the interaction behavior of ATR and FNF when incorporated into combined nanosuspension formulations.
Journal of Liposome Research, (Nasrin *et al.,* 2025),	The research investigates impact of oral resveratrol nanoliposomes on lipid disorders in an animal model. It demonstrates that these nanoliposomes modulate protein expression of TLR3 and its adaptor TRIF, leading to improved lipid profiles.	Indicates the potential of nanoliposome-based delivery systems in modulating immune responses and treating hyperlipidemia; nevertheless, translational studies involving clinically established lipid-lowering combinations such as ATR and FNF remain limited.

Pharmaceutics, (Rani, Alankrita, and Gunther Marsche. 2023),	This review discusses the role of HDL-based nanomedicine in targeting macrophages in cardiovascular disease. It concludes that HDL-mimicking nanoparticles can effectively deliver therapeutic agents to macrophages, reducing inflammation and atherosclerotic plaque formation.	Supports the development of HDL-based nanocarriers for targeted therapy in cardiovascular diseases; however, challenges associated with formulation scalability, long-term safety, and incorporation of combination antihyperlipidemic drugs are yet to be fully addressed.
Artificial Cells, Nanomedicine, and Biotechnology, (Gupta, Nidhi *et al.,* (2018)	The article reviews advancements in nanotechnology-based approaches for the treatment and diagnosis of hypercholesterolemia. It highlights various nanocarriers, including liposomes, nanoparticles, and dendrimers, that enhance drug targeting and imaging.	Emphasizes the multifaceted applications of nanotechnology in managing hypercholesterolemia; however, comparative studies evaluating the effectiveness of nanosuspension systems against conventional dosage forms for combined lipid-lowering therapy are still inadequate.
Biomaterials Research, (Jacob, Shery et al., 2020),	This review explores the expanding role of nanosuspensions in enhancing drug delivery. It discusses their advantages in promoting solubility, stability, and approaches to augment the systemic availability of limited soluble drugs and their various	Reinforces the utility of nanosuspensions in improving oral bioavailability of lipid-lowering agents; however, limited research has focused on the formulation optimization, stability assessment, and patient-compliant dosage form development of ATR-FNF

	formulations.	nanosuspension combinations.

2.3 Solid dispersion techniques for enhancing drug solubility

Table 2.3 presents a compilation of reported studies on solid dispersion techniques employed for enhancing the solubility and dissolution rate of poorly water-soluble drugs.

Table 2. 3: Solid dispersion techniques for enhancing drug solubility

Title & Reference	Main findings / conclusion	Remarks
Drug Development and Industrial Pharmacy, (Borde, Shambhavi *et al.,* 2021)	The paper classifies ternary solid dispersions and discusses formulation considerations. It concludes that incorporating a third component can augment the solubility and stability of limited soluble drugs by improving wettability with inhibiting crystallization.	Provides insights into optimizing solid dispersion formulations for better drug solubility; however, limited studies have explored ternary solid dispersion systems for combined antihyperlipidemic drugs such as ATR and FNF.
Current Pharmaceutical Design, (Tran, Phuong H L *et al.,* 2021)	This study presents fast-dissolving solid dispersions for controlled release of poorly water-soluble drugs. It finds that such dispersions can achieve rapid dissolution and sustained release, improving bioavailability and therapeutic efficacy.	Suggests a viable approach for enhancing the performance of lipid-lowering drugs; nevertheless, patient-compliant dosage forms incorporating controlled-release solid dispersions of combined lipid-lowering agents remain insufficiently investigated.

Pharmaceutics, (Budiman, Arif *et al.,* 2023)	The review elaborates on the preparation, characterization, mechanism of drug release, and physical stability of ternary solid dispersions. It emphasizes their role in enhancing solubility and maintaining stability of amorphous drugs.	Highlights the potential of ternary systems in overcoming solubility challenges; however, further studies are needed to evaluate long-term stability, scalability, and in vivo performance of dual-drug ternary solid dispersion systems.
International Journal of Pharmaceutics, (Tran, Phuong H L, and Thao T D Tran. 2020)	This article discusses dosage form designs for controlled drug release using solid dispersions. It concludes that appropriate design can modulate drug release profiles, enhancing therapeutic outcomes.	Offers guidance on designing solid dispersion-based dosage forms for controlled release; however, there is limited evidence regarding the integration of solid dispersions into dispersible or patient-friendly oral formulations for combination therapy.
Drug Development and Industrial Pharmacy, (Sonar, P A *et al.,* 2015)	The study involves the preparation and profiling of simvastatin solidified dispersion of skimmed milk. Results show optimized dissolution rate and systemic availability of simvastatin.	Demonstrates an innovative use of natural carriers in solid dispersion formulations; however, the applicability of such natural carrier systems for combination antihyperlipidemic therapy

		has not been adequately explored.
Drug Development and Industrial Pharmacy, (Silva and Taízia D *et al.,* 2010)	This research focuses on the preparation and characterization of simvastatin solid dispersion. Findings indicate enhanced solubilization and dissolution level, contributing to better systemic availability.	Supports the effectiveness of solid dispersion techniques in improving simvastatin delivery; however, comparative studies involving newer lipid-lowering drugs and multidrug formulations are still limited.
Archives of Pharmacal Research, (Park, Young-Joon et al., 2010)	The study develops a novel itraconazole-loaded solid dispersion without crystalline change, achieving improved bioavailability. It highlights the importance of maintaining the amorphous state for solubility enhancement.	Provides a model for developing solid dispersions without compromising drug stability; however, maintaining long-term amorphous stability in combination formulations remains a major challenge.
Drug Development and Industrial Pharmacy, (Luo, Yanfei *et al.,* 2013)	This research involves the design, physicochemical characterization, stability studies, and *in vitro–in vivo* correlation evaluation of pellet-layered simvastatin nanosuspensions. Results show enhanced stability and bioavailability.	Combines nanosuspension and solid dispersion techniques for optimal drug delivery; however, hybrid systems involving ATR and FNF for synergistic lipid-lowering therapy have not been extensively investigated.

European Journal of Pharmaceutics and Biopharmaceutics, Jun, Seoung Wook *et al.,* (2007)	The study prepares and characterizes a simvastatin/hydroxypropyl-beta-cyclodextrin inclusion complex using the supercritical antisolvent process. Findings indicate improved solubility and dissolution rate.	Demonstrates the utility of cyclodextrin complexes in enhancing statin solubility; however, incorporation of such complexes into scalable and commercially viable dosage forms requires further investigation.
International Journal of Pharmaceutics, (Yan, Yi-Dong *et al.,* 2012),	This research develops a novel valsartan-loaded solid dispersion with enhanced bioavailability and no crystalline changes. The formulation shows improved dissolution and stability.	Highlights the importance of maintaining the amorphous state for bioavailability enhancement; however, there remains a lack of studies focusing on dual-drug solid dispersions with synchronized dissolution and release behavior.

2.4 Nanosuspensions techniques for enhancing drug solubility

Table 2.4 summarizes various reported studies on nanosuspension techniques developed for enhancing the solubility and dissolution behavior of poorly water-soluble drugs.

Table 2. 4: Nanosuspensions techniques for enhancing drug solubility

Title & Reference	Main findings / conclusion	Remarks
Journal of Advanced	Nanosuspensions enhance	Focused on advantages, limitations,

Pharmaceutical Technology & Research. (Patel, Vishal R., and Y. K. Agrawal. 2011)	solubilization and bioavailability of limited soluble drugs by optimizing particle dimensions.	and preparation techniques of nanosuspensions; however, limited emphasis was given to combination drug delivery systems and long-term physical stability of nanosuspensions.
International Journal of Advances in Pharmaceutics (Shah, D. C. 2016)	Comprehensive review on formulation methods like precipitation, homogenization, and milling.	Emphasized stabilizers and scaling-up challenges; nevertheless, industrial translation and reproducibility of combination nanosuspension formulations remain inadequately explored.
Advances in Pharmacology and Pharmacy. (Jadhav, Shivraj Popat*, et al.,* 2023)	Nanosuspension is a robust method to overcome solubility-limited bioavailability; also discusses new polymeric stabilizers.	Covers recent trends and novel formulation strategies; however, there is insufficient research on the application of novel stabilizers in dual antihyperlipidemic nanosuspension systems.
Pharmaceutics. (Jacob, Shery, *et al.,* 2025)	Discusses advanced innovations like dual drug nanosuspensions and hybrid nanocarriers.	Highlights next-generation nanosuspension systems; however, clinical translation, toxicity evaluation, and large-scale manufacturing aspects of such advanced systems are still limited.
International Journal of Nanomedicine (Aldeeb, Oula, *et al.,*	Nanosuspensions improve drug deposition, permeation, and	Specific to dermatological and ocular delivery; however, studies related to oral nanosuspension

2024)	therapeutic index in topical formulations.	systems for cardiovascular and lipid-lowering therapy remain comparatively limited.
Advances in colloid and interface science. (Malamatari, Maria, *et al.,* 2015)	Examines physicochemical properties, formulation aspects, and biodistribution after injection.	Focused on injectable nanosuspensions; however, oral delivery applications and patient-compliant dosage forms require further investigation for chronic disease management.
International Journal of Pharmaceutical Sciences and Research (Verma, Sandeep*, et al.,* 2012)	Reviews techniques and stabilizers used to produce stable nanosuspensions for oral delivery.	Useful overview for formulation scientists; nevertheless, the influence of stabilizer combinations on long-term storage stability and drug release kinetics remains inadequately addressed.
Research j. Pharm and Tech (Shah, D. C. 2016)	Focused on technological approaches and patent status related to nanosuspension systems.	Emphasized industrial applicability; however, limited patented technologies are available for fixed-dose combination nanosuspension formulations targeting dyslipidemia.
Asian Journal of Pharmacy and Technology (Tupe, A., and S. D. Mankar. 2023)	Highlights enhanced pharmacokinetics and faster onset of action in poorly soluble drugs using nanosuspensions.	Summarizes recent clinical and preclinical outcomes; however, comprehensive in vivo studies evaluating safety, therapeutic efficacy, and pharmacokinetic behavior of combined lipid-lowering nanosuspensions are still lacking.

Int J Adv Pharm (Patel, H. M., *et al.,* 2016)		

2.5 Dispersible tablets

Table 2.5 presents an overview of studies related to dispersible tablet formulations developed to improve patient compliance and ease of administration.

Table 2. 5: Dispersible tablet for patient compliance

Title & Reference	Main findings / conclusion	Remarks
Journal of Drug Delivery Science and Technology (Alshehri SM *et al.,* 2015).	Hot melt extrusion improved solubility and masked the bitter taste of mefenamic acid in ODTs.	Demonstrates the use of solid dispersion via HME for enhancing solubility and patient compliance.
Therapeutic Advances in Gastroenterology, (Kukulka M *et al.,* 2016)	ODTs were bioequivalent to capsules; suitable for patients with swallowing difficulties.	Supports development of ODTs for equivalent therapeutic efficacy.
Journal of Pharmaceutical and Biomedical Analysis (Tambe A *et al.,* 2019)	Poloxamer-based solid dispersions improved intestinal absorption of boswellic acid.	Demonstrates the absorption-enhancing potential of solid dispersion systems.
Sensors (Szymańska-Chargot M *et al.,* 2011)	Used FTIR and Raman spectroscopy to characterize cellulose sources.	Relevant for evaluating polymer-excipient interactions in tablet formulations.
Advanced Drug Delivery	Crystal modification	Key reference for crystal

Reviews (Blagden N *et al.,* 2007)	improved dissolution of poorly soluble APIs.	engineering approaches to solubility enhancement.

2.6 **Research gap**

Despite the substantial body of research supporting the efficacy of ATR and FNF in managing dyslipidemia, notable gaps remain in optimizing their therapeutic potential, particularly through advanced drug delivery systems. Clinical studies have extensively compared the lipid-lowering effects of statins, including ATR and rosuvastatin, with findings highlighting the superior LDL-C reduction of rosuvastatin (Zhou *et al.,*2024; Zhang *et al.,*2020). However, the synergistic benefits of combining ATR with FNF—especially in mixed dyslipidemia and metabolic syndrome—are not yet fully harnessed through modern delivery platforms. The pharmacokinetic limitations of ATR and FNF, including poor aqueous solubility, extensive first-pass metabolism, and variable bioavailability, hinder their clinical efficacy, particularly in combination therapies. Although several studies (e.g., Elsebay *et al.,* 2023; Jacob *et al.,* 2020) emphasize nanosuspensions, solid dispersions, and nanoliposomes as promising strategies to enhance drug solubility and stability, the application of these approaches specifically to the co-delivery of ATR and FNF is underexplored. Furthermore, existing nanocarrier research often remains in the preclinical stage, lacking robust translational and clinical validation. Drug–drug interaction concerns, as highlighted by Liang et al. (2025), further underscore the need for pharmacokinetic studies focused on dual-drug nanosystems. Solid dispersion and nanosuspension techniques have demonstrated improved bioavailability for drugs like simvastatin and valsartan (Silva *et al.,* 2010; Yan *et al.,* 2012), yet similar frameworks for ATR - FNF combinations are either nascent or non-existent. Moreover, while advanced hybrid nanosystems and targeted nanocarriers (e.g., HDL-mimicking nanoparticles) have shown therapeutic promise in cardiovascular diseases (Rani & Marsche, 2023), these technologies are not yet applied to the dual delivery of lipid-modifying agents. Therefore, a critical research gap lies in the design, formulation, and clinical validation of nanotechnology-enabled combination therapies of

ATR and FNF. Such systems should aim to overcome solubility and bioavailability barriers, ensure pharmacokinetic compatibility, minimize systemic side effects, and enhance therapeutic outcomes in patients with complex lipid disorders.

CHAPTER 3

AIM. OBJECTIVES AND PLAN OF WORK

3. AIM OBJECTIVE AND PLAN OF WORK

3.1 Aim of the study

The aim of this study was to formulate and evaluate ATR and FNF (Fixed drug combination) loaded nanosuspension (NS) and solid dispersions (SDs) using sonoprecipitation and solvent evaporation method to enhance solubility, dissolution rate and *in vivo* bioavailability for a better drug delivery in management of high cholesterol and to reduce the levels of triglycerides.

3.2 Objectives of the study

The major objectives of the present investigation are as following:

1. To enhance the solubility and bioavailability of a poorly aqueous-soluble drug using the nanosuspension method.
2. To enhance the solubility and bioavailability of a poorly aqueous-soluble drug using the solid dispersion method.
3. To study the solubility, dissolution rate, and stability of the formulation.
4. To investigate and compare the bioavailability of the optimized formulation prepared using the two methods for ATR and FNF.

It was hypothesized that formulation of ATR and FNF into nanosuspension and solid dispersion systems would significantly enhance their aqueous solubility, dissolution rate, and oral bioavailability compared to conventional formulations. Furthermore, incorporation of the optimized formulations into dispersible tablets was expected to improve patient compliance and therapeutic performance in the management of dyslipidemia and hypercholesterolemia.

3.3 Plan of work FDCs nanosuspension

Figure 3.1 present the flow of the work.

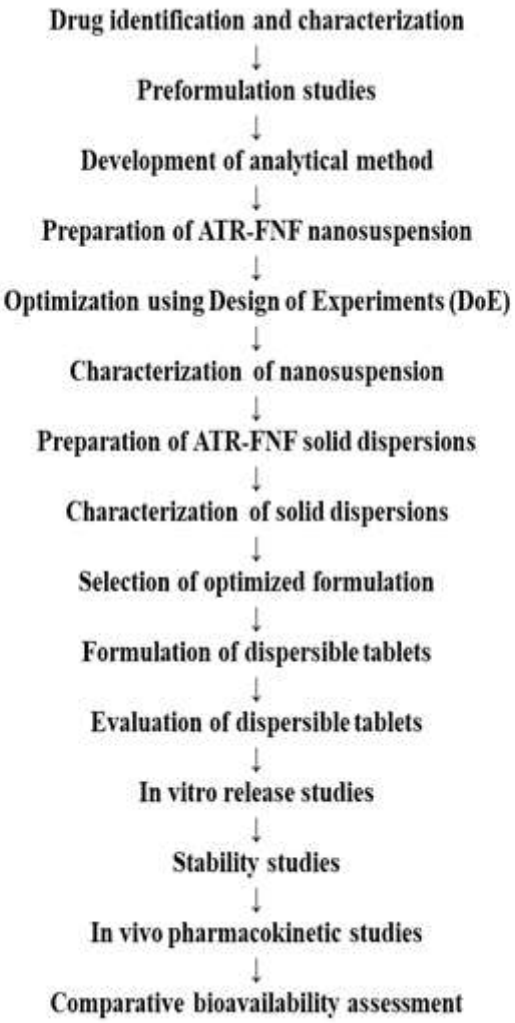

Figure 3. 1: Flow of the work

Identification of drug

- FTIR spectroscopy
- DSC thermogram

Pre-formulation parameters evaluations

- Development of UV method
- Preparation of standard calibration curve
- Physico-chemical characterization

- Organoleptic properties
- Melting point determination
- Solubility study by equilibrium solubility method
- Hygroscopicity
- Particle size and shape analysis

Preparation of nanosuspension

Formulation development of nanosuspension

Design of experiments

Characterization of nanosuspension

- Particle size
- Polydispersity index
- Zeta potential
- Encapsulation efficiency
- Scanning electron microscopy
- Fourier transformed infrared spectroscopy
- Differential scanning calorimetry

Evaluation of FDCs drug loaded nanosuspension formulation

- *In vitro* release study of drug nanosuspension
- Stability studies
- *In vivo* pharmacokinetics studies

Dispersible Tablets

- Formulation of dispersible tablets
- Evaluation of dispersible tablets
    - Weight variation
    - Hardness

- Thickness
- Friability
- Disintegration time
- Wetting time
- Water absorption ratio
- Content uniformity
- Cumulative percentage ATR drug release
- Stability studies

CHAPTER 4

MATERIALS AND METHODS

4. MATERIALS AND METHODS

4.1 Materials

Table 4.1 provides a comprehensive list of materials utilized during the course of the research work, including active pharmaceutical ingredients, polymers, stabilizers, solvents, excipients, and other analytical reagents.

Table 4. 1: List of materials utilized

S. No.	Materials	Suppliers
1.	Atorvastatin (ATR) (purity: ≥ 98%)	Innomedix Pharma Pvt Ltd. Jaipur, India
2.	Fenofibrate (FNF) (purity: ≥ 98%)	Innomedix Pharma Pvt Ltd. Jaipur, India
3.	Poloxamer 407	TCI chemicals, India
4.	Polyvinylpyrrolidone K30 (PVP)	TCI chemicals, India
5.	Soluplus®,	TCI chemicals, India
6.	Kollidon® VA 64,	TCI chemicals, India
7.	Kolliphor® P 407	TCI chemicals, India
8.	Acetonitrile	Qualigens HPLC grade (India)
9.	Methanol	Qualigens HPLC grade (India)
10.	Ethanol	Qualigens HPLC grade (India)
11.	Disodium hydrogen phosphate buffer (0.01 M	Qualigens (India)
12.	Acetonitrile HPLC grade	MERCK, India.
13.	Sodium carboxy methyl cellulose	Sd fine chem Ltd, India.
14.	Orthophosphoric acid	MERCK, India.

15.	Glacial acetic acid	MERCK, India.
16.	PEG 6000	Sd fine chem Ltd, India.
17.	Ethanol	
18.	Microcrystalline cellulose	
19.	Mannitol	
20.	Crospovidone	
21.	PVP K30	
22.	Magnesium stearate	
23.	Talc	

Table 4.2 summarizes the various equipment and instruments used for the formulation development, characterization, and analytical evaluation carried out during the study.

Table 4. 2: Equipments used for formulation and analysis

S. No.	**Equipment**	**Model**	**Manufacturer**
1.	Analytical balance	CPA225D	Sartorius AG, Germany
2.	High-speed homogenizer	IKA T25	IKA, India
3.	Melting point apparatus	MP30 melting point device	Mettler Toledo with LabXTM software
4.	Bath sonicator	Power sonic 405	Hwashin Technology & Co.
5.	Centrifuge	R-24	Remi electro-technik Ltd.
6.	Zeta Sizer	Nano ZS	Malvern instruments, UK

7.	UV-Visible spectrophotometer	V 650	Jasco, Japan
8.	Cyber Scan pH Meter	Ecphtutor-S	Eutech
9.	Freeze dryer	FD5508	Skadi, Europe
10.	HPLC	2707	Waters, Miliford, USA
11.	Optical microscope	Magnus	New Delhi
12.	Magnetic stirrer	IKA	Bangalore
13.	Vortex shaker	VG 3 S22	IKA, India
14.	High speed homogeniser	Ultra turrax T 25	IKA, Germany
15.	Centrifuge	Sigma 3-30KS	Sigma Labor centrifuge, Germany
16.	Attenuated total reflection fourier-transform infrared spectroscopy	Tensor 27	Bruker Optics
17.	Incubate shaker	SI-300	Jeio Tech, Korea
18.	Differential scanning calorimetry	DSC- 60	Seiko (Japan) DSC
19.	Scanning electron microscope	FEI Quanta 250 FEG,	Netherlands
20.	Tablet punching machine (16 station)	CIB-4 GMP Model	Create Industries, Ahmedabad, India
21.	Dissolution apparatus	DS 8000	Lab India, Mumbai, India
22.	Disintegration apparatus	S-981	Systonic, Panchukla, India
23.	Friabulator	Not available	Pharma Chem Machineries, Hyderabad,

			India
25.	Sieve set	Not available	Swastik Scientific Instruments Private Limited, India
26.	Sieve shaker	Not available	Bio Techno Lab Pvt. Ltd., Mumbai, India
27.	Stability chamber	Not available	Enviro Technologies, India

4.2 Experimental methodology

4.2.1 Pre-formulation studies

Pre-formulation studies were carried out to evaluate the physicochemical properties of the drug and excipients, which are essential for the successful development, stability, and performance of the pharmaceutical formulation.

Drug identification by fourier transforms infrared spectroscopy:

FT-IR has employed to confirm the identity of ATR and FNF using a Bruker Tensor-27 FT-IR instrument. Spectral scanning was performed across the 4000–400 cm^{-1} wavenumber region. Approx. 1 mg drug was finely grounded with ~200 mg of anhydrous, powdered KBr to obtain a uniform blend suitable for pellet formation (disc diameter ~13 mm).

The drug–KBr mixture was homogenized thoroughly, transferred into a die, and subsequently compressed under vacuum at ~800 MPa to form a transparent pellet. The prepared disc was then placed in the sample holder of the spectrometer, and the characteristic IR spectrum was recorded for each drug. The spectra were evaluated to verify the presence of functional groups corresponding to the reference range of 400–4000 cm^{-1} (Domenighini, Alberto & Giordano Mario, 2009).

DSC thermogram

Differential Scanning Calorimetry (DSC) was conducted to identify the pure drug with the Seiko (Japan) DSC model 60/DTA 60. This approach quantifies gain or dissipation of thermal energy from alterations (physical, chemical, or both); a sample undergoes a controlled temperature variation. Transitions— similar to fusion, de-solvation, and breakdown can be investigated through thermal analysis for several polymorphs to ascertain the optimal form in lieu of further applications. The instrument was calibrated with iridium. Drug samples (ATR and FNF) of 5 mg were subjected to heating in Al pans utilizing dry N_2 as the effluent gas. Investigation was conducted within a temperature between 20 to 200°C at a frequency of 20°C/ minute. Sample was hermetically packed in Al pans, followed by DSC analysis undertaken at ramp heating rate of 10°/min from 20° to 200°. Sole restriction of this technology is its destructive nature (Chiu MH & Prenner EJ, 2011).

4.2.1.1. Physico-chemical characterization of ATR

Physico-chemical characterization of ATR was performed to evaluate its physical and chemical properties, including solubility, melting point, partition coefficient, drug-excipient compatibility, and spectral characteristics, which are essential for the design and optimization of stable and effective pharmaceutical formulations.

Organoleptic properties

Organoleptic properties, including hue, aroma, and flavor, function as descriptive features of substances. While these features are recorded via physical inspection, they are not designed for identification testing.

Melting point of drugs

Melting point evaluation of ATR and FNF was carried out utilizing the capillary tube approach with an MP30 melting point device (Mettler Toledo, integrated with LabX™ software). A trace amount of the drug was transferred into a capillary tube, introduced into the device, and the melting point was subsequently monitored. (John & Young, 2013).

Solubility

Solubility studies were performed by dispersing excess 5 mg to 100 mg of the respective drug in 10 mL of various solvent media in a 25 mL conical flask. The mixture was subjected to sonication for 48 hours to ensure proper solubility. further samples were filtered and diluted with methanol and measured with the absorbance using a UV spectrophotometer at respective lamda max of the drug.

The solvents used included distilled water, ethanol, methanol, benzene, dimethyl sulfoxide (DMSO), dimethyl formamide (DMF), propylene glycol. All experiments were conducted in triplicates to ensure accuracy and reliability of the results (Krisztina Takács *et al.,* 2017).

Hygroscopicity: It was evaluated to determine the extent of moisture uptake by the drug. Initially, the mass of an empty 50 mL beaker was recorded (W_1). A weighed quantity of the sample was transferred to the same beaker, and the combined mass was noted (W_2). The beaker without a lid was then placed inside a desiccator maintained at 25 °C, containing a saturated ammonium chloride or ammonium sulfate solution to establish a controlled humid environment. After 24 hours, the beaker was reweighed (W_3). The percentage moisture sorption was determined using:

(W3-W2/W2-W1) **x 100**

Interpretation criteria:

Deliquescent: absorbs water sufficiently to liquefy

Highly hygroscopic: ≥15% increase (weight)

Hygroscopic: 2–15% increase (weight)

Slightly hygroscopic: 0.2–2% increase (weight)

Partition coefficient by shake flask method

The partition coefficient of the drugs (ATR and FNF) was ascertained in $C_8H_{18}O$(Octanol): H_2O, C_6H_{14}(Hexane): H_2O, $C_{18}H_{36}O$(oleyl): H_2O, and CH_2Cl_2(Dichloromethane): H_2O systems at ambient temperature. 5 mL:10 mL, organic and aqueous phase respectively placed in a graduated glass tube with a stopper, to which

100 mg of drug-quantity was added. Mixture was subsequently agitated with an instrument (mechanical agitator / sonication) intermittently for 24 hours at ambient temperature. The mixture was placed in a separate funnel and permitted to normalize upto 6 hours. The separated phases passed through filter (membrane), and the drug portion in each phase was measured via simultaneous estimation by UV spectrophotometry at 246 and 286 nm. The apparent partition coefficient was determined by the percentage of drug presence in the separated phases (Ruelle Paul, 2000).

$$Ko/w=C_o/C_w$$

4.2.1.2. Development of UV method for the estimation of ATR and FNF

Preparation of phosphate buffer pH 7.4

Preparation of 0.2 M potassium di hydrogen ortho phosphate (KH_2PO_4**)**

Accurately weighed 27.218 gm of KH_2PO_4 was taken in a clean and dry 1000 mL volumetric flask and dissolved in distilled water (D/W)and the volume was made up to mark to produce 0.0 2M potassium dihydrogen ortho phosphate.

Preparation of 0.2 M NaOH

Accurately weighed 8.0 gm of NaOH pellets while using an analytical balance for preparing a 0.2 M sodium hydroxide solution. After that, the NaOH was placed in a beaker along with a small volume of distilled water to completely dissolve it with stirring using a glass rod. Carefully pour the solution to a 1 L volumetric flask by rinsing the beaker with more D/W, add those rinsing's to the flask. Finally fill the volumetric flask with D/W up to the 1 L mark and mix it well to have homogeneity. Label the flask as 0.2 M NaOH, the date of preparation, and store in a safe manner.

Mixing of standard solution

As per the standard procedure adopted from Indian Pharmacopeia placed 50 mL of 0.2 M KH_2PO_4 in a clean and dry 200 mL volumetric flask and added the specified quantity of 0.2 M NaOH as per the volume mentioned in the below table and final volume was made with distilled water (**Table 4. 3**).

Table 4. 3: Mixing of standard solutions

pH	Volume of 0.2 M NaOH	pH	Volume of 0.2 M NaOH
5.8	3.6	7.0	29.1
6.0	5.6	7.2	34.7
6.2	8.1	7.4	34.9
6.4	11.6	7.6	42.4
6.6	16.4	7.8	44.5
6.8	22.4	8.0	46.1

Selection of wavelength of maximum absorbance and calibration curve:

Pre-weighed quantity of ATR (10 mg) added in volumetric flask of 100 mL capacity, and methanol was added up to mark (100 mL) to get 1000 µg/mL (Stock Solution-I). Stock solution-1, 10 mL was taken and diluted to 100 mL with methanol (Stock solution-II; 100 µg/mL). From Stock solution-II, working solution 10 µg/mL was constituted and scanned over 200-400 nm. In case of FNF accurately 100 mg was added in 100 mL volumetric flask with methanol up to mark (100 mL) to get 1000 µg/mL (Stock Solution-I). Stock solution-1, 10 mL was brought to 100 mL with methanol to generate 100 µg/mL (Stock solution-II).

Preparation of combined reference stock solution:

Standard solutions were diluted from the standard stock sample to include a mix of ATR calcium (2 µg/mL) and FNF (32 µg/mL). Simultaneous equation technique was employed and estimated ATR calcium and FNF.

Simultaneous equation method:

The analytical λ selected for the assays were 246 nm and 286 nm, corresponding to the respective spectral maxima of ATR calcium and FNF in CH_3OH. Stocks were serially diluted with methanol to prepare calibration standards ranging from 2–16 µg/mL for

ATR-Ca with 2–20 µg/mL for FNF. Spectrophotometric measurements were recorded at the specified λ, and the concentrations of the analytes in the samples were determined using the corresponding calibration equations.

$$Cx=A1\ ay2-A2ay1ax1ay2-ax2ay1\text{-----}1$$

$$Cy=A1\ ax2-A2ax1ax1ax2-ax2ax1\text{-----}2$$

Where

A1 & A2: Absorbance of the combination at 246 nm and 286 nm,

ax1 & ax2: absorptivity of ATR calcium at λ1 and λ2

ay1 & ay2: absorptivity of FNF at λ1 and λ2.

Cx & Cy: concentrations of ATR calcium and FNF (Hirave Rupali *et al.,* 2013)

Method validation: Analytical procedure was accessed in accordance with ICH Q2B guidelines to assess linearity, sensitivity, precision, and accuracy of the method for quantifying the analytes.

Accuracy: Recovery experiments were conducted at three concentration points- 80%, 100%, and 120%—to establish the accuracy of the proposed method. The percent recoveries for ATR-Ca and FNF were observed in the range of 98.99–99.92%, indicating high accuracy of the analytical procedure.

Linearity: Linearity was evaluated by analyzing a series of standard solutions of varying concentrations for both ATR-Ca and FNF. Using the simultaneous equation method, the quantity ranges exhibiting adherence to Beer-Lambert's law were determined to be 2–16 µg/mL for ATR-Ca and 2–20 µg/mL for FNF, demonstrating a linear response over the selected range.

4.2.2 Formulation of nanosuspension

Sono-precipitation high speed homogenization method was used with slight modification. An accurately weighted amount of the selected stabilizer Poloxamer 407 (P 407) and Polyvinylpyrrolidone (PVP) was taken and dissolved in deionized water (20 mL) to form the non-organic phase (NOP). Drugs were dissolved in ethanol to form the organic phase (2 mL) and injected rapidly using a syringe (gauge 18) into NOP under a magnetic stirrer

at 1000 rpm. The mixture was subjected to homogenization at an rpm of 9000 for 60 mins under ice cold conditions. The mixture was again placed on a magnetic stirrer at 1000 rpm for the complete evaporation of OP. The nanosuspension was subjected to freeze drying to get a stable product as per the standard protocol (Sahu, B.P *et al.,* 2016)

Optimization of the nanosuspension

A complete study of how several factors affect the final formulation is desirable. Therefore, to create FDC-loaded NS, we adopted the QbD strategy- a methodical approach with encoded goals. Regulatory bodies back QbD's use in the creation of pharmaceutical items. Both academia and industry have increasingly acknowledged this strategy. Unlike conventional approaches, it promises a quality product while enabling a better knowledge of the process in a cost-effective manner. Making a QTPP, or quality-targeted product profile, is essential to the FbD process. The area using during design specifies workable and impractical regions by including various variable combinations. The next step in the FbD process is the CFAs and CPPs phase. This is where possible formulation and process factors that affect CQAs are found. While process elements are connected to CPPs, formulation ones are related to CFAs and the same for this study is given in Table 4. 4 (Chary S.S *et al.,* 2024).

Table 4. 4: Factors for DOE (ATR (20 mg) and FNF (145 mg)

S. No.	**Variable**	**Low level**	**Medium level**	**High level**
A	Drug to stabilizer proportion	0. 5	1	1.5
B	Homogenization speed of stirring (RPM)	6000	9000	12000
C	Homogenization duration (HD; min)	60	90	120
Responses		*Restrictions*		

X1	PS	Minimum
X2	PI	Minimum
X3	ZP	Maximum

4.2.3 Pre-screening research

Various features may influence CQA's, and a lot of work may be needed to evaluate them throughout the design of experiments comprehensively. Generally, in this way, the variables are filtered most often by an OFAT approach so that their interaction can be minimized and the predicting power of the statistical model could be increased. CQAs included PS and polydispersity index (PdI).

4.2.3.1. Optimization of OP:API ratio and stabilizer for performance

A comparison may be made in reference to organic, anti-solvent, and stabilizer component optimization for enhanced performance.

The ratio of OP to the AP is optimized as it affects the size and polydispersity of the NS. The current study AP was changed from 40 to 10 mL, keeping the OP constant at 2 mL. The change in size and polydispersity were evaluated and recorded (Gera S *et al.,* 2017).

Preparation to remain stable at a nanoscale involves using stabilizers. Choosing appropriate stabilizers is not easy; hence a method relying on an experimental process using independent or mixed stabilizers was used. Using the OFAT approach, size, PdI, and stability determined multiple strengths at which stabilizers were rated.

Experimental design

Box-Behnken Design (BBD) implemented to lower the sample size needed for coefficient estimate via an incomplete block and exponential method. This experiment examined the independent variable's impact (i.e., amount of stabilizer-to-drug ratio (%), rpm of homogenization, and time of homogenization (C)) affecting the three dependent variables (i.e., PS, PI, and ZP) at three different levels, using three variables in the BBD design. Using Design Expert® software (Version 12, Stat-Ease Inc., Minneapolis, MN),

Response Surface Analysis was performed; the outcomes were shown via 2D contour plots and Response Surface Charts.

Search to optimized design

The feature of desirability permitted the identification of the ideal formulation with greater ease. Target values are used to determine the attractive value, which is then scaled from 0 to 1. A higher rating shows more confidence in attaining the desired results. Moreover, the design area was used for pictorial optimization. Design validation was done using checkpoint analysis. The outcomes were contrasted with the projected values after three confirmation trials.

HPLC method:

The concentrations of FNF and ATR were ascertained utilizing a Water HPLC System equipped with a UV-DAD detector with slight modification as reported by Jain et al. The mobile phase was of acetonitrile (ACN) and H_2O in the ratio of 70 and 30 v/v. C18 column RP-18, 5 microns, 125 x 3 mm was used in investigation with elution rate of 1.0 mL/min., FNF and ATR spotted at ƛ 286 nm and 246 nm. The retention time of FNF and ATR was 3.4 and 2.3 mins. The standard calibration curve covering 0.3 to 250 µg/mL and 0.2 to 200 µg/mL with correlation values over 0.999 was plotted graphically (Jain N *et al.,* 2008)

For detection of drugs in the plasma specimen the protein precipitation method was utilized. The drugs were separated from serum (50 µL) by mixing 300 µL of ACN by mixing the contents 10 mins, centrifuged 12 mins at 8000 rpm before analysis by HPLC.

4.2.4 Nanosuspension characterization

4.2.4.1. Size and zeta potential measurement

The PS, PI and ZP of the NS were measured by dynamic scattering techniques after diluting the sample by 10 times (Malvern nano S90). The measurement was conducted at 25 °C at a scattered angle of 90 degrees. The ZP of the samples was also determined using a disposable cell for zeta potential analysis employing the principle of

electrophoretic mobility technique. All the reading was done in triplicates (Gera S *et al.,* 2017).

4.2.4.2. SEM (Scanning Electron Transmission)

The NS size and topography were checked and images were captured by FESEM (field emission scanning electron microscopy), with 10 KV accelerating voltage by coating the samples with a layer of platinum for 40 sec at 20 mA (Jain N *et al.,* 2008)

4.2.4.3. Solubility studies

Saturation solubility for the NS was assessed by adding an excess quantity of lyophilized formulation (1 mg of ATR and 10 mg of FNF) to 10 mL 7.4 pH buffer. The specimen was homogenised on a shaker for 48 h at 37ºC. After suitable dilutions the drug dissolved was enumerated using UV Visible spectrophotometer at a lambda max of 246 nm (ATR) and 286 nm (FNF).

4.2.4.4. Drug release

For determining drug kinetics from NS and plain drug using USP dissolution (Type 2) was employed. F-NS and pure drugs (100 mg of sample) were weighted accurately and added into the dissolution vessels containing 900 mL, 0.5 % sodium lauryl sulfate ($C_{12}H_{25}SO_4Na$/SLS; pH 7.4). The dissolution was carried out at 37±0.5ºC at an rpm of 50. Sampling was done at predetermined time, filtered and estimated, calculated and plotted the percentage of drug release from L-NS and plain drugs respectively (Górniak A *et al.,* 2023).

4.2.4.5. Compatibility studies

FT-IR analysis of the selected drugs (ATR, FNF), stabilizers and L-NS were performed by Bruker FT-IR. Approximately 5 mg of the sample were placed on the holder crystal and recorded the results 4000 cm^{-1} to 400 cm^{-1} (Afifi *et al.,* 2015).

4.2.4.6. DSC Study (Differential Scanning Calorimeter)

Using Perkin Elmer DSC apparatus, the compatibility study for the samples, such as selected drugs (ATR, FNF), stabilizers, and L-NS, was achieved under heat, at a frequency 5ºC/min exceeding a 200ºC.

4.2.4.7. XRD (X-ray diffraction)

XRD was executed with diffractometer (Philips PW-1710) with the graphite monochromator and with Ni-filtered Cu K± illumination. The tests were done on pure drugs, a physical mixture (PM), and L-NS. They were scanned at 2 theta between 80 and 2 degrees, with step increment of 0.045° and a time between steps 0.5 sec (Górniak *et al.,* 2023).

4.2.4.8. Stability studies

Stability testing of the optimized ATR–FNF nanosuspension was performed following ICH Q1A-E guidelines. Optimized formulation aliquot into amber glass container with airtight caps and stored at three specified conditions: refrigerated (2 to 8 °C), room temperature (23 to 27 °C /55 to 65% RH), and accelerated (38 to 42 °C/ 70 to 80 % RH). Aliquots were withdrawn at predefined intervals (initial, 30 days, 90 days, and 180 days) and analyzed in triplicate (n = 3) for particle dimension (DLS), size distribution index (PDI), and zeta potential (Surface charge) using a calibrated Zetasizer. Appearance was assessed visually for clarity, turbidity, and aggregation. Drug content (assay) and impurity profiling were performed by validated HPLC methods using gradient elution and UV detection; assay values are reported as percent of label claim (mean ± SD). Dissolution testing of dried nanosuspension-loaded tablets (or dispersible aliquots reconstituted per method) was performed with USP II paddle bowl at 50 rpm, 37 ± 0.5 °C with 900 mL 6.8 pH phosphate buffer, through aliquot withdrawal at 30 mins to quantify % drug release. All analytical instruments were calibrated, and method validation parameters were within acceptable limits before sample analysis (linearity, accuracy, precision, LOD/LOQ) (Górniak *et al.,* 2019).

4.2.4.9. Exploration of Pharmacokinetic parameters

Male Wistar rats were animals regularly supplied by the Nutritional National Institute (NIN) in Hyderabad, India, 4-5 weeks of age and weigh of an average 200 ± 20 g. The IAEC (Protocol No. 1447/PO/Re/S/11/CPCSEA-102/A) approved the study, which adhered to CPCSEA guidelines. After a week of getting used to the outside light and dark cycle, the temperature (20 ± 2°C), and the controlled humidity (40–60%), the animals

were split into two groups of six by chance. Either NS (ATR of 08 mg/kg and FNF of 20mg/kg BW) or 0.5% w/v sodium carboxymethylcellulose pure drugs suspension was given to the animals (Willett, 1981)

At set times, every 0.25 to 12 hours, 200 µL blood was retracted from the eye (orbital venous plexus), placed into EDTA-coated container tubes and spun down (10 mins.) at 7500 rpm. We analyzed the plasma using HPLC (Yousaf *et al.,* 2015) (Hashem *et al.,* 2015).

Pharmacokinetic data were analyzed utilizing Kinetica software employing a non-compartmental approach for the data generated considering concentration analyzed at different time points. Statistical interpretation was accomplished utilizing GraphPad-Prism (version 8.05, GraphPad Software Inc., CA), with pharmacokinetic variables expressed as Mean ± SD.

4.2.5 Formulation of solid-dispersion

The FDCs' solid-polymer dispersion was compounded using the solvent-evaporation process. Using different drug-to-polymer ratios the various BSD prepared using, Soluplus and Kolliphor. The TSD of a binary formulation that has been refined with the inclusion of polymers, namely PVP and Kollidon. Solid dispersions in binary and ternary configurations can be found in Table 5. 10. The right amount of methanol (20 mL) was used to dissolve 120 mg of ATR and 840 mg of FNF, both of which were precisely measured. In a separate 20 mL CH_3OH, the chosen carrier/polymer was dispersed while being constantly stirred. For a more consistent mixture, these two solutions were sonicated for 10 mins. An apparatus for rotational evaporation was used to evaporate the solvent at a temperature of 45 °C. We dried the end result at 40 °C for 24 hours. We dried the result after pulverization and then ran it through a No. 80 mesh screen. For future use, the powder was sealed in a bottle with desiccants.

A ternary solid dispersion was created by combining 30 mL of the obtained binary solid dispersion with 20 mL of the preferred carrier solubilized in CH_3OH. Sonication was used to combine the two solutions. The next procedures for preparation were identical to those for making a binary solid dispersion. After combining the enhanced TSD with

microcrystalline cellulose, sodium starch glycolate, and a tablet-forming punching machine, a dispersible tablet was produced (Akram *et al.,* 2022).

4.2.6 Evaluation of BSD and TSD

4.2.6.1. Solubility studies

Solubility was assessed by blending a plain API and weighed quantity prepared BSD and TSD formulations containing 2 mg of ATR and 10 mg of FNF to buffer of pH 7.4. The specimen was stirred followed by vertexing on a shaker for 48 h at 37ºC. After centrifugation and suitable dilutions, the drug dissolved was determined using UV Visible spectrophotometer at a lambda max of 246 nm (ATR) and 286 nm (FNF) (Hirave *et al.,* 2013).

4.2.6.2. Practical yield and drug content

The yield of the formulation was determined by taking the difference between dried BSDS and TSD (W1) and actual API mass and polymers (W2). The percentage experimental yield is computed using below mentioned formula:

$$\% \text{ Yield} = W1W2x\ 100$$

For the determination of drug contents an equivalent amount of BSD and TSD formulations containing 2 mg of ATR and 10 mg of FNF was mixed with 10 mL of organic solvent like methanol and subjected to 10 mins sonication to ensure the complete solubility of drug. After suitable dilutions the samples were filtered and analyzed by using UV Visible spectrophotometer at a lambda max of 246 nm (ATR) and 286 nm (FNF) (Basha *et al.,* 2020).

4.2.6.3. Drug release

For determining drug release from BSDF, TSDF, TSDF-T and plain drug USP dissolution (Type 2) was employed. Pure drugs and SDs containing an equivalent quantity of drugs (20 mg of ATR and 145 mg of FNF) were weighted accurately and added into the dissolution vessels containing 900 mL 7.4 pH, 0.5 % $CH_3(CH_2)_{11}OSO_3Na$ (SLS). The dissolution was carried out at 37±0.5ºC at an rpm of 50. At pre-determined

intervals, aliquots were removed and filtered, and analyzed and quantified, plotted the percentage of drug release (Akram *et al.,* 2022).

4.2.6.4. SEM

The sample of plain drugs, BSD and TSD were checked and images were captured by FESEM (field emission scanning electron microscopy) with 10 KV accelerating voltage by coating the samples with a layer of platinum for 40 sec at 20mA.

4.2.6.5. Compatibility studies

FT-IR analysis of the selected drugs (ATR, FNF), stabilizers and optimized BSD and TSD were performed by Bruker FT-IR. Approximately 5 mg of the sample were placed on the sample holder crystal and scanned the samples (4000 cm^{-1} to 400 cm^{-1}).

4.2.6.6. DSC Study (Differential Scanning Calorimeter)

Using Perkin Elmer DSC apparatus, the compatibility study for the samples, such as selected drugs (ATR, FNF), stabilizers, and optimized BSD and TSD, was achieved under heat, at a frequency 5ºC/min exceeding a 200ºC.

4.2.6.7. XRD (X-ray diffraction)

XRD was executed with diffractometer (Philips PW-1710) with the graphite monochromator and with Ni-filtered Cu K± illumination. The tests were done on pure drugs, a physical mixture (PM), and optimized BSD and TSD. They were scanned at 2θ between 80 and 2º, with step increment of 0.045° and a time between steps 0.5 seconds (Górniak *et al.,* 2023).

4.2.6.8. HPLC method

The concentrations of FNF and ATR were ascertained utilizing a Water HPLC System equipped with a UV-DAD detector with slight modification as reported by Jain et al, 2008. The mobile phase was of ACN and H_2O in the ratio of 70 and 30 v/v. C18 column RP-18, 5 microns, 125 x 3 mm was used in investigation with elution rate of 1.0 mL/min. FNF and ATR spotted at ƛ 286 nm and 245 nm. The retention time of FNF and ATR was 3.4 and 2.3 mins. The standard calibration curve covering 0.3 to 250 µg/mL and 0.2 to

200 µg/mL with correlation values over 0.999 was plotted graphically (Jain N *et al.,* 2008).

For detection of drugs in the plasma specimen the protein precipitation method was utilized. The drugs were separated from serum (50 µL) by mixing 300 µL of ACN by mixing the contents 10 mins, centrifuged 12 mins at 8000 rpm before analysis by HPLC.

The developed analytical methods for simultaneous estimation of ATR and FNF were validated according to International Council for Harmonisation (ICH) guideline Q2(R1) for analytical method validation.

Specificity was assessed by evaluating interference from excipients, blank plasma, and degradation products at the retention times of ATR and FNF. Linearity was established over the selected concentration ranges with correlation coefficients (R^2) greater than 0.99. Accuracy was evaluated through recovery studies at different concentration levels, while intra-day and inter-day precision studies were performed to determine method reproducibility.

Robustness of the analytical method was determined by introducing deliberate variations in chromatographic conditions such as mobile phase composition, flow rate, and detection wavelength. System suitability parameters including theoretical plate count, tailing factor, and resolution were evaluated prior to sample analysis to ensure chromatographic reliability and reproducibility.

4.2.6.9 Stability studies

Stability testing of the optimized ATR–FNF nanosuspension was performed following ICH Q1A-E guidelines. Optimized formulation aliquot into amber glass container with airtight caps and stored at three specified conditions: refrigerated (2 to 8 °C), room temperature (23 to 27 °C /55 to 65% RH), and accelerated (38 to 42 °C/ 70 to 80 % RH). Aliquots were withdrawn at predefined intervals (initial, 30 days, 90 days, and 180 days) and analyzed in triplicate (n = 3) for particle dimension (DLS), size distribution index (PDI), and zeta potential (Surface charge) using a calibrated Zetasizer. Appearance was assessed visually for clarity, turbidity, and aggregation. Drug content (assay) and impurity profiling were performed by validated HPLC methods using gradient elution

and UV detection; assay values are reported as percent of label claim (mean ± SD). Dissolution testing of dried nanosuspension-loaded tablets (or dispersible aliquots reconstituted per method) was performed with USP II paddle bowl at 50 rpm, 37 ± 0.5 °C with 900 mL 6.8 pH phosphate buffer, through aliquot withdrawal at 30 mins to quantify % drug release. All analytical instruments were calibrated, and method validation parameters were within acceptable limits before sample analysis (linearity, accuracy, precision, LOD/LOQ) (Górniak *et al.,* 2019).

4.2.6.10. Exploration of pharmacokinetic parameters

Male wistar rats were animals regularly supplied by the Nutritional National Institute (NIN) in Hyderabad, India, 4-5 weeks of age and weigh of an average 200 ± 20 g. The IAEC (Protocol No. 1447/PO/Re/S/11/CPCSEA-102/A) approved the study, which adhered to CPCSEA guidelines. After a week of getting used to the outside light and dark cycle, the temperature (20 ± 2°C), and the controlled humidity (40–60%), the animals were split into two groups of six by chance. Either NS (ATR of 08 mg/kg and FNF of 20mg/kg BW) or 0.5% w/v sodium carboxymethylcellulose pure drugs suspension was given to the animals (Willett, 1981). At set times, every 0.25 to 12 hours, 200 µL blood was retracted from the eye (orbital venous plexus), placed into EDTA-coated container tubes and spun down (10 mins.) at 7500 rpm. We analyzed the plasma using HPLC (Yousaf *et al.,* 2015) (Hashem *et al.,* 2015).

Pharmacokinetic data were analyzed utilizing Kinetica software employing a non-compartmental approach for the data generated considering concentration analyzed at different time points. Statistical interpretation was accomplished utilizing GraphPad-Prism (version 8.05, GraphPad Software Inc., CA), with pharmacokinetic variables expressed as Mean ± SD.

4.2.7 Dispersible tablets

4.2.7.1. Formulation

Dispersible tablets containing solid dispersions of ATR (20 mg) and FNF (145 mg) were formulated by direct compression. The objective was to develop tablets that disintegrate

rapidly in a small volume of water, thereby facilitating the solubilization rate and *in vivo* availability of the hydrophobic molecules.

The solid dispersion powders obtained were used as the core drug components (**Table 4. 5**). Microcrystalline cellulose (MCC PH 102) was incorporated as a diluent and binder due to its excellent compressibility and flow properties. Polyethylene glycol 6000 (PEG 6000), used during solid dispersion preparation, also acted as a plasticizer and solubilizing agent in the final formulation. To facilitate rapid disintegration, various super-disintegrants crospovidone, croscarmellose sodium (CCS), and sodium starch glycolate (SSG) were employed and evaluated either alone or in combination at varying concentrations (10–30 mg/tablet) across different formulations (F1–F5) to examine their implication on disintegration and drug release kinetic. Magnesium stearate and talc were used as a lubricant and glidant, respectively, to ensure proper flow and ease of tablet ejection from the die cavity during compression. The blended powders were mixed using the geometric dilution method to ensure uniform distribution of all components. The final powder blends were subjected to pre-compression evaluation and then compressed into tablets using a rotary tablet compression machine fitted with 9 mm flat-faced punches.

Table 4. 5: Composition of dispersible tablets

Ingredient	**F1**	**F2**	**F3**	**F4**	**F5**
	mg				
Atorvastatin 20mg	407 mg TSD dried material				
Fenofibrate 145mg					
PEG 6000	28	28	28	28	28
MCC (Avicel PH 102)	50	50	50	50	50
Crospovidone	10	15	20	25	30
Mg Stearate	2	2	2	2	2

Talc	3	3	3	3	3
Total Weight	500	505	510	515	520

4.2.7.2. Evaluation of dispersible tablet

Pre-compression Parameters

For a tableting operation to be successful, the flow characteristics of powders are essential. In order to ensure effective mixing and tolerable weight consistency of the compressed tablets, an optimistic flow is required. When a medicine is "poorly flowing" during the pre-formulation stage, the issue can be fixed by choosing the right excipients. To optimize their flow characteristics, medication powders may occasionally need to be pre-compressed or granulated. Evaluation of the drug material and its flow characteristics should be studied during pre-formulation, especially when a substantial drug dose is anticipated (Kukulka *et al.,* 2016).

Angle of repose

A sheet of paper was laid on a flat surface, and a funnel was held vertically in a stand at a certain height above it. 10 gm of sample material was placed inside the funnel, which has a closed bottom. The powder was then released from the funnel, creating a smooth, conical mound on the paper. Different directions of measurement were taken in order to determine the heap's radius. Using the scale, the heap's height was determined. The following formula is used to compute the angle of repose values, and standard values are shown in Table 2 of the appendix.

$\text{Tan}\theta = h/r \ \theta = \tan^{-1} h/r$

Where h=heap height & r-heap radius

Bulk density

Filling a measuring cylinder with powder determined the bulk density in gm/mL. The cylinder was cautiously leveled without compacting powder. The unsettled apparent volume was measured in graded units (Pan *et al.,* 2015).

Bulk density (ρbulk) = m/Vo

Where, m=mass of the powder, Vo=unsettled apparent bulk volume,

Tapped density

Machine-tapping is accomplished with cylinder and letting it to fall (by one of two methods) at a predetermined distance after noting the initial volume. To reduce any potential mass separation during tapping down, a device that rotates the cylinder may be preferred (14±2 mm at a standard rate 300 drops/min for cylinders).

Tapped density (ρtap) = m/Vf

Where m=mass, Vf=final tapped volume

Post-compression parameters

Weight variation

Twenty tablets were picked randomly and each one is weighed a calibrated digital balance. Mean tablet mass was calculated and compared with individual tablet. Percent deviation for each tablet was determined to assess compliance with pharmacopeia specifications (as per IP/BP/USP standards). Tablets weighing over 250 mg, the permissible limit is ±5%.

Hardness

Tablet hardness was accessed using a Monsanto hardness tester. Each tablet was placed between the spindle and the anvil of the tester, and force was applied until broke. The pressure necessitate to fragment the tablet was recorded in kg/cm². The mean of six determinations was calculated to ensure mechanical integrity and resistance during handling and transportation.

Thickness

A vernier caliper was employed to record tablet thickness. Three tablets were selected at random, and their thickness was recorded independently. The mean and standard deviation were calculated. Uniform thickness is important for uniform packaging and proper fitting in blister packaging.

Friability

The friability of the tablets was evaluated using a Roche friabilator. A sample of 10 pre-weighed tablets was positioned in the friabilator and spinned 4 mins at 25 rpm, equivalent to 100 rotations. The tablets were then removed, dusted, and reweighed (less than 1 acceptable). The friability value was computed using the formula:

Disintegration time

Disintegration time was determined using the USP disintegration test apparatus. Six tablets were placed in individual tubes of the disintegration basket rack and operated in distilled water sustained at 37±0.5°C. Complete disintegration time for each tablet without leaving any palpable residue was assessed and recorded. The average time for six tablets was calculated.

Wetting time

Wetting time was measured to assess the hydrophilicity of the tablet surface. A tissue paper doubly folded was cited in a Petri dish (diameter 10 cm) with 6 mL of d/w. The tablet was set gently on the tissue, and the elapsed time needed for water to wholly wet the superficial portion of the tablet was recorded using a stopwatch. The mean wetting time of three tablets was calculated.

Water absorption ratio

The water absorption ratio was calculated to verify the extent of H_2O uptake by the tablet. A pre-weighed tablet (W1) was laid on the wetted tissue paper in a Petri dish, as described above. After the whole hydration of the tablet, it was withdrawn and re-measured weight (W2). Water absorption ratio was derived with formula:

$$R\% = [(W2 – W1) / W1] \times 100$$

This parameter indicates the tablet's ability to absorb water and initiate disintegration.

Drug content uniformity

Arbitrarily Ten tablets were selected, crushed singularly, and accurately weighed to obtain a quantity equivalent to one tablet. Each sample was dispersed in a suitable solubilizing medium (e.g., methanol or phosphate buffer), filtered, and analyzed for drug

content using UV-visible spectrophotometry at the drug's λ max. Drug content was quantified from a standard calibration curve, and the mean percent composition was determined. The test ensures uniformity of drug distribution in the formulation.

***In vitro* dissolution studies**

Dissolution studies were carried out using a Type II USP dissolution bowl. The test was conducted at 37±0.5°C in 6.8 pH 900 mL of phosphate buffer with the rotating paddle at 50 rpm. At predetermined time intervals (e.g., 5, 10, 15, 30, 45, and 60 mins), 5 mL aliquots were retrieved and instantly replenished with an equivalent quantity of dissolution medium. Aliquots were quantified using spectrophotometrically. Percent of drug released was recorded and graphed against time to generate the dissolution profile.

Stability studies

Stability testing of the dispersible tablet formulations was performed following ICH Q1A-E guidelines. Optimized formulation aliquot into amber glass container with airtight caps and stored at three specified conditions: refrigerated (2 to 8 °C), room temperature (23 to 27 °C /55 to 65% RH), and accelerated (38 to 42 °C/ 70 to 80 % RH). Aliquots were withdrawn at predefined intervals (initial, 30 days, 90 days, and 180 days) and analyzed in triplicate (n = 3) for particle dimensions (DLS), PdI, and zeta potential using a calibrated Zetasizer. Appearance was assessed visually for clarity, turbidity, and aggregation. Drug content (assay) and impurity profiling were performed by validated HPLC methods using gradient elution and UV detection; assay values are reported as percent of label claim (mean ± SD). Dissolution testing of dried nanosuspension-loaded tablets (or dispersible aliquots reconstituted per method) was performed with USP II paddle bowl at 50 rpm, 37 ± 0.5 °C with 900 mL 6.8 pH phosphate buffer, through aliquot withdrawal at 30 minsto quantify % drug release.

Impurity profiling was carried out using HPLC, comparing retention times and peak areas with known standards. Triplicate measurements were performed and outcomes are expressed as mean ± SD (Górniak *et al.,* 2019).

4.3 Statistical Analysis

All experiments were carried out in triplicate, and the results were expressed as mean ± standard deviation (SD). Statistical analysis of the obtained data was performed using GraphPad Prism® software. Comparison between multiple formulations was carried out using one-way analysis of variance (ANOVA), followed by Tukey's post hoc test to determine statistical significance among groups. For comparison between two groups, Student's t-test was applied wherever appropriate. A probability value of $p < 0.05$ was considered statistically significant. Design Expert® software was utilized for optimization studies based on Quality by Design (QbD) principles. Response surface methodology and polynomial equations were employed to evaluate the influence of independent formulation variables on critical quality attributes such as particle size, PDI, and entrapment efficiency. Regression analysis, contour plots, and 3D response surface plots were generated to identify the optimized formulation conditions.

CHAPTER 5

RESULTS AND DISCUSSION

5. RESULTS AND DISCUSSION

5.1 Pre-formulation studies

Pre-formulation studies revealed the essential physicochemical characteristics of the drug candidates, including solubility behavior, melting point, spectral properties, and compatibility with excipients, which confirmed their suitability for the development of stable and effective pharmaceutical formulations.

5.1.1. Identification of drug by FTIR

The FTIR spectrum of ATR was performed and it is showing characteristic absorption bands corresponding to its key functional groups. An extensive absorption region 3200–3550 cm^{-1} is associated to O–H stretching vibrations from hydroxyl and carboxylic acid groups. Sharp peaks observed near 1700–1720 cm^{-1} indicate the presence of carbonyl (C=O) stretching, associated with both ester and acid functionalities. Aromatic C=C stretching vibrations appear near 1600 and 1500 cm^{-1}, while C–O stretching bands from ester and phenolic groups are evident in the range of 1100–1300 cm^{-1}. A weak to moderate band around 3300–3400 cm^{-1} corresponds to N–H stretching of amide or secondary amine groups. The presence of a fluoroaryl group is confirmed by C–F stretching vibrations near 1000–1100 cm^{-1}, and aliphatic and aromatic C–H stretching bands are observed between 2850 and 2950 cm^{-1}. These spectral features collectively confirm the structural identity and functional group composition of ATR (**Figure 5. 1**).

The FTIR spectrum of FNF reveals distinct absorption bands that correspond to its key functional groups (**Figure 5.2**). A strong and sharp peak around 1735–1750 cm^{-1} is indicative of the ester carbonyl (C=O) stretching vibration, which is a prominent feature due to the presence of an isopropyl ester moiety. Aromatic C=C stretching vibrations typically appear in the region of 1600–1500 cm^{-1}, confirming the presence of a substituted aromatic ring. The C–O stretching associated with the ester functional group is observed in the range of 1100–1300 cm^{-1}. Additionally, alkyl C–H stretching vibrations occur between 2850 and 2950 cm^{-1}, while aromatic C–H out-of-plane bending can be seen around 700–900 cm^{-1}. These functional group absorptions in the FTIR spectrum collectively verify the chemical structure of FNF. The combination FTIR

profile shows combination of the two drugs and is not showing any additional peaks indicating the physical compatibility between the two drugs (**Figure 5.3**). No significant shifting, disappearance, or broadening of the characteristic absorption bands was observed in the combination FTIR spectrum, indicating the absence of major chemical interactions between the drugs and confirming their compatibility and stability within the formulation system.

5.1.2 Identification of drugs by DSC

The API (ATR and FNF) was found to be a highly crystalline in nature and the drugs exhibited sharp melting endotherm 155ºC, with onset peak at a temperature of 157.66ºC and end set peak at a temperature of 167.69ºC in case of ATR while, FNF exhibited sharp melting endotherm at 83.65ºC with onset peak at a temperature of 81.2ºC and end set peak at a temperature of 87.64ºC. The combination DSC profile shows combination of is not showing any additional peaks indicating the compatibility between the two drugs (Ajmera *et al.,* 2012). The DSC endotherm shown in Figure 5.4, Figure 5.5, and Figure 5.6.

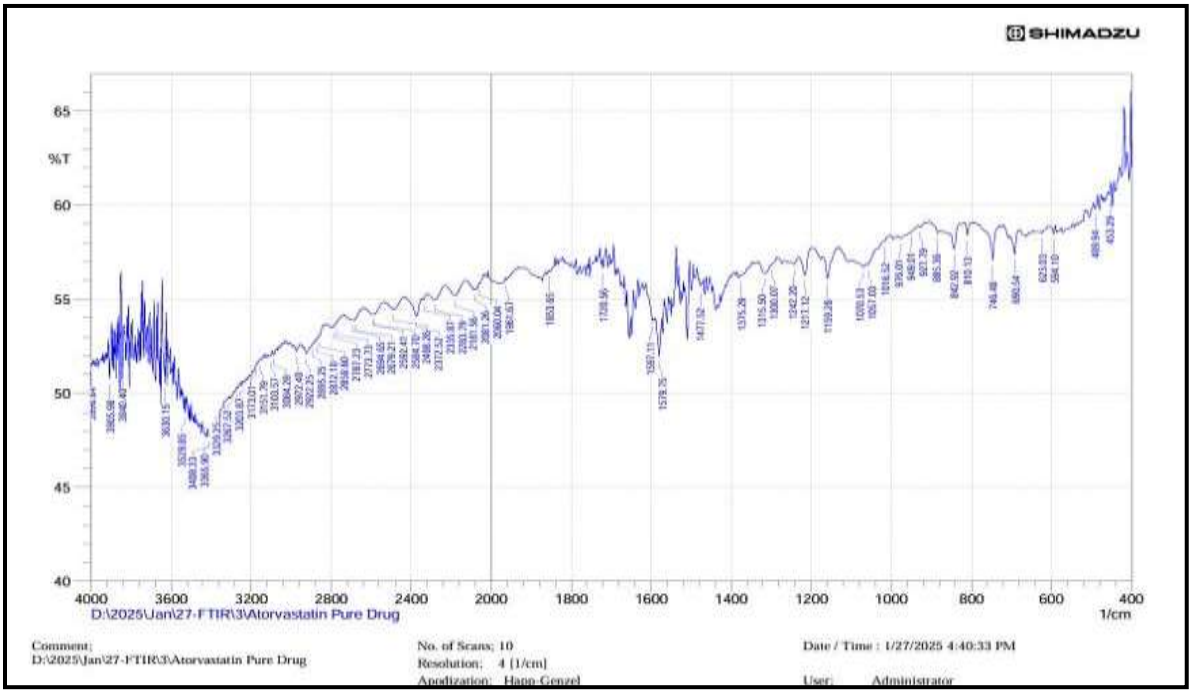

Figure 5. 1: FTIR Spectra of ATR

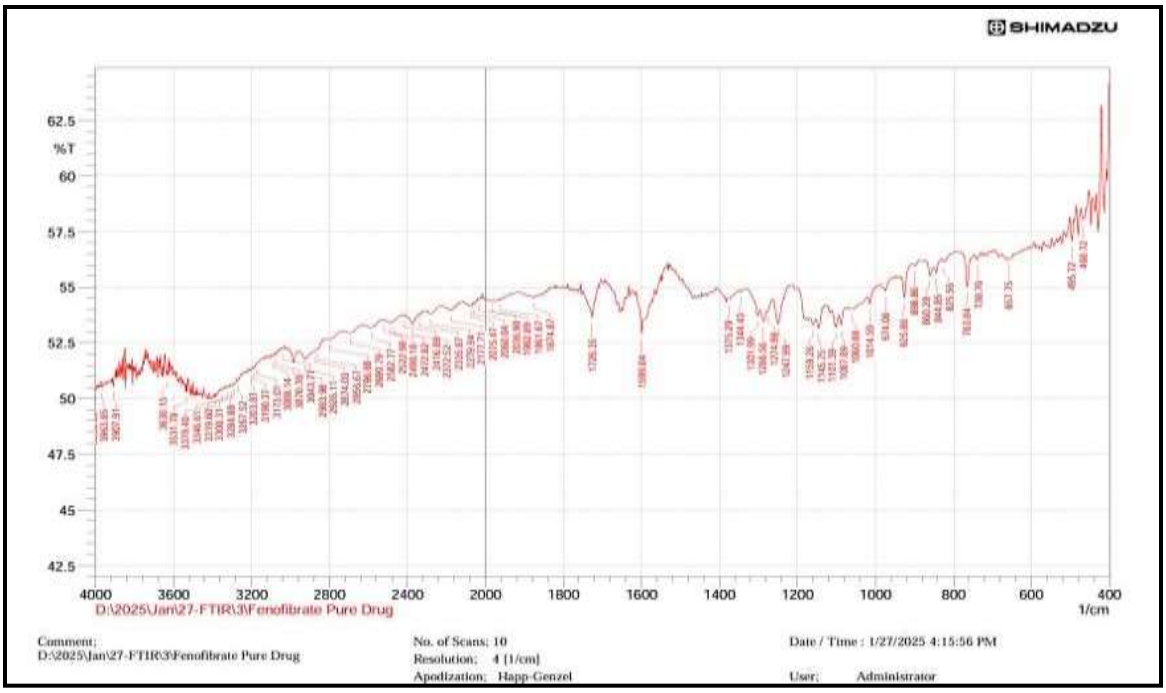

Figure 5. 2: FTIR Spectra of FNF

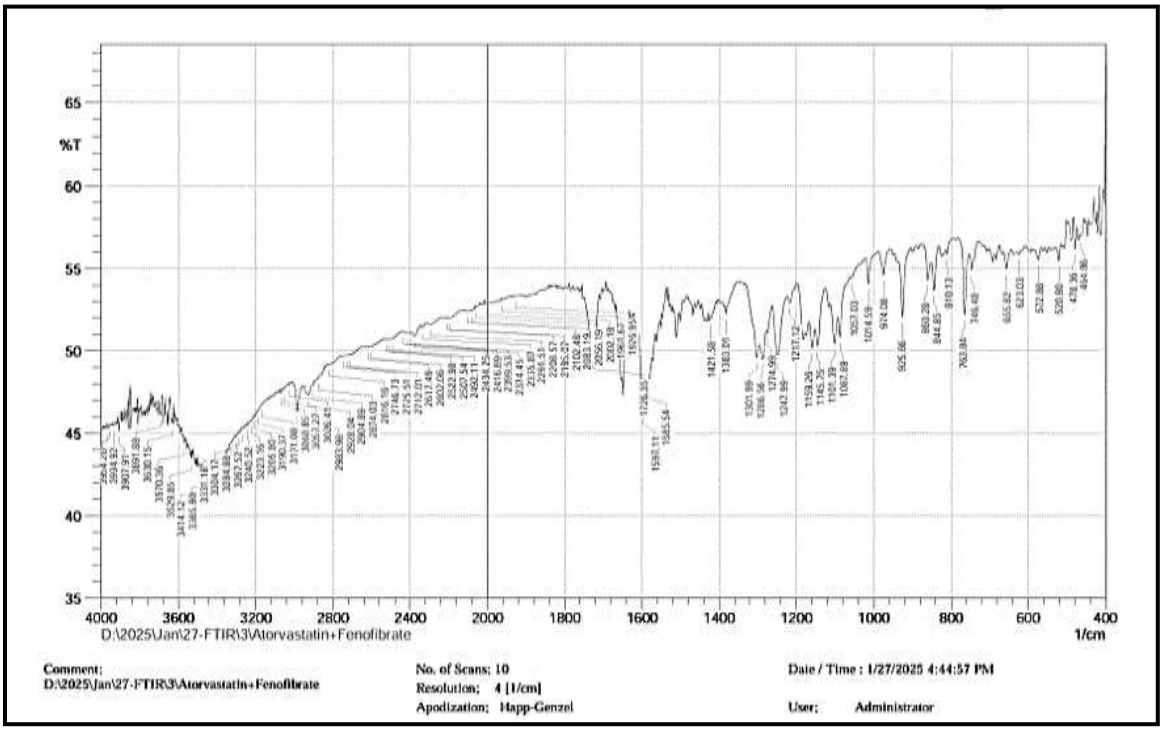

Figure 5. 3: FTIR of combination ATR and FNF plain drugs

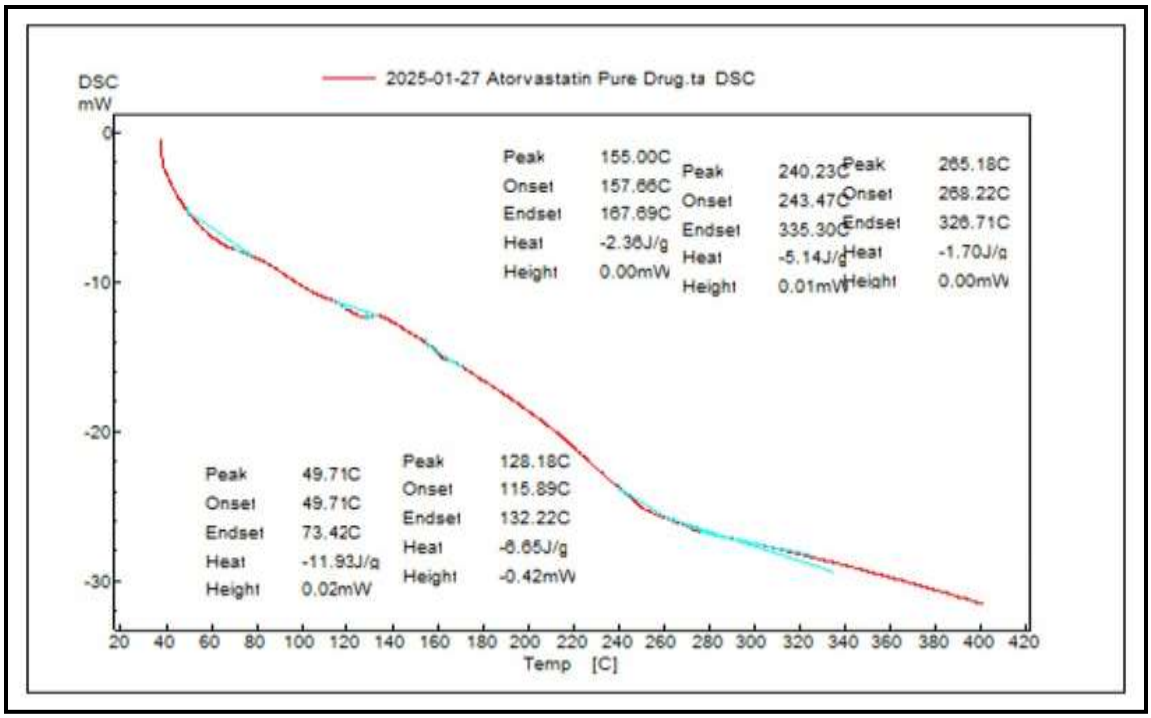

Figure 5. 4: DSC thermogram of ATR.

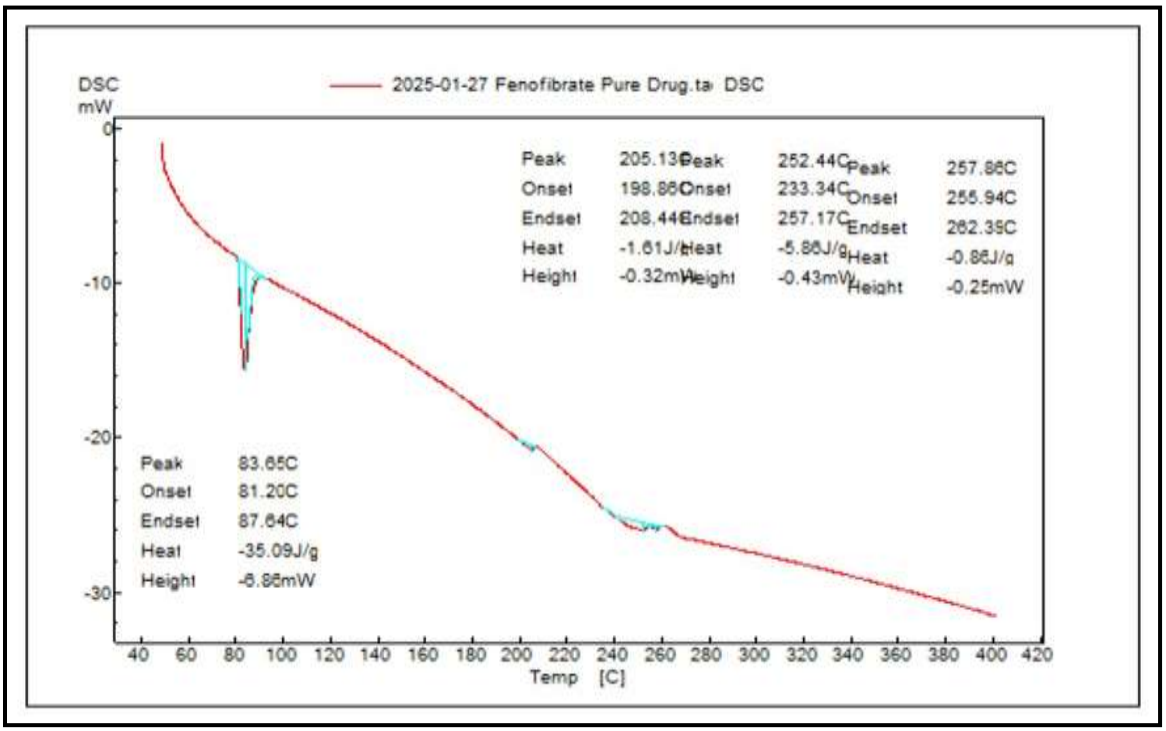

Figure 5. 5: DSC thermogram of FNF.

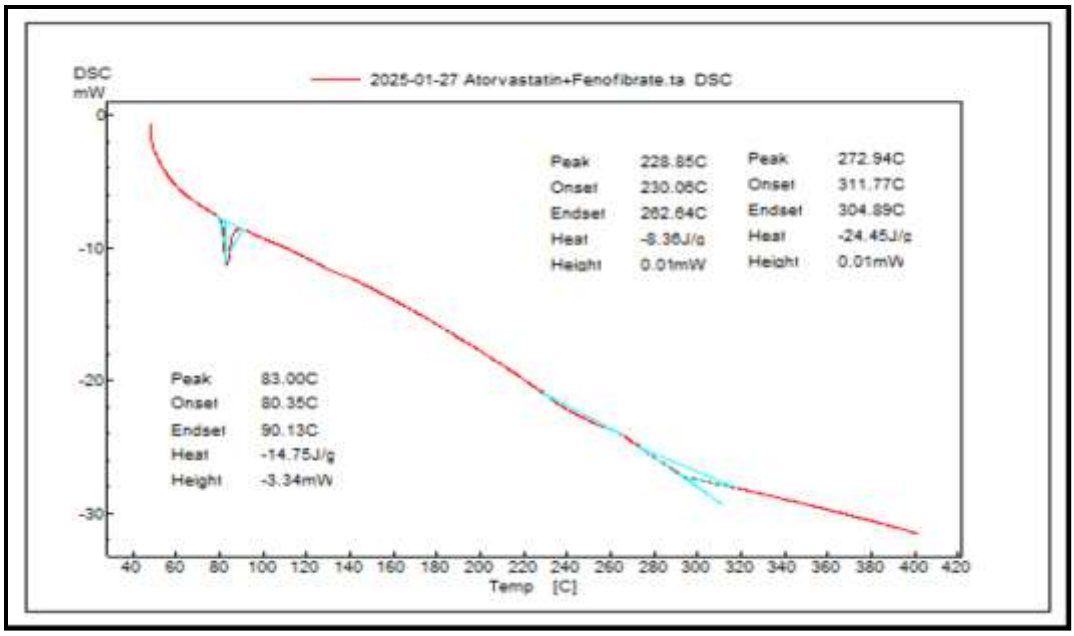

Figure 5. 6: DSC thermogram of combination ATR and FNF API

5.1.3 Physico-chemical characterization of ATR and FNF

The physico-chemical characterization of ATR and FNF demonstrated their characteristic physical and chemical properties, including solubility profile, melting behavior, and spectral characteristics, which confirmed the identity, purity, and suitability of the drugs for further formulation development.

5.1.3.1. Organoleptic properties

API (ATR and FNF) had been characterized and noted the properties mentioned in Table 5. 1.

Table 5. 1: ATR and FNF with respect to color, nature, odor and taste

Description	**Atorvastatin (ATR)**	**Fenofibrate (FNF)**
Color	White to off-white	White to off-white
Solid Nature	Crystalline powder	Crystalline powder
Odor	Characteristic	Odorless
Taste	Bitter	Tasteless or slightly bitter

5.1.3.2. Melting point

Melting point of the selected drugs (ATR and FNF) was determined by capillary method and found to be 160.21°C for ATR, and 80.84°C for FNF and the values were found to correlate with that of standard melting point value of drugs indicating its purity. The data of the MP of ATR and FNF is provided in the Table 5.2 and Table 5. 3. The slight variations observed may be attributed to minor experimental or instrumental variations during analysis. The close agreement between the observed and reference melting point values indicates the purity and authenticity of both drug samples and confirms their suitability for further formulation and characterization studies.

Table 5. 2: Melting point data of the ATR in comparison to the reference.

S. No	Reference MP	Observed MP	Average MP
	°C		
1	159–160	160.44	160.21
2		159.6	
3		160.6	

Table 5. 3: Melting point data of the FNF in comparison to the reference

S. No	Reference MP	Observed MP	Average MP
	°C		
1	80–81	80.44	80.84
2		81.8	
3		80.28	

5.1.3.3. Solubility study by equilibrium solubility method

Aqueous and lipophilic solubility of API are of crucial in determining it is capability to reach absorption sites and its interaction with therapeutic targets along with its eventual metabolism and elimination. Therefore, solubility profiling is often undertaken first during pre-formulation work. The solubility of ATR and FNF were measured in different solvents at room temperature and the results are as shown in Table 5. 4**.** The aqueous solubility of drug was found to be around less than 2.16 µg/mL and maximum solubility of drug (96.13 µg/mL) was observed in dimethyl formamide.

Table 5. 4: Solubility of ATR and FNF in various solvents

S. No	Solvent	Concentration ATR (µg/mL)	Concentration FNF (µg/mL)
1	0.1 N HCl	306 ± 26.19	9.33 ± 2.28
2	Ethanol	936.29 ±58.48	8268± 128.01
3	Methanol	911.04 ± 23.15	9036± 236.16
4	Benzene	09.16 ± 00.89	331± 49.15
5	DMSO	10,000 ± 37.04 (freely soluble)	>10,000 ± 272.15 (freely soluble)
6	DMF	10,000± 21.23 (freely soluble)	>10,000 ± 466.29 (freely soluble)
7	Acetone	131.7± 25.10	1944 ± 240.92
8	PB (pH 7.4)	36.13 ± 14.09	9.65 ± 1.28
9	Water	1.16 ± 0.76	0.0

Note: All experiments were performed in triplicate and values were expressed as mean±S.D., n=3

5.1.3.4. Hygroscopicity

Hygroscopicity denotes the capacity of a solid material to absorb moisture from its environment. The degree of moisture absorption is contingent upon the material's chemical and physical qualities. Comprehending hygroscopicity is essential for choosing suitable packaging to safeguard the final dosage form from moisture during transit and storage. This aids in preserving the product's stability, averting chemical or microbial degradation, and preventing physical alterations such as disintegration or discoloration, especially in tablets. The moisture absorption of ATR was found to be little hygroscopic and FNF drugs was found to be non-hygroscopic in nature.

5.1.3.5. Determination of partition coefficient by shake flask method

Partition coefficient (Log P) value is defined as ratio of unionized drug dispersed across aqueous and organic layers. Log P value indicates the drug's potential to permeate lipid membranes. An appropriate lipophilic/hydrophilic ratio plays a vital role in achieving efficient drug absorption and delivery. Lipid composition of biological membranes makes drug absorption highly dependent on lipophilicity. Greater lipophilicity observed in the unionized state plays a crucial role in pharmacokinetics and drug delivery. The partition coefficient values of ATR and FNF in different solvent systems are shown in Table 5. 5.

Table 5. 5: Partition coefficient of ATR and FNF in different solvents

Name of the solvent system	Log P	Log P
Octanol-water	4.6	5.3
Hexane-water	2.6	4.2
Oleyl Alcohol-water	3.0	5.6
Dichloromethane-water	3.7	4.8

5.2. Development of UV method for the estimation of ATR and FNF

This UV-Spectrophotometric simultaneous method is quite simple, accurate, precise, reproducible, and sensitive when two drugs are used in the same formulation. The UV –

Vis spectrophotometric calibration curves for analysis in phosphate buffer of pH 7.4 was developed. The operational two wavelengths were chosen to be 246 nm and 286 nm for ATR and FNF. The stock solutions of both the drugs were diluted with methanol to get a standard solution (1-10 µg/mL) of ATR-Ca and 2-20 µg/mL concentrations of FNF. Absorbance reading was taken at the predetermined λ and sample concentrations were obtained using the corresponding calibration equations.

$$Cx=A1\ ay2-A2ay1ax1ay2-ax2ay1\text{-----}1$$

$$Cy=A1\ ax2-A2ax1ax1ax2-ax2ax1\text{-----}2$$

Where, A1 & A2= absorbance of the mix at 246 nm and 286 nm

ax1 & ax2= absorptivity of ATR-Ca λ1 and λ2

ay1 & ay2=absorptivity of FNF at λ1 and λ2

Cx & Cy=concentrations of ATR calcium and FNF

The drug follows linearity in the concentration range of 2-16 and 2-20 µg/mL for ATR and FNF with a correlation coefficient value of 0.999 and 0.998 in pH 7.4 for both the drugs. The linear regression analysis along with the respective absorption values are given in the Table 5. 6. The concentration versus absorbance values and plots was shown in the Table 5. 7, Table 5. 8, Figure 5. 7, Figure 5. 8, Figure 5. 9, and Figure 5. 10.

Table 5. 6: Data of the Standard calibration curve with corresponding absorption values

Parameter ATR	**Parameter ATR**	**Parameter ATR**
Detection of wavelength	246 nm	286 nm
Beer's law limit (µg/mL)	1-16	1-20
Correlation coefficient (r)	0.9998	0.9999
Molar absorptivity (lit/mol/cm)	47237.94	18757.32
Sandell's sensitivity (µg/Sq.cm/0.001)	0.025604	0.019235

Slope	0.039056	0.0524
Intercept	- 0.001	+ 0.012
LOD	0.0376	0.4183
LOQ	0.1139	1.227

Table 5. 7: Standard calibration graph of ATR in PB pH 7.4

Concentration (µg/mL)	Absorbance
0	0
2	0.142
4	0.266
6	0.388
8	0.494
10	0.625
12	0.762
14	0.881
16	0.994

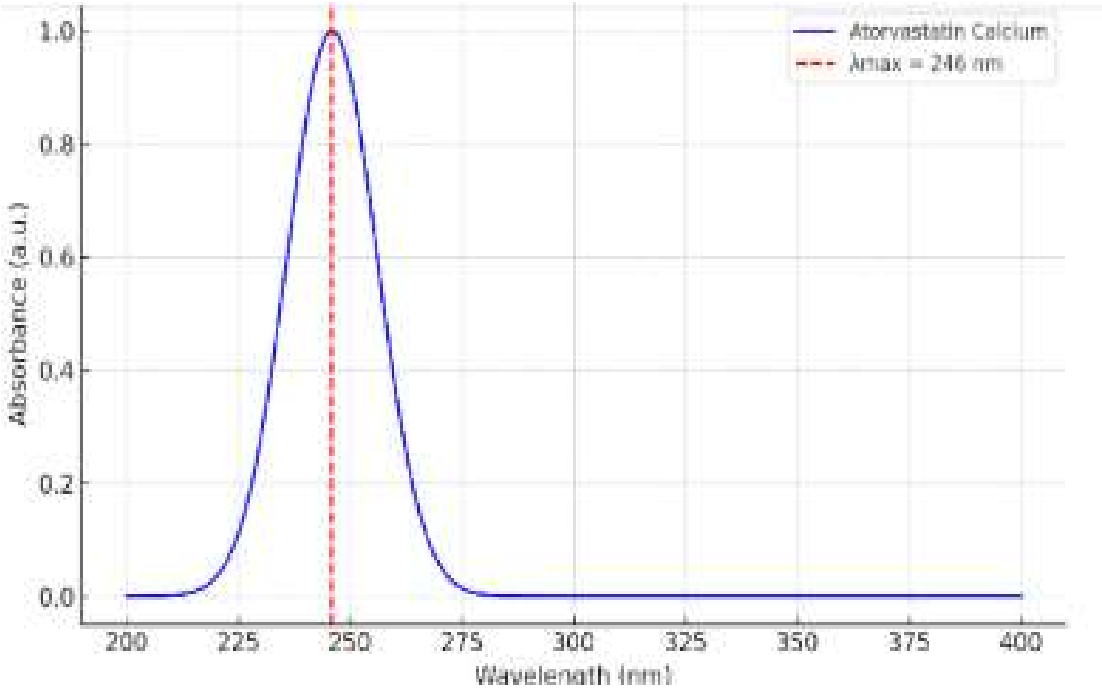

Figure 5. 7: Absorption spectra of ATR-Ca at 246 nm

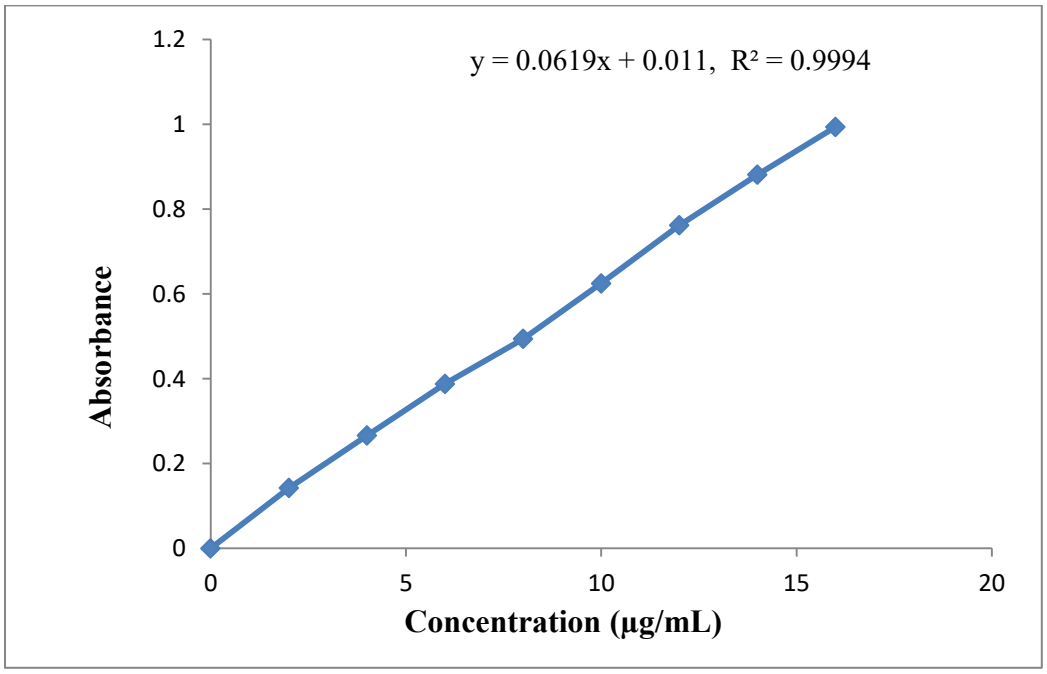

Figure 5. 8: Standard calibration graph of ATR in PB pH 7.4

Table 5. 8: Standard calibration graph of FNF in PB pH 7.4

Concentration (µg/mL)	Absorbance
0	0
2	0.128
4	0.23
6	0.339
8	0.431
10	0.534
12	0.639
14	0.732
16	0.825
18	0.912
20	0.998

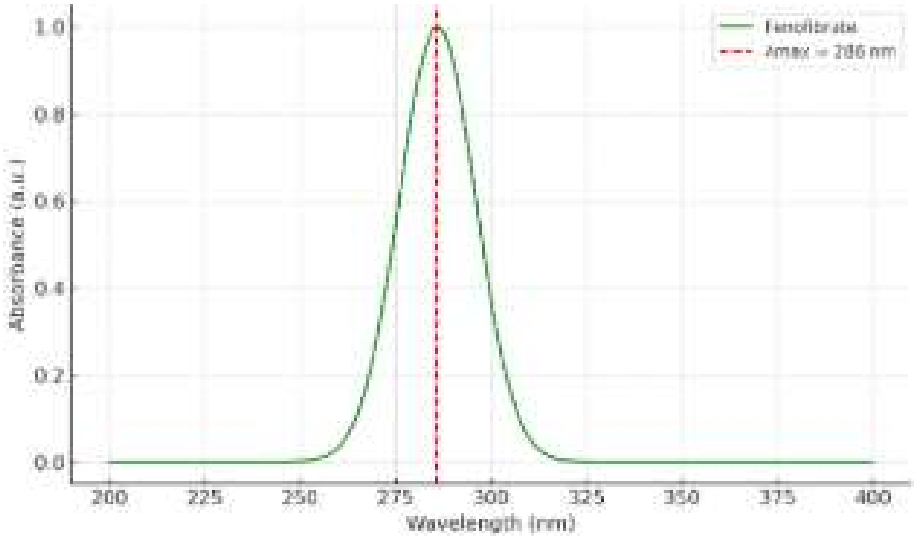

Figure 5. 9: Absorption spectra of FNF at 286 nm

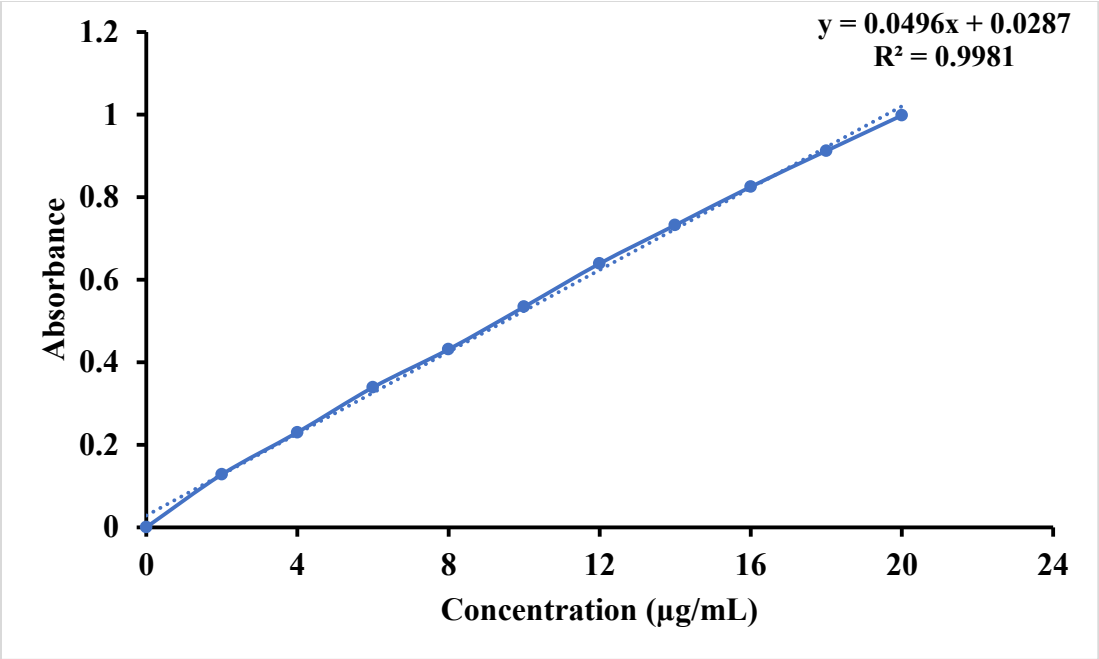

Figure 5. 10: Standard calibration graph of FNF in PB pH 7.4

5.3. Formulation of nanosuspension of FDC of ATR and FNF:

This study applied the sonoprecipitation homogenization technique for developing NSs. It can be briefly stated in the following way: Drugs were mixed in one organic phase (OP), whereas the selected stabilizer was dispersed in the aqueous phase (AP). Intense desolvation causes immediate precipitation of the drug, resulting in the formation of nanoparticulate drug particles. Based on the Ostwald-Miers theory, the system is said to be in a regime of supersaturation, whereby nucleation and crystallization occurs. This regime is reached once an AP is introduced to a solution saturated with drug. Afterward, progressive solvent evaporation leads to the formation of numerous nuclei conducive for further crystal growth (Figure 5. 11).

Damköhler number (Da = Tmix/Tppt), which defines the endpoints in time for precipitation, provides the theoretical basis for the technique. A mixing-controlled progression is triggered when Da is more than or equal to one, meaning that the mixing period (Tmix) is lengthier than the precipitation interval (Tppt). Larger units form due to increased growth over nucleation, caused by delayed supersaturation. When Da is less than 1, quick supersaturation tranopires, signifying that Tmix is inferior to Tppt, which

help in the formation of several tiny nuclei and finally to crystal formation. To obtain smaller particles, maintaining Da<1 is ideal. Stabilizers increase Tppt, while ultrasonic waves help reduce Tmix (Ferreira *et al.,* 2024).

Figure 5. 11: Prepared optimised formulation of nanosuspensions

DBF approach for formulating optimized NS

The NS of combination drugs was designed to enhance solubility and as well bioavailability. To reach Quality Target Product Profiles (QTPP), QbD emphasizes finding and tracking CQAs. Nanoscale particle size reduction increases solubility for medications with low water solubility. PS, PI, and ZP were used as CQAs in this work. Table 5.9 presents an outline of the chosen CQAs.

Table 5. 9: Logical basis for defining QTPP and related CQA

QTPP	Goal	Application
Preferred formulation	NS	The chosen combination drugs are classified as BCS II and hence NS can address the same

Drug delivery route	p.o	The formulation currently marketed is meant for p.o., and an attempt is being done to enhance the same.
Dissolution	Should be better than conventional marketed formulation	An increased solubility leads to better dissolution
Pharmacokinetics	Need to be much superior than pure drug	This is needed to reduce the dose of the drugs as these drugs are life time consuming drugs
Stability	Should not show any signs of aggregations	Maintaining size is an important criteria and particle size affects the efficacy of the formulation
CQA	**Goal**	**Rationale**
PS	In Nano-metric range	A small size will have high surface area and this will ultimately boost the surface area which in turn increases the drug release
PI	Below 0.4	A PI of less than 0.4 indicates a stable and uniform particle size
ZP	Value should be high than 25 ±mV	High ZP indicates a stable system and we want a stable NS

5.4. Pre-screening research

Optimizing the proportion of OP to the AP and stabilizer

The screening tests were conducted by using the OFAT approach to isolate to select the ideal stabilizer and to analyse the optimal-to-precipitant (OP to AP) ratio so that the design becomes simple and avoid unnecessary trials. Different formulation and process

parameters were evaluated to determine the optimal condition to meet the requirements of the nanoprecipitation process, including important variables: selection of the solvent system for drug dissolution, the ratio of solvent to antisolvent, the kind and concentration of stabilizer, speed of mixing (rpm), and temperature. The consequences of these variable's impact on particle size and PI were studied OFAT by keeping other parameters constant. The solubility maximum for the drug in organic vehicles such as methanol or ethanol would therefore provide an OP of equal 1:1 mixture of both solvents. Since distilled water is mixable with many vehicles and drugs being insoluble in water, water was used as AP. The ratio of OP to AP is necessary to prevent the aggregation of size, so we have changed the ratio of the same and its effect of PS and PI was observed and the same is shown in Figure 5. 12.

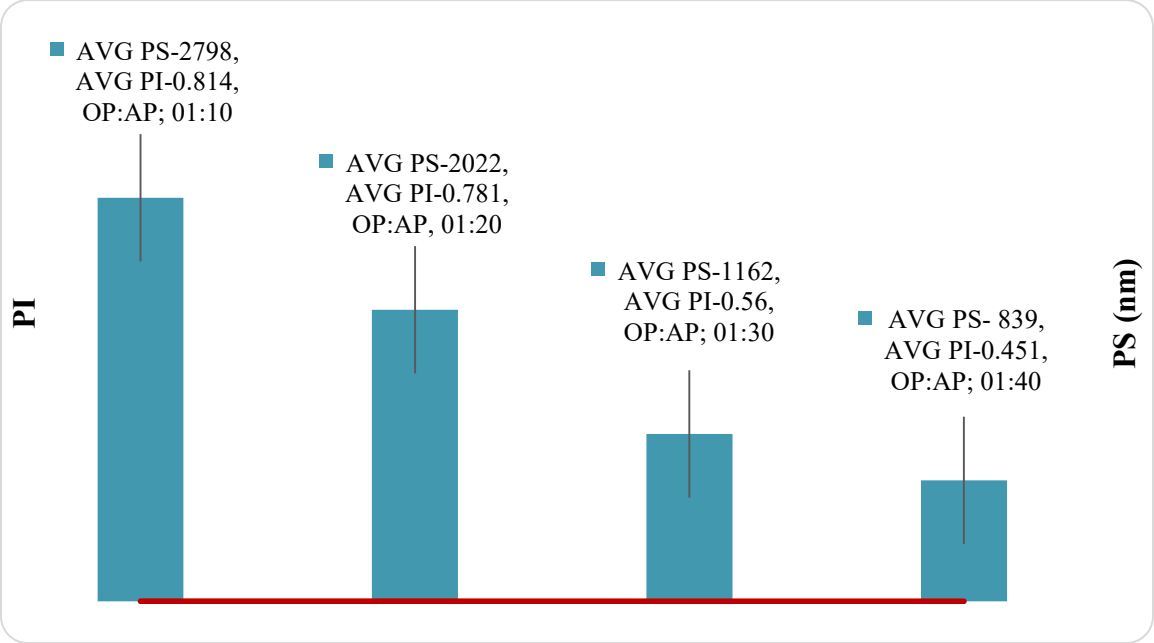

Figure 5. 12: Graphical depiction of influence of OP:AP proportion on PS and PI (n=3)

The OP to AP ratio was set at 1:30 to assess the stabilizer's influence on particle size (PS) and polydispersity index (PI) using 8 mg of ATR and 20 mg of FNF in first trials. Composed of very active but thermodynamically unstable nanoparticles, nanosuspensions need stabilizers to stop agglomeration and Ostwald ripening. The

optimum concentration of the stabilizer should be such that it reduces the tension between the two surfaces, prevents crystal growth, and imparts electrostatic or steric stability. With PS and PI readings, several stabilizers were tried to find the most successful one. The stabilizing efficiency was in the following sequence: PVP K-30 < Poloxamer 407 < Poloxamer 188 < SLS < PVA <Pluronics 338 < HPMC E 15 < TPGS. With low PS and PI, PVP K-30 and Poloxamer 188 created a uniform nanosuspension. While Poloxamer 407 and PVP K-30 avoided this problem, stability testing showed cake formation in HPMC, TPGS, Pluronics 338, and SLS-containing formulations. While PVA-stabilized formulations showed clear particle segregation, HPMC E15 produced a hard, non-dispersible cake. Zeta potentials for Poloxamer 407 formulations varied from -20.9 to -23.3 mV and stayed steady. Due to steric stabilization via a polymeric coating, PVP K-30 produced smaller particle sizes but had lower zeta potential (13.24 to 11.98 mV) (Sinha *et al.,* 2013).

A combination of stabilizers was used to improve electrostatic stability. Due to their hydrophilic nature, consistency, surface activity, and functional groups, poloxamers (also known as Pluronics) exhibited better stability. These are A–B–A type triblock copolymers consisting of a central hydrophobic polypropylene oxide block surrounded by hydrophilic polyethylene oxide chains (**Figure 5. 13**).

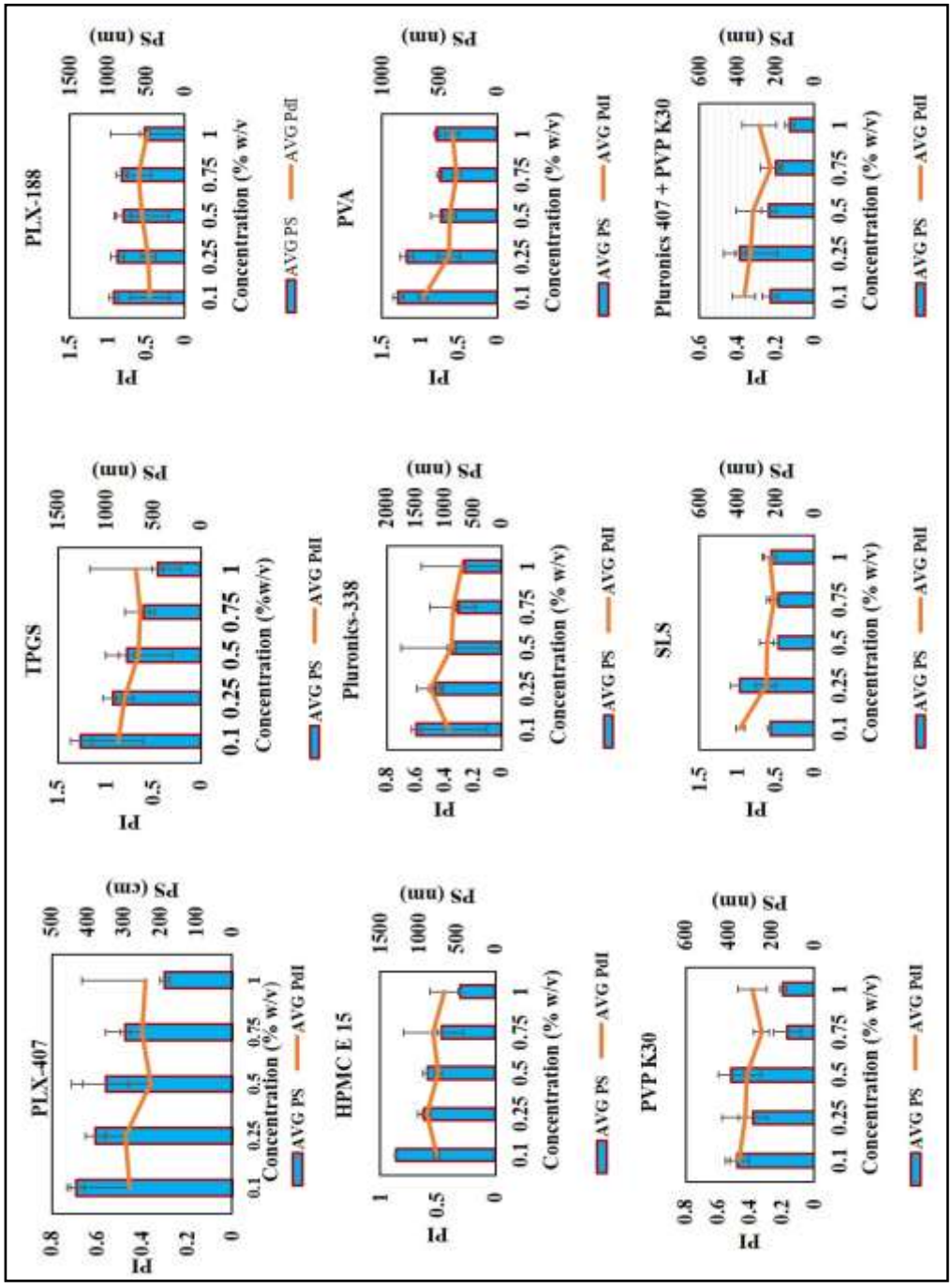

Figure 5. 13: Effect of stabilizer and its concentration of PS and PI (n=3)

5.5 Experimental design

There were three center points among fifteen leads in the investigation (see Table 5.10). The model selection technique employed R^2, projected R^2, adjusted R^2, and

coefficient of variation (C.V). ANOVA was also applied to assess how different factors affected the responses.

Table 5. 10: Runs planned for the trials

	Factor 1	**Factor 2**	**Factor 3**	**Response 1**	**Response 2**	**Response 3**
Run	A: Stabilizer to drug ratio	B: HS	C:HT	PS	PI	ZP
	% w/w	rpm	mins	nm		mV
1	0.5	12000	90	402.2	0.588	-36.45
2	1	9000	90	252.8	0.428	-36.45
3	1	9000	90	250.2	0.488	-33.45
4	1.5	6000	90	251.89	0.529	-49.88
5	1	9000	90	253.6	0.444	-33.35
6	1	12000	120	258.44	0.388	-29.78
7	1	6000	120	193.2	0.598	-30.69
8	1.5	9000	120	210	0.129	-48.06
9	0.5	6000	90	356.3	0.468	-16.43
10	1	12000	60	237.12	0.332	-37.92
11	1.5	9000	60	244.12	0.192	-39.44
12	1	9000	90	249.7	0.244	-38.35
13	**1.5**	**12000**	**90**	**199.64**	**0.132**	**-29.11**
14	1	9000	90	255.26	0.384	-36.65
15	1	6000	60	302.03	0.428	-37.89

	Factor 1	Factor 2	Factor 3	Response 1	Response 2	Response 3
Run	A: Stabilizer to drug ratio	B: HS	C:HT	PS	PI	ZP
	% w/w	rpm	mins	nm		mV
16	0.5	9000	120	354	0.426	-16.46
17	0.5	9000	60	397.88	0.296	-32.46

5.5.1. PS

The particle size and PI extended from 193.2 to 402.2 nm after 15 rigorous trials. The F value of the model is 1058.90, hints a mere 0.01 percent likelihood of being owed to noise. The projected model is 'quadratic' and proved notable with an inconsequential lack of fit. As per the ANOVA, p-values corresponding to the factors less than 0.05 are said to indicate an important factor on the response. R^2, corrected R^2, and predicted R^2 remained 0.9993, 0.9983, and 0.9930, respectively. The design meticulousness of the model was measured as 101.474, which indicated that it was certainly above the threshold value of 4.

It was also observed that the typical effects (A, C, AB, BC, and A2) had a major consequence on the results with p-values under 0.05. Therefore, these variables are now regarded as significant; the subsequent regression equation is:

Particle size=+252.31-75.59-0.7525B-20.69C -24.54AB+2.44AC +32.54BC+52.00A2 -1.80B2 -2.81C2

The given quadratic equation represents how the particle size (PS) is influenced by three factors: A (stabilizer-to-drug ratio), B (homogenization speed), and C (homogenization time), along with their interactions and squared terms. The positive constant 252.31 suggests the base particle size. A, B, and C have negative coefficients, indicating that increasing these parameters individually reduces particle size. However, interactions such

as AC (+2.44) and BC (+32.54) contribute positively, meaning their combined effect increases particle size, while AB (-24.54) reduces it. The squared terms A^2 (+52.00), B^2 (-1.80), and C^2 (-2.81) indicate that increasing the stabilizer-to-drug ratio significantly increases particle size, while higher homogenization speed and time have a minor decreasing effect. This equation helps in optimizing formulation parameters for achieving the desired particle size as stated by Alexandridis *et al.,* at an increased stabilizer ratio, multilayers will form, providing thicker particles that are larger in size when the minimum micellar temperature is taken as 25°C (Lin & Alexandridis, 2002).

Overall, increasing homogenization speed (B) and homogenization time (C) tends to decrease particle size (Table 5.11 and 5.12). This is evident from the negative coefficients of B (-0.7525) and C (-20.69) in the equation, indicating that as these factors increase individually, the particle size reduces. The ultrasonic waves may be breaking down the particles, causing lower T_{mix}, which gives Da<1. The 3D surface plot is shown in Figure 5.14.

Table 5. 11: Model summary statistics - ANOVA of the quadratic model for the response of particle size (Y1)

Source	Sum of squares	df	Mean square	F-value	p-value	
Model	67196.45	9	7466.27	1058.90	< 0.0001	significant
A-Stabilizer to drug ratio	45712.30	1	45712.30	6483.13	< 0.0001	
B-HS	4.53	1	4.53	0.6425	0.4492	
C-HT	3424.20	1	3424.20	485.64	< 0.0001	
AB	2408.36	1	2408.36	341.56	< 0.0001	
AC	23.81	1	23.81	3.38	0.1087	

BC	4234.76	1	4234.76	600.59	< 0.0001	
A^2	11384.83	1	11384.83	1614.65	< 0.0001	
B^2	13.70	1	13.70	1.94	0.2061	
C^2	33.27	1	33.27	4.72	0.0664	
Residual	49.36	7	7.05			
Lack of Fit	27.49	3	9.16	1.68	0.3082	not significant
Pure error	21.87	4	5.47			
Cor Total	67245.81	16				

Table 5. 12: Sequential model sum of squares

Source	**Sum of squares**	**df**	**Mean square**	**F-value**	**p-value**	
Mean vs Total	1.282E+06	1	1.282E+06			
Linear vs Mean	49141.02	3	16380.34	11.76	0.0005	
2FI vs Linear	6666.93	3	2222.31	1.94	0.1867	
Quadratic vs 2FI	**11388.51**	**3**	**3796.17**	**538.39**	**< 0.0001**	**Suggested**
Cubic vs Quadratic	27.49	3	9.16	1.68	0.3082	Aliased
Residual	21.87	4	5.47			
Total	1.349E+06	17	79366.61			

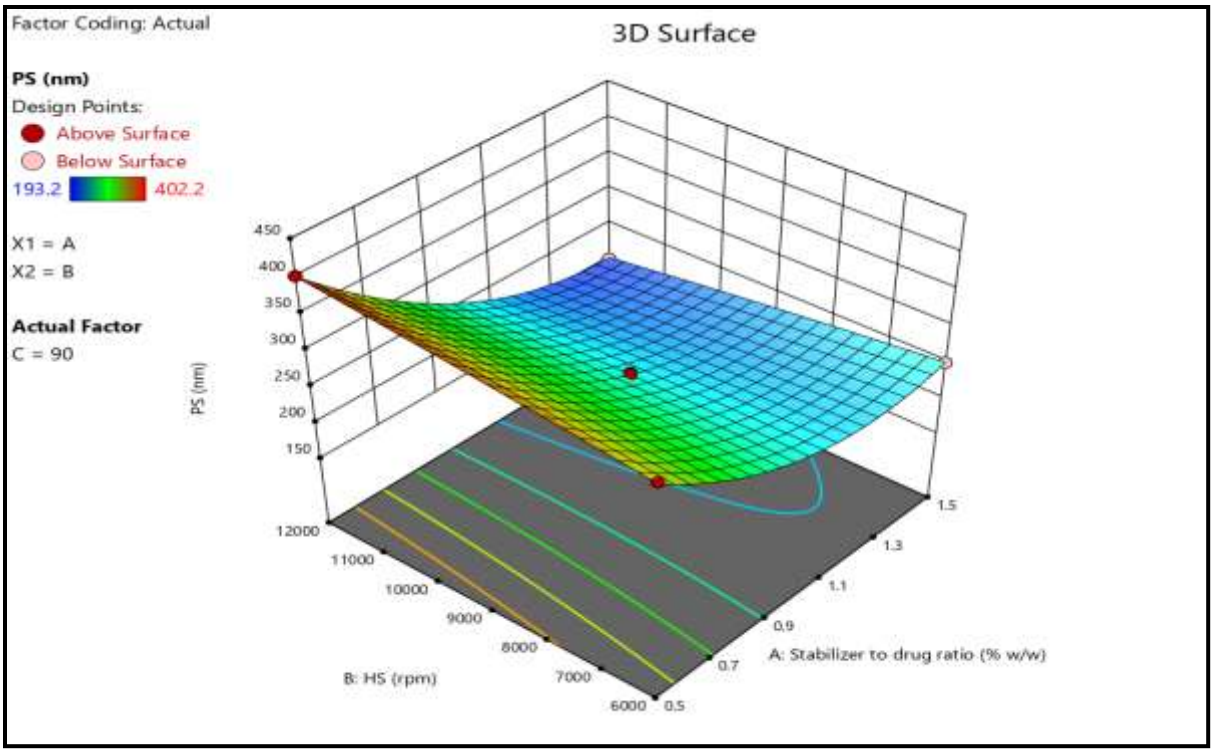

Figure 5. 14**: Graphical representation of 3D-contour plot showing the influence of (A) Stabilizer to drug ratio and (B) Homogenization Speed (HS; RPM) on mean particle size fixed level of C (homogenization time; HT).**

5.5.2. PI

The PI represents in a dimensionless way the range in the particle size distribution. It mostly lies in the range of 0 to 1 (Danaei *et al.,* 2018). Particles are hetero-dispersed systems if their values are greater than 0.5 and are considered widely distributed. PIs of the formulations under development ranged from 0.129 to 0.598%. The projected model is "quadratic" was substantial value of F value 5.94, 0.01% probably due to noise, while it exhibited inconsequential unsatisfactory fit.

Based on the F-value (0.123) for unsatisfactory fit, the statistical significance of the unsatisfactory fit has not been established by the pure error. 89.08% chance that this big F-value for unsatisfactory fit occurred due to noise. The R^2 (regression coefficient), adjusted R^2, and expected R^2 values stayed at 0.8843, 0.7355, and 0.6765. The sufficient

precision of the model was confirmed to be 8.0646, which is greater than the required value of 4, affirming its usefulness in the analysis of the layout.

The p-values for the variables in the model A, B, AB, and B^2 were found to be under 0.050, suggesting that they had a significant influence and hence considered essential, and the equation of regression is given as below:

PI=+0.3976-0.0995A-0.0729B+0.0366C -0.1293AB-0.0483AC -0.0285BC-0.0721A2 +0.1037B2 -0.0648 C2

The positive constant 0.3976 represents the baseline PI value. The negative coefficients of A (-0.0995) and B (-0.0729) indicate that increasing the stabilizer-to-drug ratio and homogenization speed reduces PI, leading to a more consistent particle size distribution. The small positive coefficient of C (+0.0366) suggests that increasing homogenization time slightly increases PI, potentially leading to broader size distribution. Interaction terms like AB (-0.1293), AC (-0.0483), and BC (-0.0285) all have negative values, indicating that combined increases in these factors reduce PI (Table 5.13 and 5.14).

The squared terms show that A^2 (-0.0721) further reduces PI, B^2 (+0.1037) increases it, and C^2 (-0.0648) reduces it. Overall, higher A and C help in achieving a more uniform particle size, while excessive homogenization speed (B) may increase PI, leading to slight variability in particle sizes (Hassani *et al.,* 2015). The 3D surface plot is shown in Figure 5.15.

Table 5. 13: Model summary statistics - ANOVA of the quadratic model for the response of PDI (Y2)

Source	Sum of squares	df	Mean square	F-value	p-value	
Model	0.2926	9	0.0325	5.94	0.0141	significant
A-Stabilizer to drug ratio	0.0792	1	0.0792	14.48	0.0067	
B-HS	0.0425	1	0.0425	7.77	0.0270	

Source	Sum of squares	df	Mean square	F-value	p-value	
C-HT	0.0107	1	0.0107	1.96	0.2041	
AB	0.0668	1	0.0668	12.21	0.0101	
AC	0.0093	1	0.0093	1.70	0.2333	
BC	0.0032	1	0.0032	0.5939	0.4661	
A^2	0.0219	1	0.0219	4.00	0.0858	
B^2	0.0453	1	0.0453	8.28	0.0238	
C^2	0.0177	1	0.0177	3.23	0.1153	
Residual	0.0383	7	0.0055			
Lack of Fit	0.0033	3	0.0011	0.1245	0.9408	not significant
Pure error	0.0350	4	0.0088			
Cor total	0.3309	16				

Table 5. 14: Sequential model sum of squares

Source	Sum of squares	df	Mean square	F-value	p-value	
Mean vs Total	2.48	1	2.48			
Linear vs Mean	0.1324	3	0.0441	2.89	0.0758	
2FI vs Linear	0.0794	3	0.0265	2.22	0.1485	
Quadratic vs 2FI	**0.0808**	**3**	**0.0269**	**4.93**	**0.0380**	**Suggested**
Cubic vs	0.0033	3	0.0011	0.1245	0.9408	Aliased

Source	Sum of squares	df	Mean square	F-value	p-value	
Quadratic						
Residual	0.0350	4	0.0088			
Total	2.81	17	0.1654			

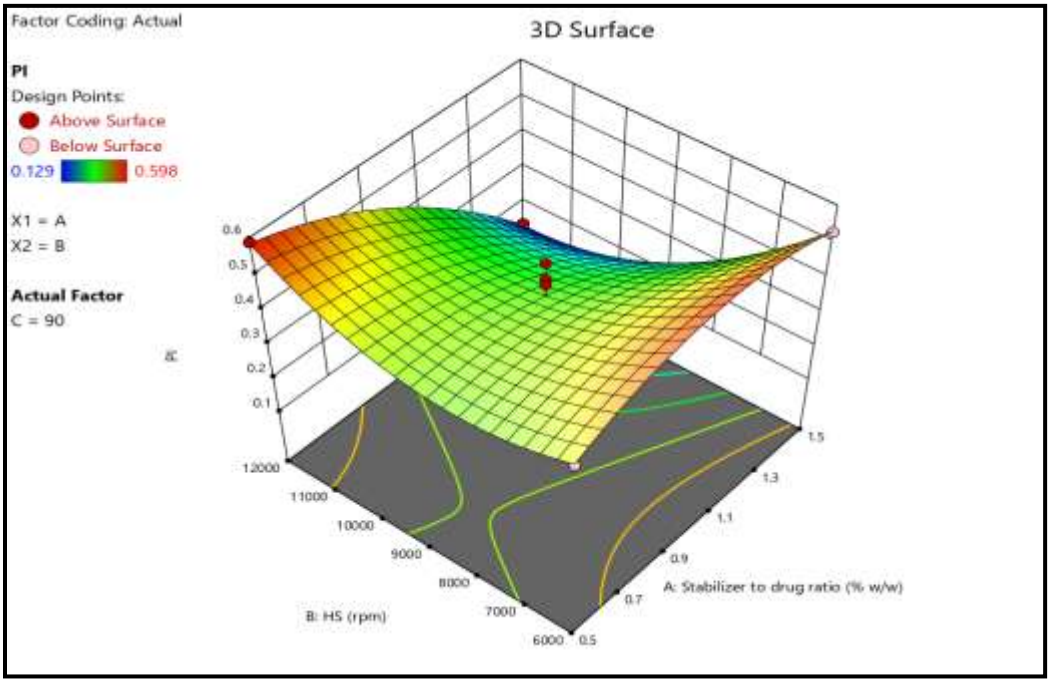

Figure 5. 14: Graphical representation of 3D surface plots showing the influence of (A) stabilizer to drug ratio and (B) homogenization speed (HS) on PdI fixed at level of C (homogenization time)

5.5.3. Zeta potential

ZP is regulated by surface charges, which plays an imperative role in the stability of colloidal solution and the primary interaction of particles with the cell membrane to make them an essential component of any successful drug delivery system. In this work, the ZP values were in the array of -49.88 to -16.43 mV. The linear model for the zeta potential has demonstrated its very significant statistical meaning through the high F-value of 30.58. The regression coefficients (R^2, adjusted R^2, and predicted R^2) remained

at 0. 9483, 0.9173, and 0.8278, respectively. The model used here has sufficient precision (S/N ratio) of 22.705. This is already exceeding four times the required amount and thus completely sufficient to be trusted in exploring the design space. "Lack of fit F-Value" (1.54) indicates that the differences in fit are not statistically significant. There is a 35.28% chance that such a "Lack of Fit F-value" will occur out of random noise, which shows that around over-sign features this model is reliable. The model is desired to be "zero" in nonsignificant lack of fit and should be fit. The model's variables (A, C, AB, and AC) indicate a significant influence on the consequence (Table 5.15 and 5.16). Thus, these terms are considered and the following formula for regression from above is:

Zeta Potential=-34.28-8.09A+0.2037B+2.84 C+10.20AB-6.16AC+0.235

The base ZP value is -34.28, indicating an initial negative charge. The coefficient of A (-8.09) suggests that increasing the stabilizer-to-drug ratio further decreases (makes more negative) the ZP. B (+0.2037) has a very small positive effect, meaning homogenization speed slightly increases ZP. C (+2.84) shows that increasing homogenization time make the ZP less negative. The interaction AB (+10.20) significantly increases ZP, meaning their combined effect reduces the overall negative charge. Conversely, AC (-6.16) decreases ZP, making it more negative. The small constant term (+0.235) has a negligible effect. Overall, increasing A makes ZP more negative, while increasing C and the AB interaction make it less negative, affecting the stability of the particles (Figure 5.16). Lower zeta potential values further point towards good stability of the colloids, emphasizing that these parameters play a pivotal role in stabilizing the nanosuspensions (Rangaraj *et al.,* 2019).

Table 5. 15: Model summary statistics - ANOVA of the quadratic model for the response of ZP (Y3)

Source	Sum of squares	df	Mean square	F-value	p-value	
Model	1155.67	6	192.61	30.58	< 0.0001	significant
A-Stabilizer to	523.10	1	523.10	83.04	< 0.0001	

Source	Sum of squares	df	Mean square	F-value	p-value	
drug ratio						
B-HS	0.3321	1	0.3321	0.0527	0.8230	
C-HT	64.52	1	64.52	10.24	0.0095	
AB	415.96	1	415.96	66.03	< 0.0001	
AC	151.54	1	151.54	24.06	0.0006	
BC	0.2209	1	0.2209	0.0351	0.8552	
Residual	62.99	10	6.30			
Lack of Fit	43.93	6	7.32	1.54	0.3528	not significant
Pure error	19.06	4	4.76			
Cor total	1218.66	16				

Table 5. 16: Sequential model sum of squares

Source	Sum of squares	df	Mean square	F-value	p-value	
Mean vs Total	19981.13	1	19981.13			
Linear vs Mean	587.96	3	195.99	4.04	0.0312	
2FI vs Linear	**567.71**	**3**	**189.24**	**30.04**	**< 0.0001**	**Suggested**
Quadratic vs 2FI	16.57	3	5.52	0.8331	0.5168	
Cubic vs Quadratic	27.36	3	9.12	1.91	0.2688	Aliased

Source	Sum of squares	df	Mean square	F-value	p-value	
Residual	19.06	4	4.76			
Total	21199.79	17	1247.05			

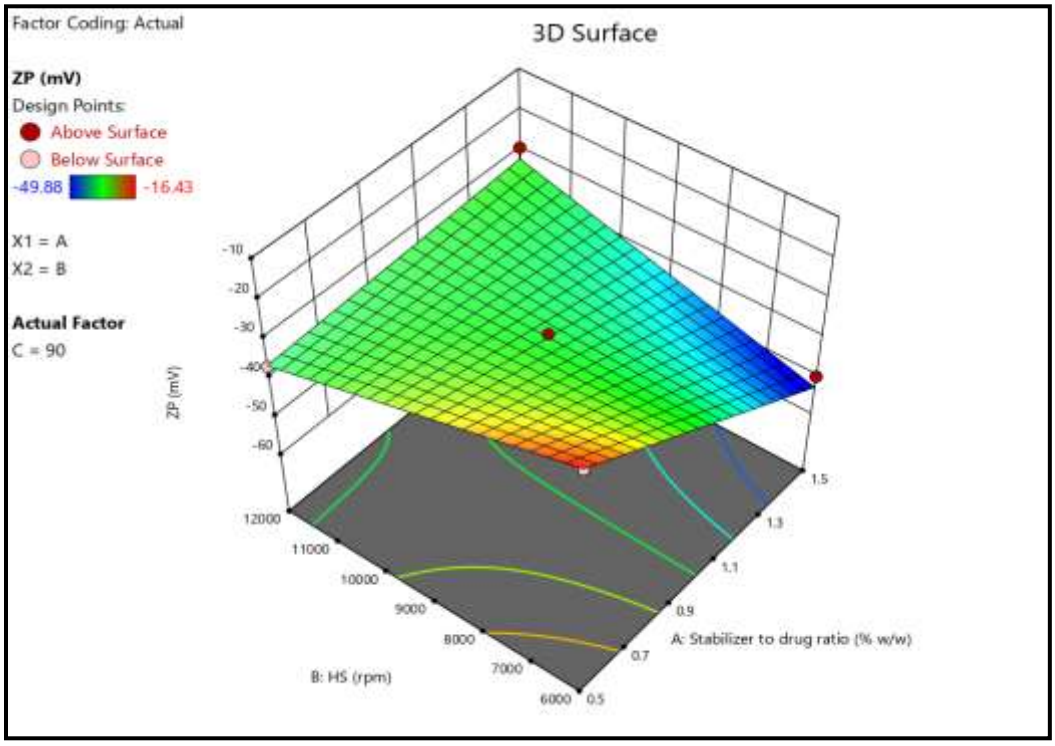

Figure 5. 15: Graphical representation of 3D response surface plots showing the influence of (A) stabilizer concentration and (B) homogenization speed on ZP fixed at level of C (homogenization time)

5.5.4. Exploration of optimal formulations

Desirability-based criteria applied in numerical optimization provided desirability values to the outcomes generated through this design. The ideal formulation that gave the highest desirability score (Fopt solution) was 0.856. The ideal conditions were 12000 rpm HS, 60 min HT, and a drug-to-stabilizer ratio of 1.48 (i.e., 250 mg of the stabilizer for every 170 mg of the medications). Additional graphical customization was made

possible by limiting the Critical Quality Attributes (CQAs) goal values, specifically low PS and PI (Figure 5.17 and 5.18).

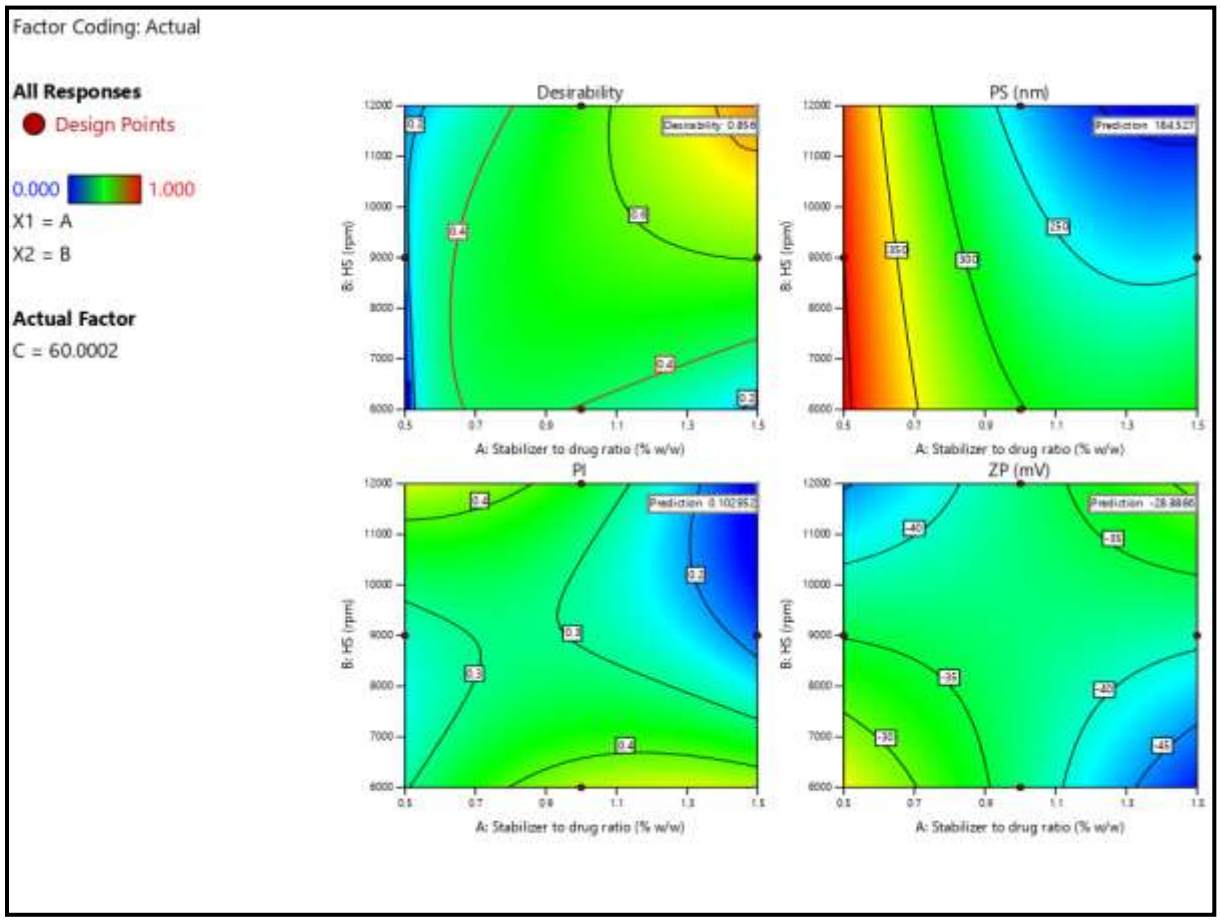

Figure 5. 16: The design space

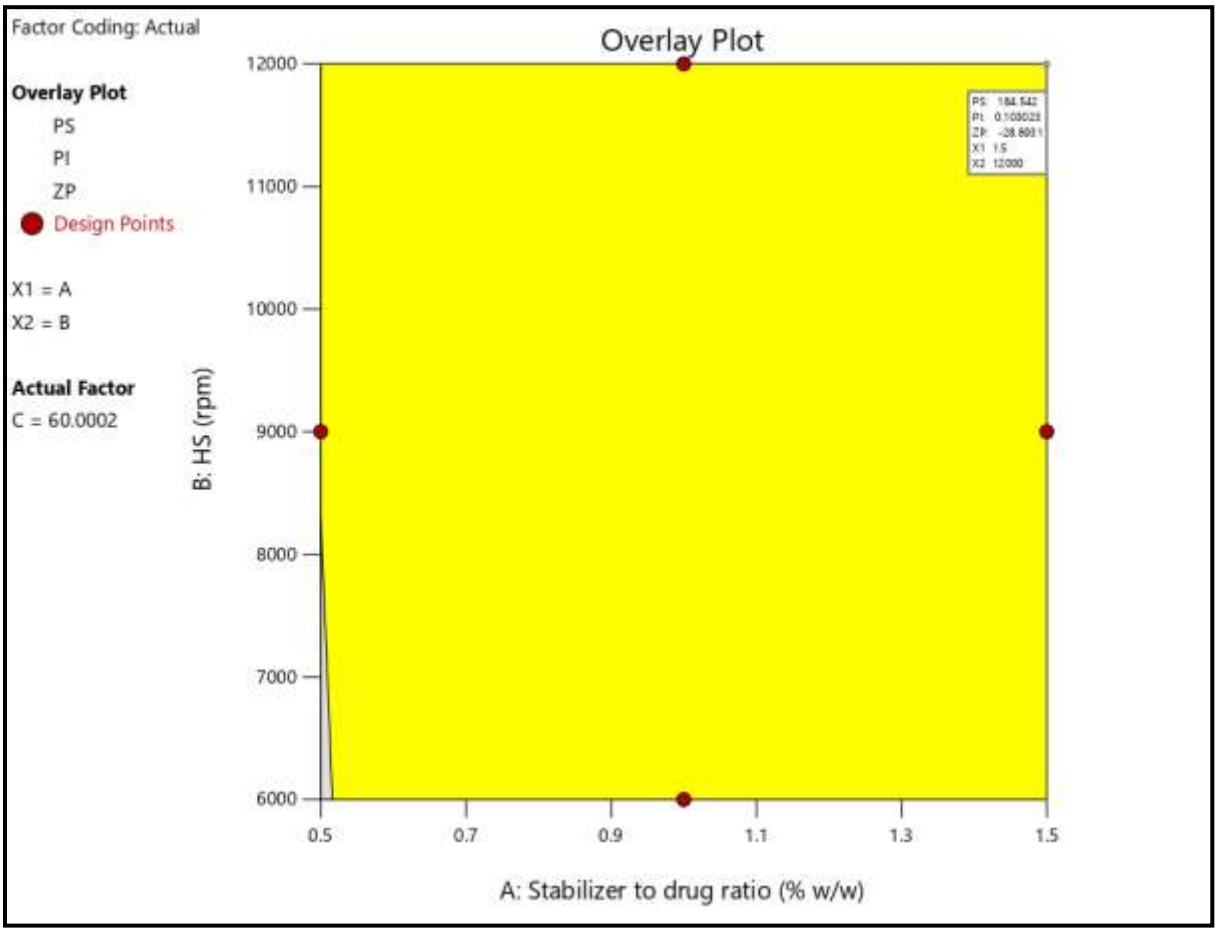

Figure 5. 17: Graphical depiction of desirability and plot of overlay

Validation was performed using three checkpoints to confirm the model's robustness and the accuracy of the formulation. The observed mean values were 189.3 nm PdI of 0.244 and -41.8 mV, while the predicted mean standards for size, PI, and ZP were 184.54 nm 0.103 and -48.8 mV. The predicted values were almost similar with that of software and results from those formulations thus validating the proposed model (Shah *et al.,* 2015).

5.5.5. HPLC method

A UV-DAD detector was used to conduct the analysis by reversed-phase high-performance liquid chromatography (RP HPLC) with a lambda max of 286 for FNF and 246 for ATR. ACN and water (70/30 v/v) assisted as mobile phase, while the flow speed was 1 mL/min. Regression coefficients (R^2) of 0.999 and 0.998 for FNF and ATR,

respectively, indicated that the concentration of the drug was linear within the tested ranges of 0.3 to 250 µg/mL and 0.2 to 200 µg/mL. Specificity was determined by comparing chromatograms of the samples and blank. The specificity of the developed RP-HPLC method was evaluated using blank plasma and plasma spiked with ATR, FNF, and internal standard (IS). No interfering peaks were observed in the blank plasma chromatogram at the retention times of the analytes. In the spiked plasma chromatogram, ATR, FNF, and IS showed distinct and well-resolved peaks at approximately 3.1 min, 5.0 min, and 6.2 min, respectively. The resolution between adjacent peaks was found to be greater than 2.0, indicating adequate peak separation and high specificity of the developed analytical method. The percent recovery was then calculated by measuring the response of the pure reference drugs and comparing it with the concentration response due to the extraction of the analyte from the biological matrices (Górniak *et al.,* 2023). The chromatogram of the drugs with IS is depicted in Figure 5. 19.

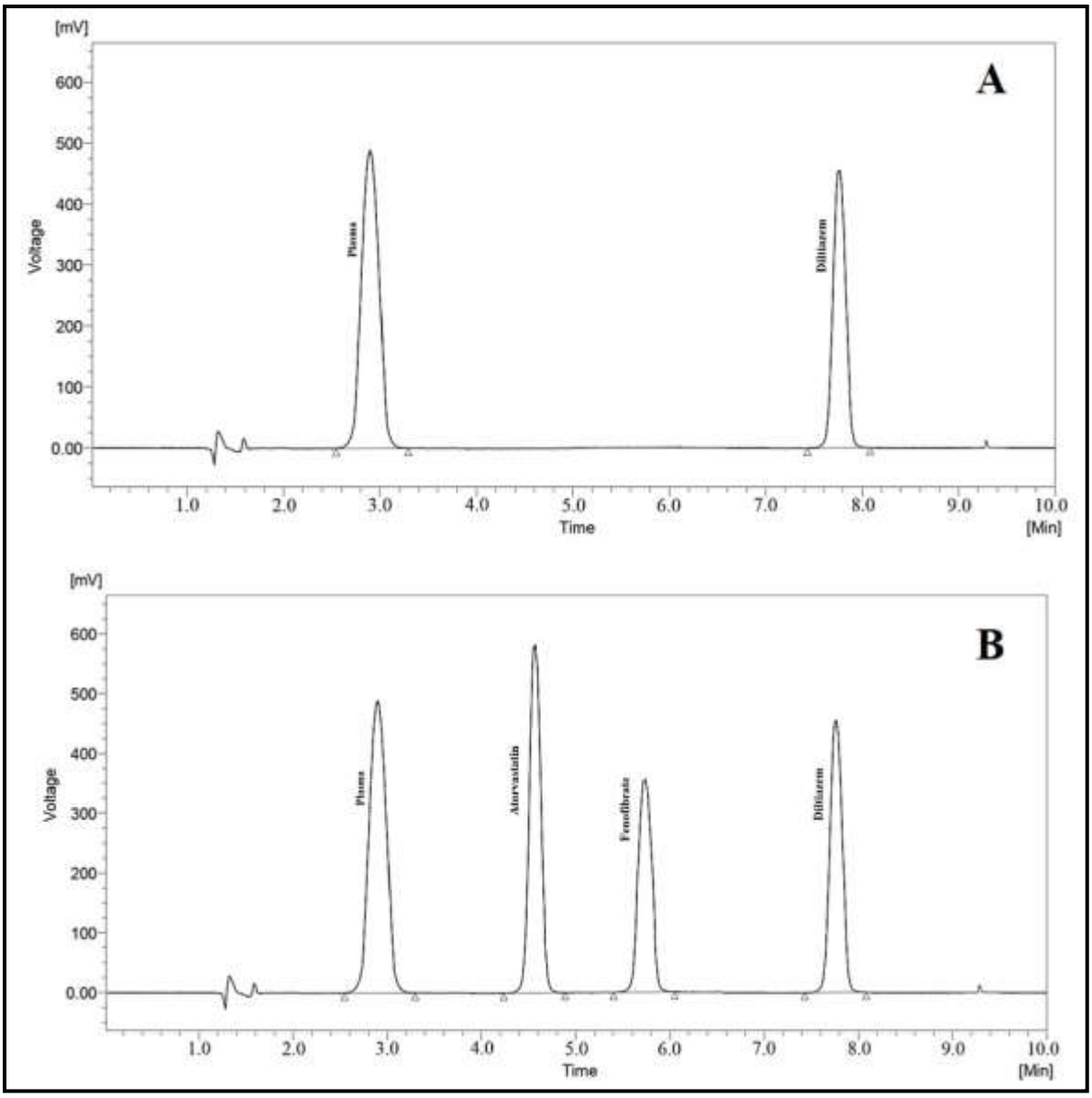

Figure 5. 18: HPLC chromatograms for specificity A) blank plasma B) plasma with drug and IS

5.6. Nanosuspension characterization

5.6.1. Measurements of PS, PI, and ZP

The parameters PS and PI of the formulation varied between 189.3 ± 4.76 nm and 0.245 ± 0.142 mV, indicating that the size of the particles is kept in a consistent range and hence indicates homogeneity of the nanosuspension. A polydispersity value less than 0.3

indicate a homogeneous system. The ZP, a characteristic associated with the DEL on the outer layer of units that are colloidal, can be used in finding the stability of NS. Optimal formulation has ZP of 41.8 ± 5.6 mV. The increased ZP was due to the steric stabilization mechanism of the stabilizer, which formed a polymeric cover around the particles (Figure 5.20). They showed that small nanoparticles need greater zeta potentials, not for sterically secured NS but only electrostatically stabilized NS (Jacob *et al.,* 2020).

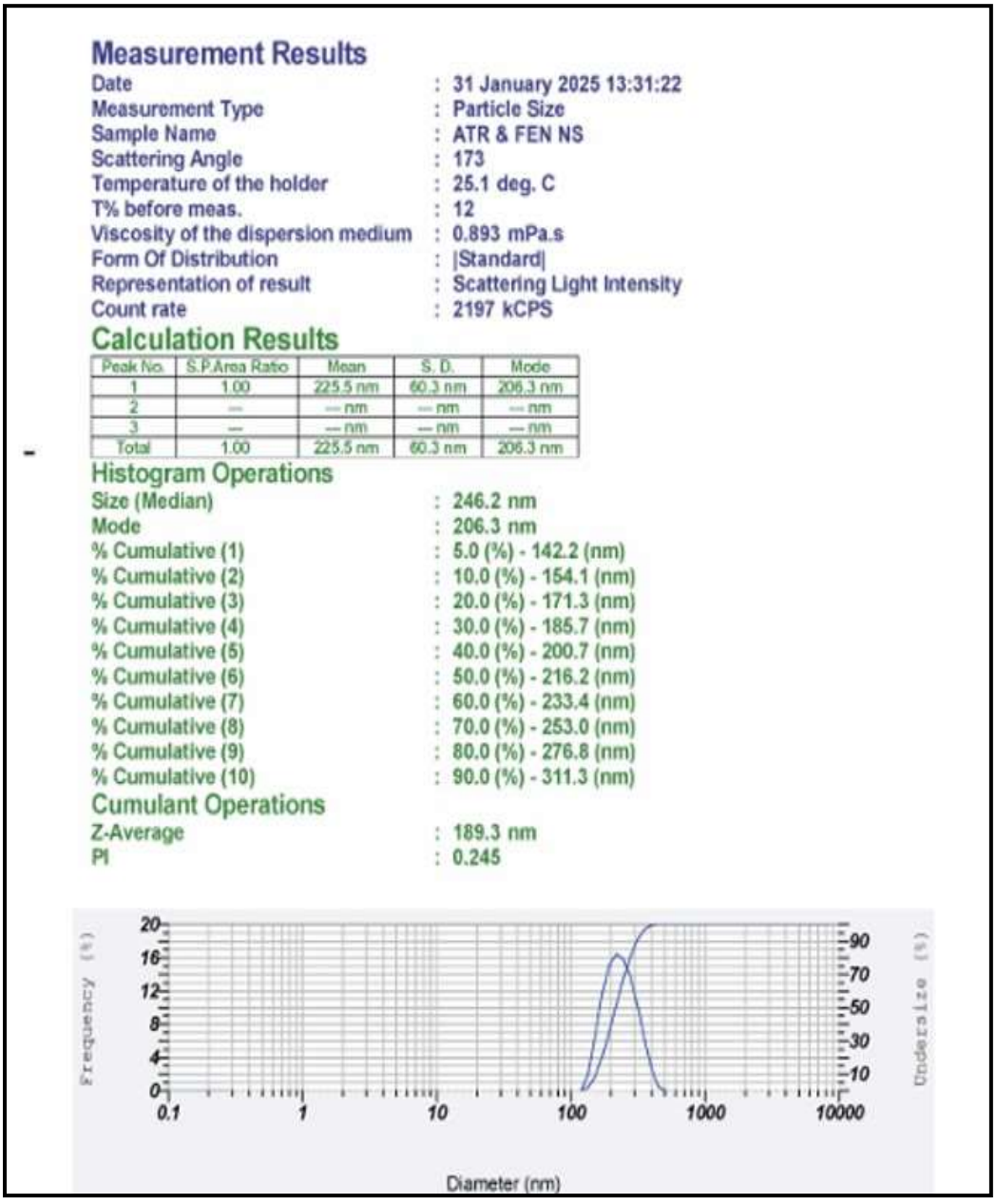

Measurement Results

Date	: 31 January 2025 13:31:22
Measurement Type	: Particle Size
Sample Name	: ATR & FEN NS
Scattering Angle	: 173
Temperature of the holder	: 25.1 deg. C
T% before meas.	: 12
Viscosity of the dispersion medium	: 0.893 mPa.s
Form Of Distribution	: |Standard|
Representation of result	: Scattering Light Intensity
Count rate	: 2197 kCPS

Calculation Results

Peak No.	S.P.Area Ratio	Mean	S. D.	Mode
1	1.00	225.5 nm	60.3 nm	206.3 nm
2	—	— nm	— nm	— nm
3	—	— nm	— nm	— nm
Total	1.00	225.5 nm	60.3 nm	206.3 nm

Histogram Operations

Size (Median)	: 246.2 nm
Mode	: 206.3 nm
% Cumulative (1)	: 5.0 (%) - 142.2 (nm)
% Cumulative (2)	: 10.0 (%) - 154.1 (nm)
% Cumulative (3)	: 20.0 (%) - 171.3 (nm)
% Cumulative (4)	: 30.0 (%) - 185.7 (nm)
% Cumulative (5)	: 40.0 (%) - 200.7 (nm)
% Cumulative (6)	: 50.0 (%) - 216.2 (nm)
% Cumulative (7)	: 60.0 (%) - 233.4 (nm)
% Cumulative (8)	: 70.0 (%) - 253.0 (nm)
% Cumulative (9)	: 80.0 (%) - 276.8 (nm)
% Cumulative (10)	: 90.0 (%) - 311.3 (nm)

Cumulant Operations

Z-Average	: 189.3 nm
PI	: 0.245

Measurement Results

Date	: 31 January 2025 00:50:33
Measurement Type	: Zeta Potential
Sample Name	: ATR & FEN NS
Temperature of the holder	: 25.0 °C
Viscosity of the dispersion medium	: 0.895 mPa·s
Conductivity	: 0.089 mS/cm
Electrode Voltage	: 3.9 V

Calculation Results

Peak No.	Zeta Potential	Electrophoretic Mobility
1	-41.8 mV	-0.000324 cm2/Vs
2	— mV	— cm2/Vs
3	— mV	— cm2/Vs

Zeta Potential (Mean)	: -41.8 mV
Electrophoretic Mobility mean	: -0.000324 cm^2/Vs

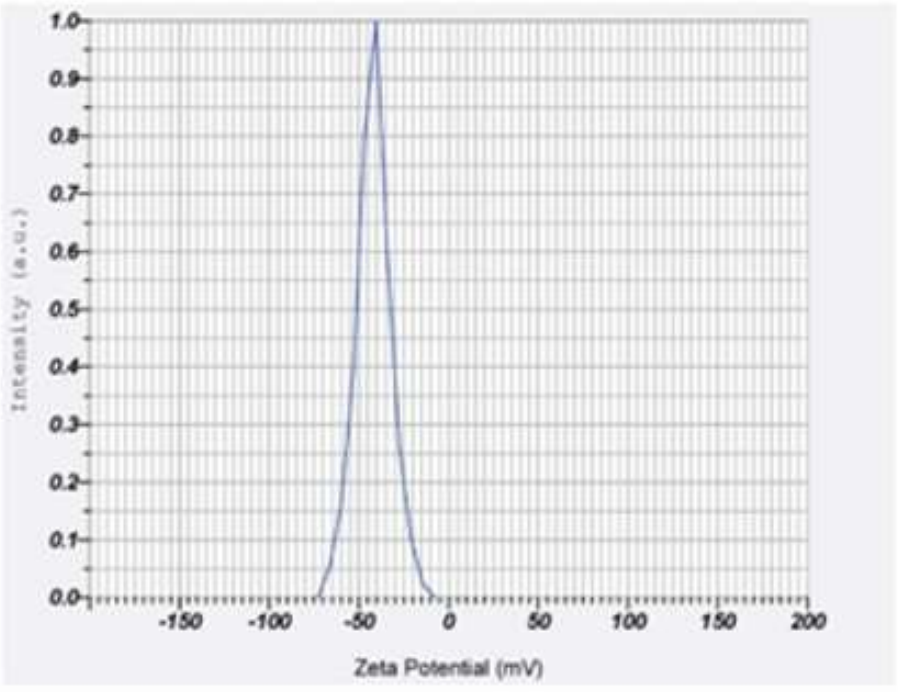

Figure 5. 19: Images of PS, and ZP of the optimized NS

5.6.2. SEM (Scanning Electron Transmission)

The formulation's material external surface properties and those of simple medication are presented in Figure 5. 21. The pharmaceutical is an irregular shape cubic in structure with micrometer-sized particles and an enormous particle size range with unique units in its natural state. Its course of transformation as the drug is, however, converted into a tiny spherical bead with a more uniform size range value between 118 and 229 nm by the solvent-antisolvent precipitation-based nanosuspension. The study illustrates that the nanosizing effect achieved by antisolvent precipitation prohibits crystal development while promoting the nucleation of several (Sampathi *et al.,* 2022).

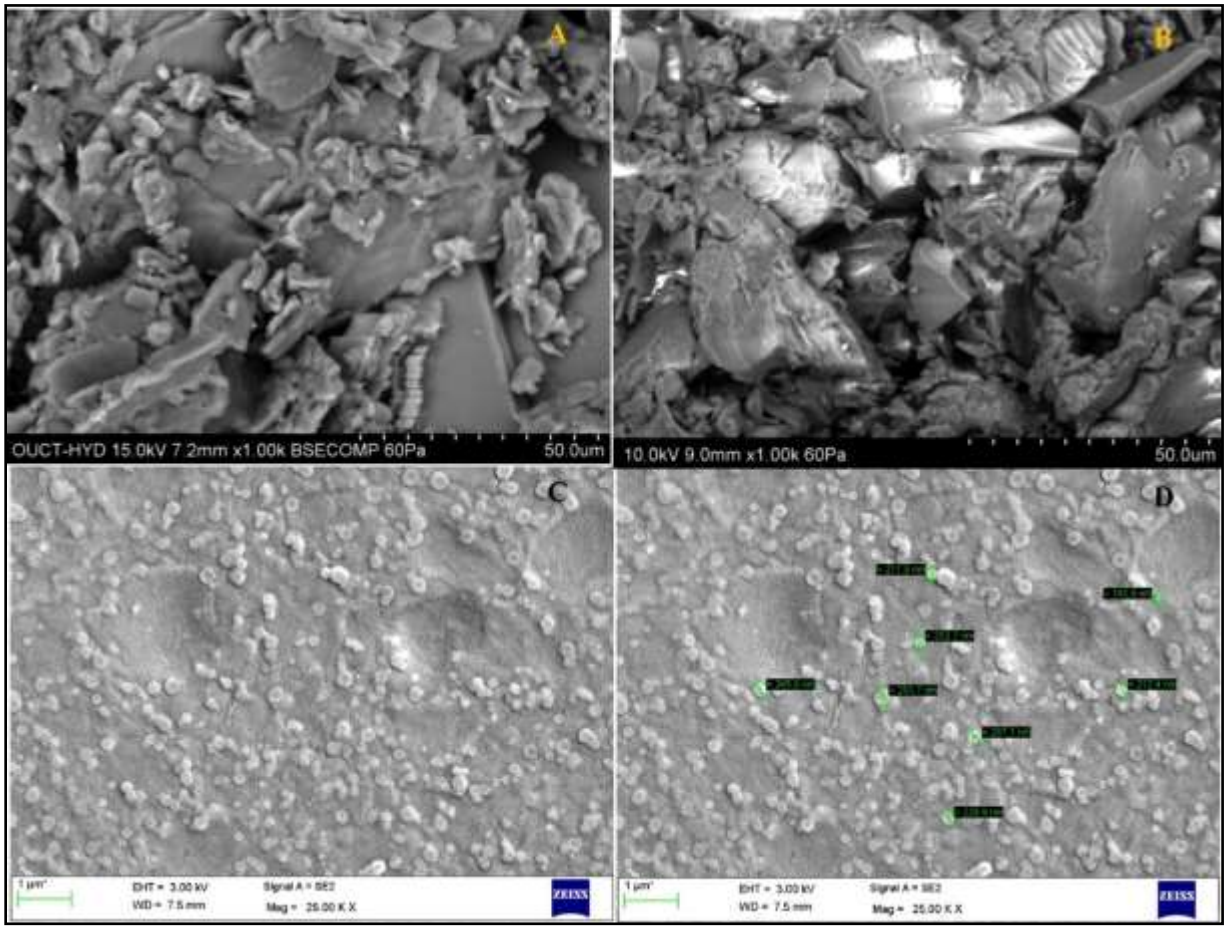

Figure 5. 20: SEM pictures of A) and B) pure drug of ATR and FNF, C) and D) NS of optimized formulation without and with scale

5.6.3. Solubility studies

Figure 5. 22 represents the assessment and graphical depiction of drug solubility in the stabilizer (distilled water) as the solubility of the drug would test the capacity for nanosuspension stability (Table 5.17). Ostwald ripening, according to the LSW deserving will very much be linked to concentration of the drug in dispersion phase. Drug's dissolution behavior in the same gives rise to concentration gradients (solubilized smaller particles versus bigger one), as a result of which relocation of particles from high to low concentration takes place. This leads to the eventual outcome of particle growth, agglomeration, and crystallization, as shown in studies carried out previously with nanosuspensions. Therefore, it is advisable to select stabilizers having minimal damaging effects on solubility of the medicine. Herein, the optimal formulation was used and yielded an expected solubility of the drug of 91.26 ± 8.24 µg/mL and 74.32 ± 9.11 with a stabilizer-to-drug ratio of 1.5% of stabilizer in a volume of 10 mL (Chary *et al.,* 2024).

Table 5. 17: Solubility studies

Sr. No	Name of the sample	Solubility (µg/mL)
1	PD (ATR)	3.83±0.05
2	PD (FNF)	2.21±0.186
3	PD (ATR) with stabilizer	8.85±2.68
4	PD (FNF) with stabilizer	6.24±1.86
5	NS (ATR)	91.26±7.03
6	NS (FNF)	74.32±6.15

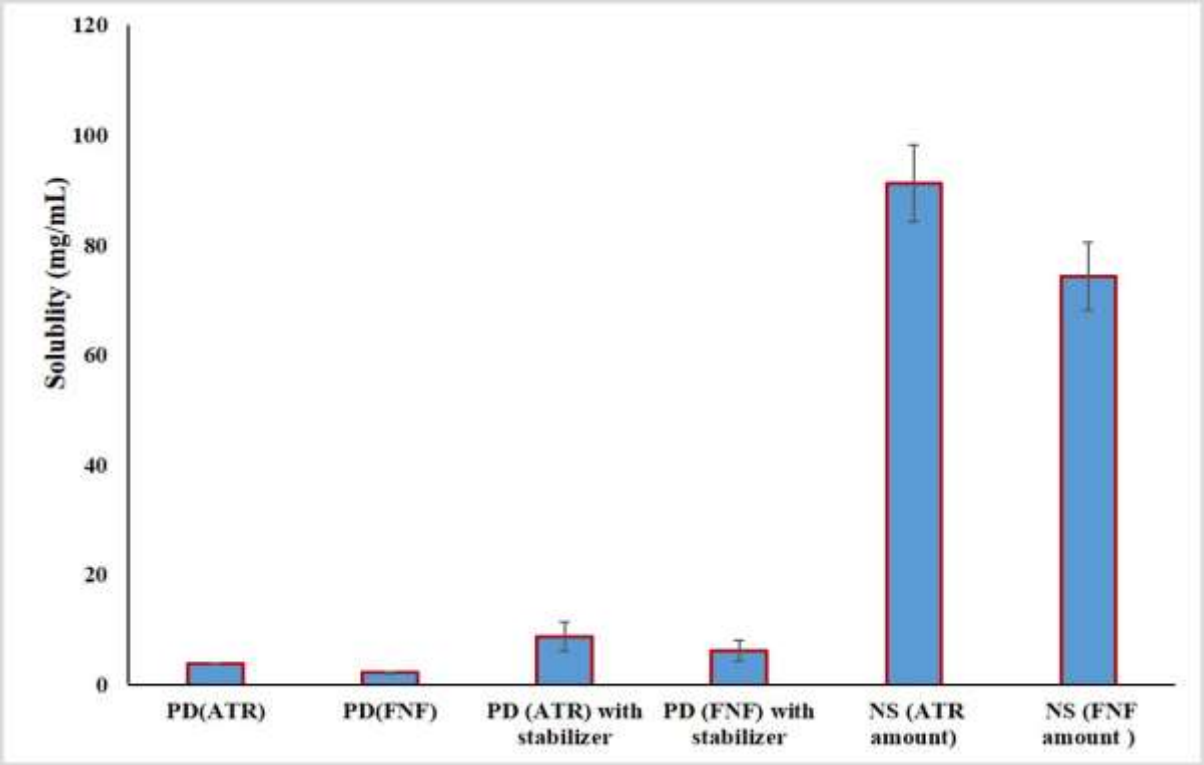

Figure 5. 21: Solubility of ATR, FNF, with stabilizer and NS

5.6.4. Drug release

Drug release endured for up to two hr, for ATR and FNF (PD) of 48.66± 11.15% and 52.8± 9.44% respectively. FNF and ATR showed drug releases of 98.66 ± 11.44% and 99.23 ± 12.06%, respectively, in case L-NS FNF, and ATR showed drug releases of 98.66 ± 11.44% and 99.23 ± 12.06% in case L-NS. The L-NS data, at 15 mins, showed that more than forty-five percent of drug release from the formulation was obviously enhanced (Table 5.18, Figure 5.23). Such a mechanism can be explained by a decrease in particle size, conversion of the substance into the amorphous state, and the use of stabilizers like surfactants that increased solubility. Increased drug release from NS further supports the Noyes-Whitney equation and Brunner-Nernst concept, which suggest that minimizing particle dimensions into the nano level augments the surface area which helps in dissolution (Chary *et al.,* 2024).

Table 5. 18: *In vitro* cumulative drug release (CDR) data of pure drugs, NS of FDC

Time (min)	CDR from PD (ATR)	CDR from PD (FNF)	CDR from NS (FNF)	CDR from NS (ATR)
0	0	0	0	0
5	8.14±1.68	10.16±2.72	22.39±4.67	69.98±6.12
10	12.89±2.01	14.22±2.58	36.72±3.66	77.54±7.68
15	18.9±3.74	21.36±4.14	46.93±7.43	86.28±9.37
30	23.44±5.16	28.89±6.03	62.76±8.45	94.49±10.22
45	28.89±6.67	34.72±8.38	84.84±6.76	98.78±9.06
60	33.12±8.41	38.84±7.35	92.02±8.48	99.18±11.35
90	36.67±9.76	44.48±8.83	99.34±10.34	99.23±12.06
120	48.66±11.15	52.8±9.44	98.66±11.44	-

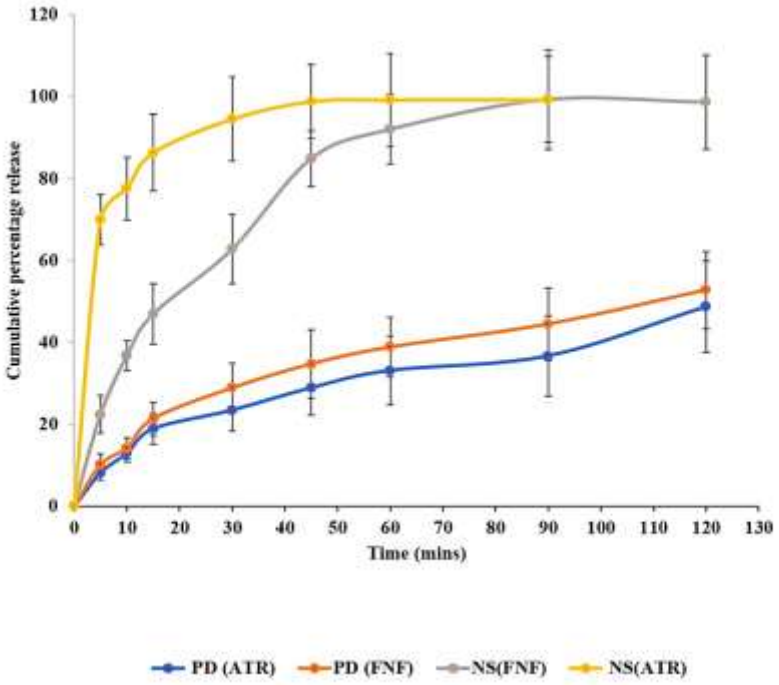

Figure 5. 22: *In vitro* release of ATR, FNF and NS loaded with ATR and FNF

5.6.5. Compatibility studies FT-IR

Figure 5. 24 depict the determination of component compatibility through IR spectra analysis of the nano-formulation, excipients, and drugs. The range of 400-4000 cm^{-1} was used to record the FTIR spectra. In the FTIR spectra of FNF, a variety of absorption bands could be identified, such as the C-H stretch (2984 cm^{-1}), ester carbonyl stretches (1725 cm^{-1}), carbonyl stretch (1648 cm^{-1}), benzene ring stretch (1597 cm^{-1}), and aryl ether (1286 cm^{-1}). Likewise, the ATR showed absorption bands corresponding to stretching of O-H (3547 cm^{-1}), aliphatic C-H vibration (2951, 2930, 2872, and 1467 cm^{-1}), ester C=O vibrations (1695 and 1266 cm^{-1}) and ester/lactone C-O-C oscillations (1162 cm^{-1}).The FTIR spectra of L-NS reflected a superimposition of bands from both drugs, and no additional bands or significant shifts were observed, confirming the absence of chemical interactions among the formulation components (Tipduangta *et al.,* 2015) (Choudhary *et al.,* 2012).

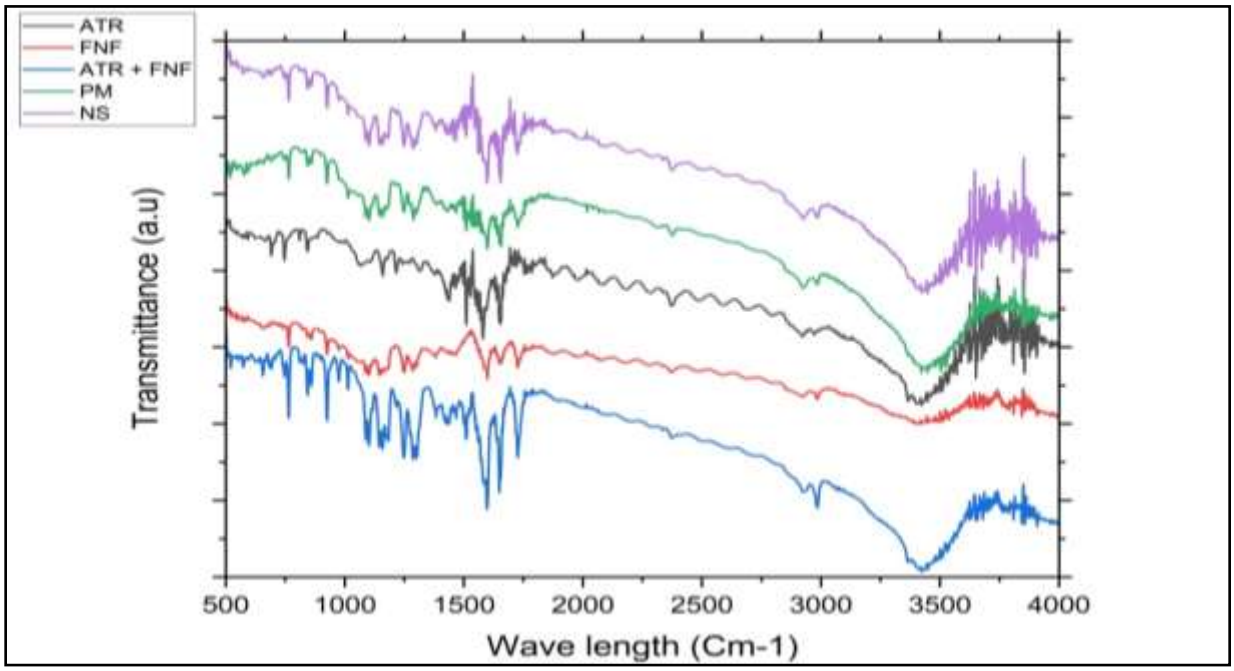

Figure 5. 23: FT-IR of plain drugs (ATR, FNF), and NS along with PM and combination plain drugs

5.6.6. DSC study

The thermal behaviour of the optimized L-NS, the physical mixture, and the pure drugs according to DSC is portrayed (Figure 5. 25). The ATR PD was reported to have a melting point of 128.18 and 240.23°C. The exceedingly crystalline structure of FNF PD was evidenced by its sharp melting endotherm at 83.65°C. The drugs have shown the characteristic peak in the physical mixture. Nonetheless, in L-NS an endothermic peak at 84.03°C of the FNF with a reduced crystallinity and another peak at 237.28 °C indicating that ATR has undergone a signified amorphous nature and might have been covered by stabilizer acting as an inhibitor for further crystal growth. Since no new additional peaks are observed we can confirm that the drugs are chemically stable and no degradation products were formed (Górniak *et al.,* 2023) (Ajmera *et al.,* 2012).

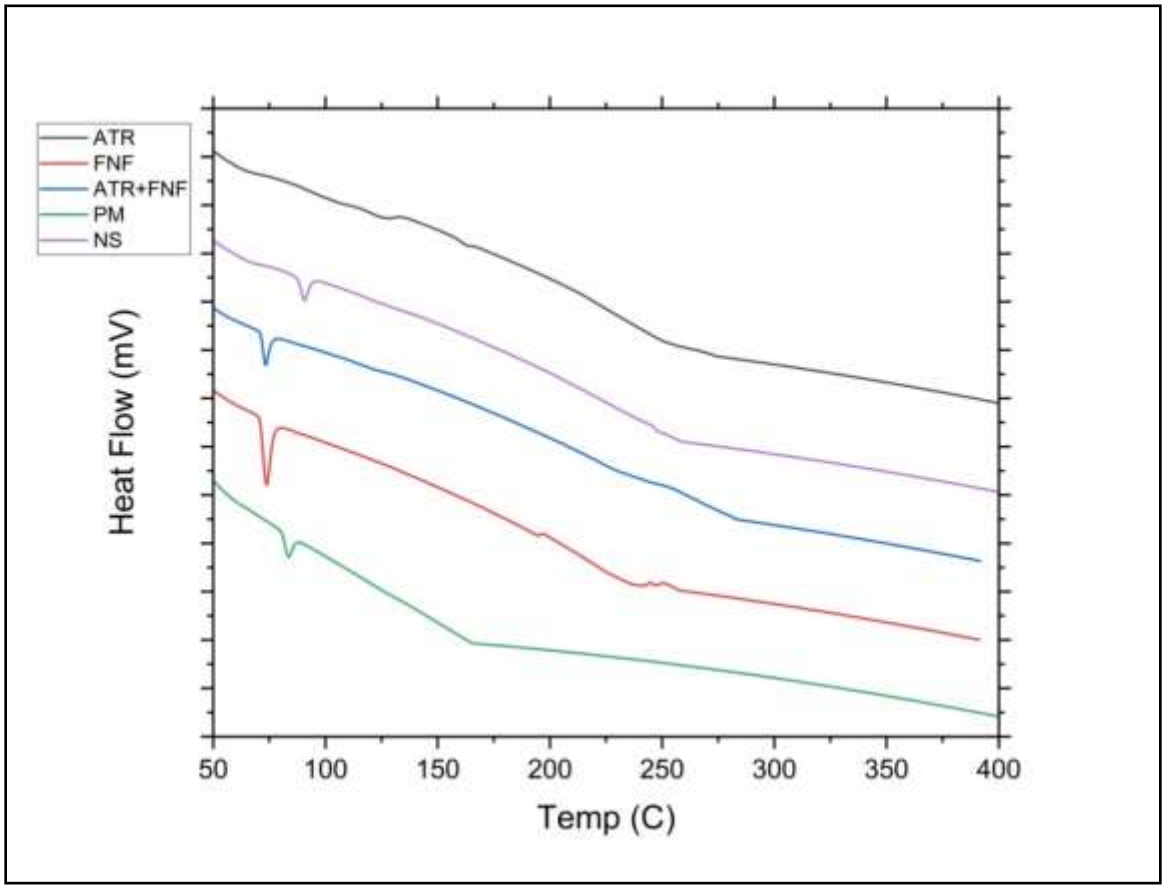

Figure 5. 24: DSC overlay of plain drugs, combination drugs, PM and NS

5.6.7. XRD (X-ray diffraction)

Another DSC pattern was observed with the pure FNF drug confirming the presence of solid peaks at different scattered 2θ angles of 6.03, 11.04, 11.6, 12.35, and 14.11°, while the ATR drug showed firm diffraction peaks at 2.97, 5.98, 9.01, 9.34, 10.13, 11.7, and 12.05°. Similar diffraction peaks for the studied material have also been reported previously. However, the characteristic diffraction peaks of L-NS were observed at scattering angles of 2θ 2.9, 5.96, 6.15, 8.95, 9.29, and 10.07, which elucidated a reduction in peak intensity compared to the pure drugs, confirming involvement of solid-state interaction at a molecular level due to the inclusion of stabilizer encasing (Górniak *et al.,* 2023) (Ajmera *et al.,* 2012) The XRD overlay is illustrated in Figure 5. 26.

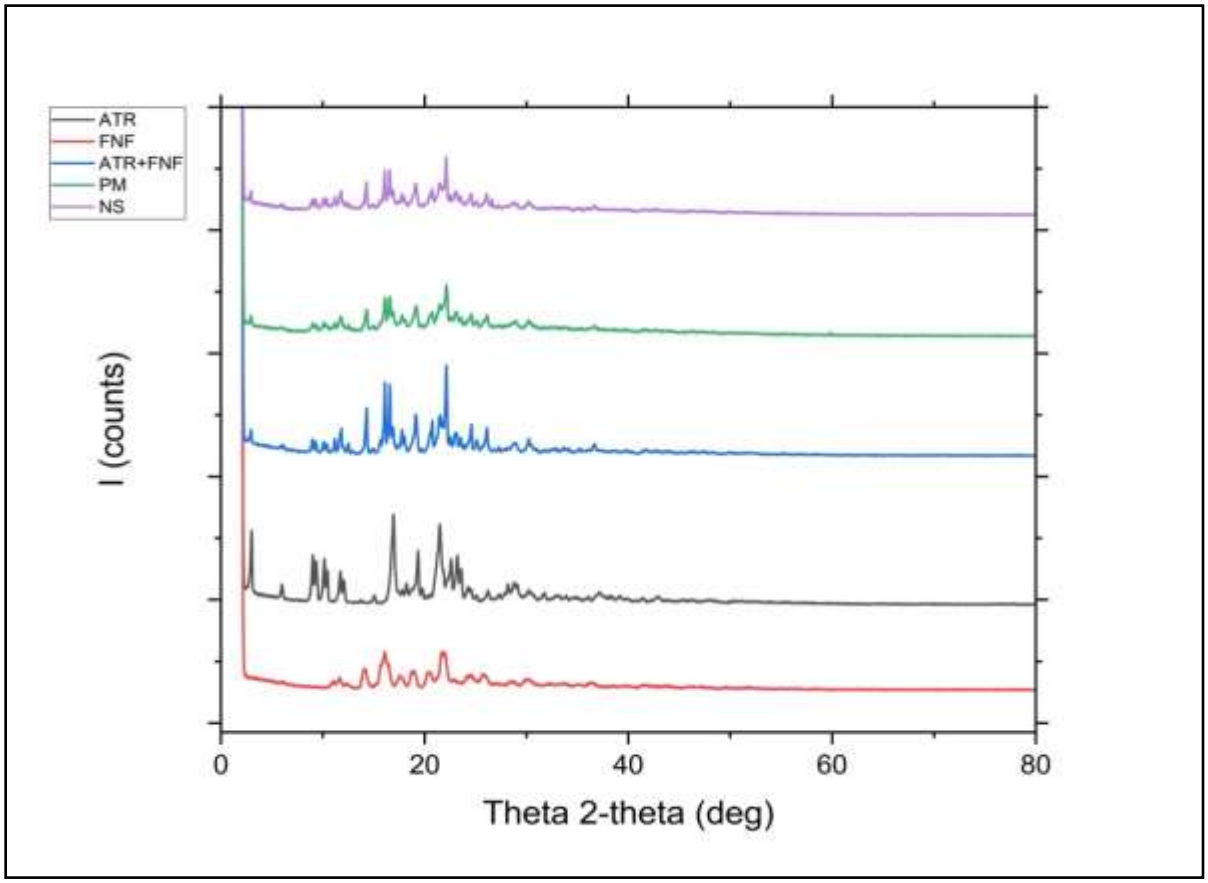

Figure 5. 25: XRD overlay of plain drugs, combination drugs, PM and NS

5.6.8. Stability studies

The optimized ATR–FNF nanosuspension demonstrated remarkable colloidal stability under refrigerated and ambient conditions and acceptable but predictable changes under accelerated stress. Particle size remained narrowly distributed across all storage conditions; at 2–8 °C the mean diameter increased marginally from 189.3 ± 4.76 nm to 193.5 ± 3.50 nm over six months, consistent with minor Ostwald ripening or limited coalescence. Under room temperature and accelerated conditions, the particle size increase was slightly greater (to 194.0 ± 7.50 nm and 196.0 ± 5.00 nm, respectively), indicating temperature-dependent mobility and potential solubility-driven growth, yet values remained within a narrow size range (< ~10 nm change), which is acceptable for nanosuspension performance stability.

PDI values exhibited a small upward trend (e.g., 0.218 → 0.232 at 2–8 °C and up to 0.255 at 40°C), which reflects slight broadening of the size distribution under stress. However, PDI remained <0.3 in all cases, indicating that the formulations maintained monomodal distributions without significant aggregation. Zeta potential showed a modest reduction in magnitude over time (e.g., −28.6 → −27.6 mV at 2–8 °C and −28.6 → −26.2 mV at 40 °C), consistent with minor surfactant or ionic environment changes at elevated temperature; nevertheless, zeta values remained sufficiently negative to confer electrostatic stabilization.

Drug content (assay) for both ATR and FNF remained high across stored samples, with only marginal declines under accelerated conditions (ATR: 99.2 → 97.0%; FNF: 98.7 → 96.8% at 6 months). These decreases are within acceptable limits and are likely attributable to slow degradation pathways (oxidation/hydrolysis) accelerated by temperature and humidity, as corroborated by the impurity profile. Impurity levels increased progressively, most notably under accelerated conditions (ATR impurities rising to 0.42% at 6 months), but remained well below ICH reporting thresholds and any safety concern levels. The impurity growth aligns temporally with assay decline and particle-level changes, suggesting that elevated temperature promotes both chemical and colloidal mobility, thereby hastening minor degradation.

Importantly, dissolution performance showed no major change across the study period, a key finding that confirms retained functional performance of the nanosuspension. At 2–8 °C and 25 °C conditions, ATR and FNF dissolution at 30 min decreased only minimally (~0.6–0.7%), remaining above 92%. Under accelerated conditions a slightly larger decline was observed (≈1.8% over six months) yet the dissolution remained >91% for both drugs. These small changes are not expected to impact bioavailability significantly, particularly given the consistently high assay values and narrow particle-size distribution, which both support maintained dissolution kinetics.

Visual appearance was stable for refrigerated and room temperature samples, with only slight turbidity/haziness under accelerated storage by month 3–6; importantly, no sedimentation or irreversible aggregation was observed, and samples could be re-dispersed easily prior to analysis. Collectively, the data indicate that the nanosuspension preserves its colloidal attributes, chemical integrity, and release characteristics over six months, with accelerated testing revealing expected stress-related changes but no critical quality failures. These results support the nanosuspension's suitability for further development and suggest a projected shelf-life exceeding six months under controlled storage, and likely >24 months under recommended conditions with appropriate packaging (Table 5.19, Figure 5.27).

Table 5. 19: Stability study of L-NS conducted every 0, 30, 90 and 180 days

Temperature condition	**Parameter**	**Initial (0 day)**	**30 days**	**90 days**	**180 days**
2–8 °C (Refrigerated**)**	Particle size (nm)	189.3 ± 4.76	190.18 ± 6.04	192.8 ± 3.22	193.5 ± 3.50
	PDI	0.218 ± 0.014	0.221 ± 0.018	0.229 ± 0.020	0.232 ± 0.022
	Zeta potential	−28.6 ± 1.7	−28.3 ± 1.4	−27.9 ± 1.6	−27.6 ± 1.5

Temperature condition	Parameter	Initial (0 day)	30 days	90 days	180 days
	(mV)				
	Appearance	Uniform, no aggregation	No visible change	No visible change	Uniform, stable
	Assay ATR (%)	99.2 ± 0.3	99.0 ± 0.3	98.6 ± 0.4	98.2 ± 0.4
	Assay FNF (%)	98.7 ± 0.3	98.5 ± 0.3	98.2 ± 0.4	97.9 ± 0.4
	Impurity ATR (%)	0.10 ± 0.01	0.12 ± 0.01	0.16 ± 0.02	0.18 ± 0.02
	Impurity FNF (%)	0.09 ± 0.01	0.11 ± 0.01	0.14 ± 0.02	0.16 ± 0.02
	Dissolution ATR (% at 30 min)	93.0 ± 0.5	92.8 ± 0.5	92.6 ± 0.4	92.4 ± 0.4
	Dissolution FNF (% at 30 min)	93.0 ± 0.5	92.9 ± 0.4	92.6 ± 0.4	92.5 ± 0.4
25 °C (Room temp)	Particle size (nm)	189.3 ± 4.76	191.9 ± 7.36	193.4 ± 7.04	194.0 ± 7.50
	PDI	0.218 ± 0.014	0.226 ± 0.017	0.233 ± 0.022	0.236 ± 0.023
	Zeta	−28.6 ± 1.7	−27.8 ±	−27.5 ± 1.5	−27.2 ± 1.6

Temperature condition	Parameter	Initial (0 day)	30 days	90 days	180 days
	potential (mV)		1.8		
	Appearance	Uniform, no aggregation	Slight increase in turbidity	Uniform, stable	Uniform, stable
	Assay ATR (%)	99.2 ± 0.3	98.9 ± 0.4	98.5 ± 0.4	98.3 ± 0.4
	Assay FNF (%)	98.7 ± 0.3	98.4 ± 0.4	98.1 ± 0.4	97.9 ± 0.4
	Impurity ATR (%)	0.10 ± 0.01	0.14 ± 0.02	0.18 ± 0.02	0.21 ± 0.02
	Impurity FNF (%)	0.09 ± 0.01	0.13 ± 0.02	0.17 ± 0.02	0.20 ± 0.02
	Dissolution ATR (% at 30 min)	93.0 ± 0.5	92.8 ± 0.5	92.6 ± 0.4	92.3 ± 0.4
	Dissolution FNF (% at 30 min)	93.0 ± 0.5	92.9 ± 0.4	92.6 ± 0.4	92.4 ± 0.4
40 °C (Accelerated)	Particle size (nm)	189.3 ± 4.76	192.2 ± 6.41	194.21 ± 4.64	196.0 ± 5.00
	PDI	0.218 ±	0.230 ±	0.241 ± 0.024	0.255 ± 0.025

Temperature condition	Parameter	Initial (0 day)	30 days	90 days	180 days
		0.014	0.019		
	Zeta potential (mV)	−28.6 ± 1.7	−27.4 ± 1.6	−26.8 ± 1.9	−26.2 ± 1.8
	Appearance	Clear, homogenous	Slight haziness	Mild turbidity, no sedimentation	Mild turbidity, no sedimentation
	Assay ATR (%)	99.2 ± 0.3	98.6 ± 0.4	97.9 ± 0.5	97.0 ± 0.6
	Assay FNF (%)	98.7 ± 0.3	98.1 ± 0.4	97.6 ± 0.5	96.8 ± 0.6
	Impurity ATR (%)	0.10 ± 0.01	0.18 ± 0.02	0.30 ± 0.03	0.42 ± 0.03
	Impurity FNF (%)	0.09 ± 0.01	0.17 ± 0.02	0.28 ± 0.03	0.36 ± 0.03
	Dissolution ATR (% at 30 min)	93.0 ± 0.5	92.5 ± 0.6	92.0 ± 0.7	91.2 ± 0.8
	Dissolution FNF (% at 30 min)	93.0 ± 0.5	92.4 ± 0.6	91.8 ± 0.7	91.0 ± 0.8

Note: F opt: Optimized formulation, n = 3 ($p < 0.05$).

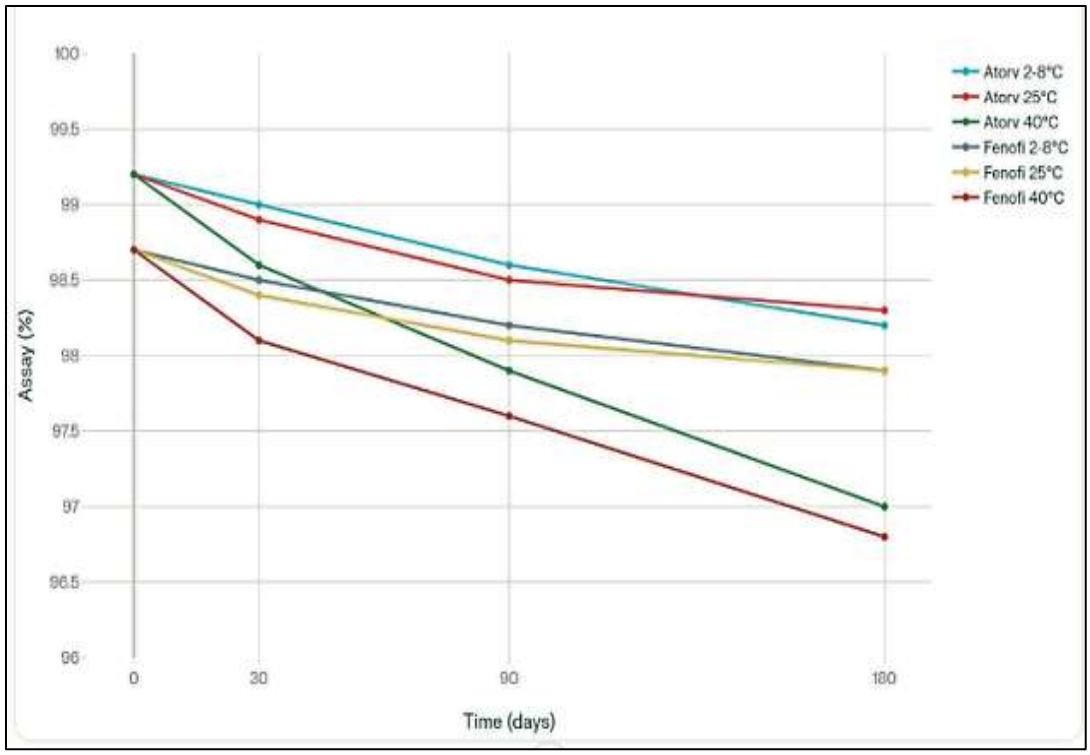
Atorv 2-8°C
Atorv 25°C
Atorv 40°C
Fenofi 2-8°C
Fenofi 25°C
Fenofi 40°C
Assay (%)
100
99.5
99
98.5
98
97.5
97
96.5
96
0
30
90
180
Time (days)

(A)

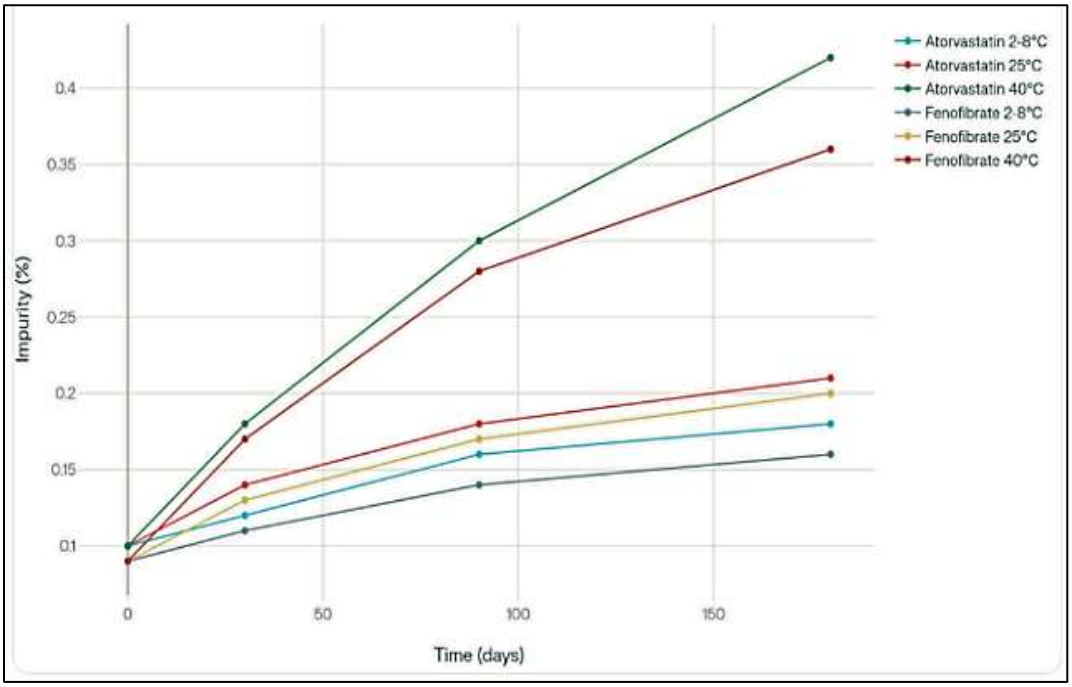
Atorvastatin 2-8°C
Atorvastatin 25°C
Atorvastatin 40°C
Fenofibrate 2-8°C
Fenofibrate 25°C
Fenofibrate 40°C
Impurity (%)
0.4
0.35
0.3
0.25
0.2
0.15
0.1
0
50
100
150
Time (days)

(B)

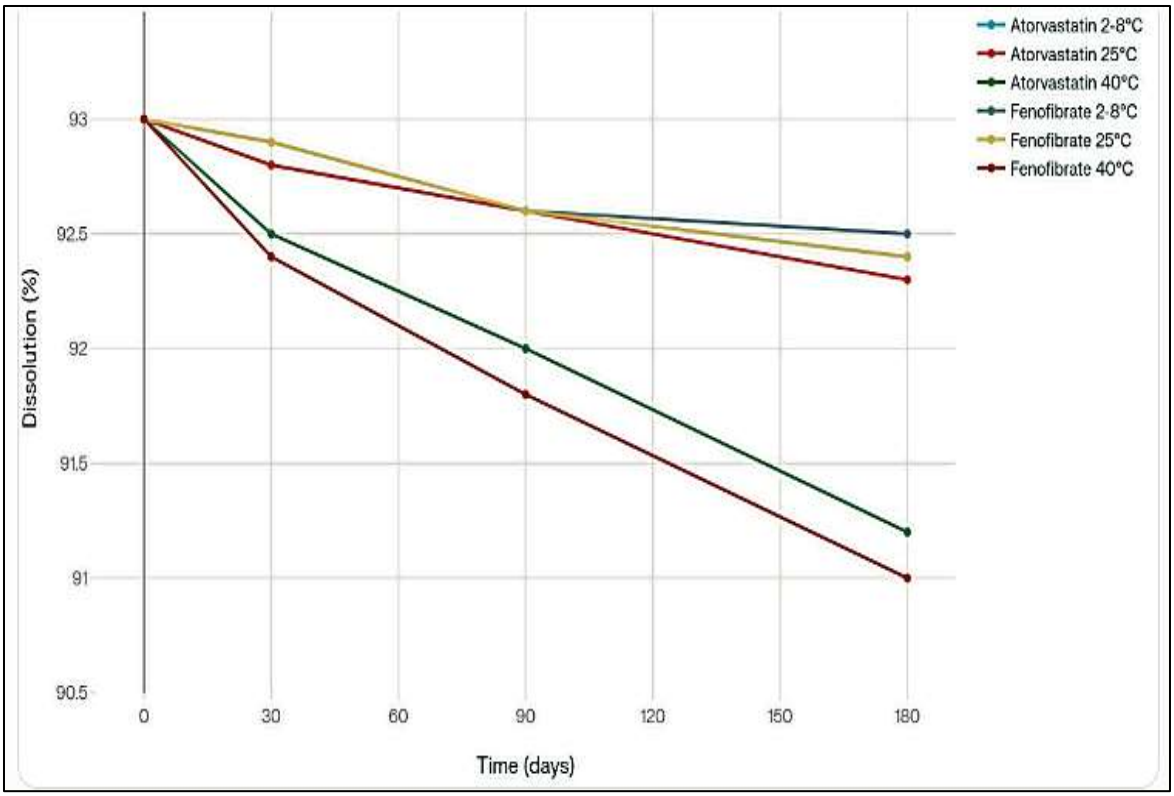

(C)

Figure 5. 26: Trends of change in drug content (A), impurity (B), and dissolution profile for 6 months stability period

5.6.9. Pharmacokinetic studies

The plasma concentration versus time curve after an oral administration of the optimized nanosuspension and a commercial PD solution (0.25% w/v HPMC) is shown in Figure 5. 28. The related pharmacokinetic information is given in Table 5. 20 and 5.21.

Table 5. 20: Pharmacokinetic information

Time (h)	PD (ATR)	PD (FNF)	NS (ATR)	NS (FNF)
0	0	0	0	0
0.25	408.22±72.98	388.98±57.08	2421.54±163.5	1818.08±188.9
0.5	946.65±89.1	779.1±66.34	3908.37±258.67	2566.34±163.67

Time (h)	PD (ATR)	PD (FNF)	NS (ATR)	NS (FNF)
0.75	1248.12±99.92	1190.92±68.98	4766.62±226.84	3478.89±184.84
1	1883.64±242.93	1742.49±229.91	5612.43±466.75	4629.91±293.75
2	1229.56±116.4	1346.4±132.04	4226.54±414.66	6522.04±388.66
3	1003.34±93.8	1133.8±85.88	2239.11±257.78	4305.88±330.78
4	846.33±51.87	945.87±117.42	1202.37±112.93	1949.4±146.93
6	458.44±42.58	393.58±64.36	661.31±88.51	866.22±99.51
8	248.22±29.58	167.34±38.36	404.87±60.57	378.93±56.81

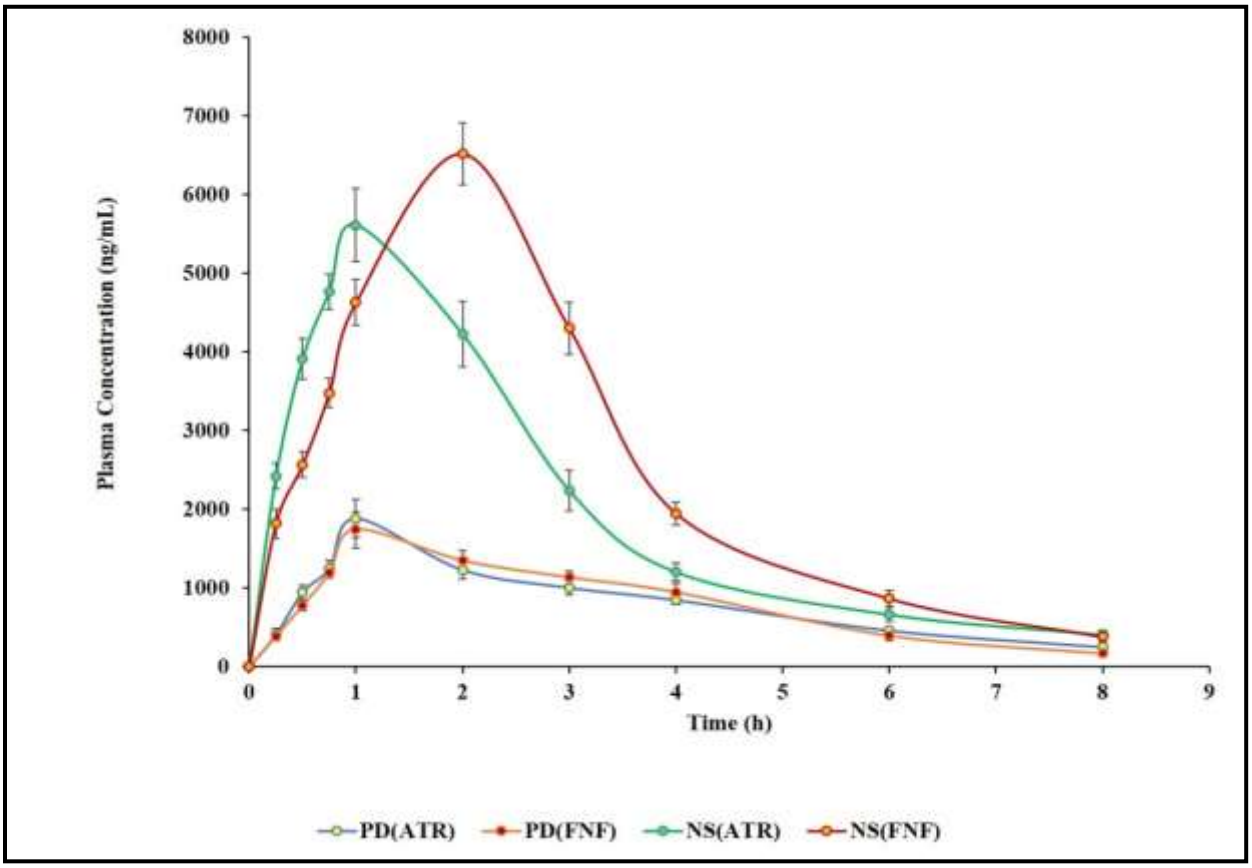

Figure 5. 27: ***In vivo*** **release studies in animals following oral administration of plain drugs (ATR, FNF), and NS**

Table 5. 21: PK data for plain ATR, FNF and for NS

Parameters	Plain drug		Nanosuspension formulation	
	ATR	FNF	ATR	FNF
C_{max} (ng/mL)	1883.64 ± 242.93	1742.49± 229.91	5612.43± 466.75	6522.04± 388.66
T_{max} (h)	1	1	1	2
Half-life (h)	2.26 ± 0.61	1.600 ± 0.34	2.54± 0.88	1.69± 0.42
AUC_{0-t} (ng.h/mL)	6495.51 ± 680.98	6532.311 ±186.34	16278.59±330.59	20722.91±329.26
$AUC_{0-\infty}$ (ng.h/mL)	7304.978 ± 566.2	6918.7604±385.52	17766.42±422.16	21648.30±458.02
MRT(h)	3.92 ± 01.21	3.36± 01.87	3.15± 0.79	2.98± 0.74
Ke	0.306	0.433	0.2721	0.409

In comparison to unformulated pure drug, kinetics exhibited higher values of C_{max} (2.97-fold) and AUC0-24h (2.49-fold) for ATR nanoformulation, while for FNF nanoformulation an increase in the value of C_{max} (3.74-fold) and AUC_{0-24h} (3.17-fold) was evident. It is the lesser particle size with a higher effective surface area that may facilitate solubility and possibly improved drug release concentration gradient across the GIT and blood walls (Gao *et al.,* 2013).

5.7. Formulation of BSD and TSD

In the current study binary solid dispersions have been produced with drug and single hydrophilic carriers for solubility enhancement. More polymer or surfactant was added in preparing ternary solid dispersions to have an extra dimension for establishing further improvement in drug release and stability. Results demonstrated that two drugs in ternary systems offer the best dissolution profiles compared to the binary counterpart, which is

due to the synergy of effects of the carriers in the ternary formulations. Thus, ternary dispersions were considerably more efficacious in both solubility enhancement and the buoyancy of the composite. For the FDCs the BSD using two polymers such as Soluplus and Kolliphor, were used in drug to polymer proportions and from the enhanced BSD, the TSD were formulated with two polymers, such as Kollidon and PVP at ratios and the compositions of the BSD and TSD is given in the Table 5. 22 and Figure 5.29.

Table 5. 22: Composition of BSD and TSD (w/w)

Formulation code (BSD)	**Drug: Soluplus / kolliphor (w/w)**
KF1	1:0.2
KF2	1:0.4
KF3	1:0.6
KF4	1:0.8
SF5	1:0.2
SF6	1:0.4
SF7	1:0.6
SF8	**1:0.8**
Formulation code (TSD)	**Drug: Kollidon / PVP (w/w)**
KDF9	1:0.8:0.2
KDF10	1:0.8:0.4
KDF11	**1:0.8:0.6**
PVPF12	1:0.8:0.2
PVPF13	1:0.8:0.4
PVPF14	1:0.8:0.6

Figure 5. 28: Optimised solid dispersion formulation

5.8. Evaluation of BSD and TSD

5.8.1. Solubility studies

The solubility of the pure drugs was evaluated in D/W, 0.1 N HCl (pH 1.2) and phosphate buffer (pH 7.4). The ATR solubility is 3.02 ± 0.09 (µg/mL), 19.78 ± 3.66 (µg/mL) and 4.72 ± 0.57 (µg/mL), whereas FNF solubility is 5.89 ± 0.84 µg/mL, 42.09 ± 5.31 (µg/mL) and 54.86 ± 4.43 (µg/mL). ATR has little high solubility in 0.1 N HCl whereas FNF has high solubility in phosphate buffer.

The solubility profiles of the formulated BSD and TSD is shown in Figure 5. 30 and the data of the same is given in the Table 5.23 and 5.24. From the BSD F8 formulation has demonstrated the highest solubility.

Table 5. 23: Solubility studies data values of ATR in BSD and TSD along with plain drugs in 0.1 N HCl and pH 7.4

Formulation code (BSD)	Solubility in 0.1N HCl (ATR)	Solubility in pH 7.4 (ATR)
ATR	9.78±1.22	3.62±0.89
KF1 (ATR)	21.27±4.09	6.99±1.26
KF2 (ATR)	30.22±3.36	15.6±2.04
KF3 (ATR)	38.08±4.09	22.02±3.66
KF4 (ATR)	42.21±2.55	26.15±4.69
SF5 (ATR)	24.28±2.65	8.41±0.99
SF6 (ATR)	36.78±1.48	16.73±1.22
SF7 (ATR)	48.43±5.1	23.68±2.76
SF8 (ATR)	**52.56±3.4**	**36.24±2.9**
KDF9 (ATR)	60.35±3.56	39.33±3.53
KDF10 (ATR)	66.83±5.01	44.05±4.92
KDF11 (ATR)	**82.84±11.4**	**51.28±5.7**
PVPF12 (ATR)	58.58±10.21	37.04±9.34
PVPF13 (ATR)	62.71±8.09	48.48±8.5
PVPF14 (ATR)	68.12±7.98	53.65±5.6

Table 5. 24: Solubility studies data values of FNF in BSD and TSD along with plain drugs in 0.1 N HCl and pH 7.4

Formulation code	Solubility in 0.1N HCl (FNF)	Solubility in pH 7.4 (FNF)
FNF	36.09±2.41	48.47±2.28
KF1 (FNF)	42.11±3.18	55.63±3.61
KF2 (FNF)	50.63±4.57	69.08±3.98
KF3 (FNF)	76.67±4.94	81.32±4.8
KF4 (FNF)	99.9±12.26	108.74±5.11
SF5 (FNF)	46±8.38	62.58±8.1
SF6 (FNF)	58.8±4.26	87.33±7.56
SF7 (FNF)	83.44±9.42	103.81±8.58
SF8 (FNF)	**112.72±10.24**	**120.22±8.96**
KDF9 (FNF)	187.24±9.69	266.48±10.04
KDF10 (FNF)	260.54±13.36	335.02±11.36
KDF11 (FNF)	**386.56±10.16**	**404.77±13.64**
PVPF12 (FNF)	140.22±5.04	146.52±11.25
PVPF13 (FNF)	176.02±9.37	190.46±9.84
PVPF14 (FNF)	226.65±13.04	258.27±7.48

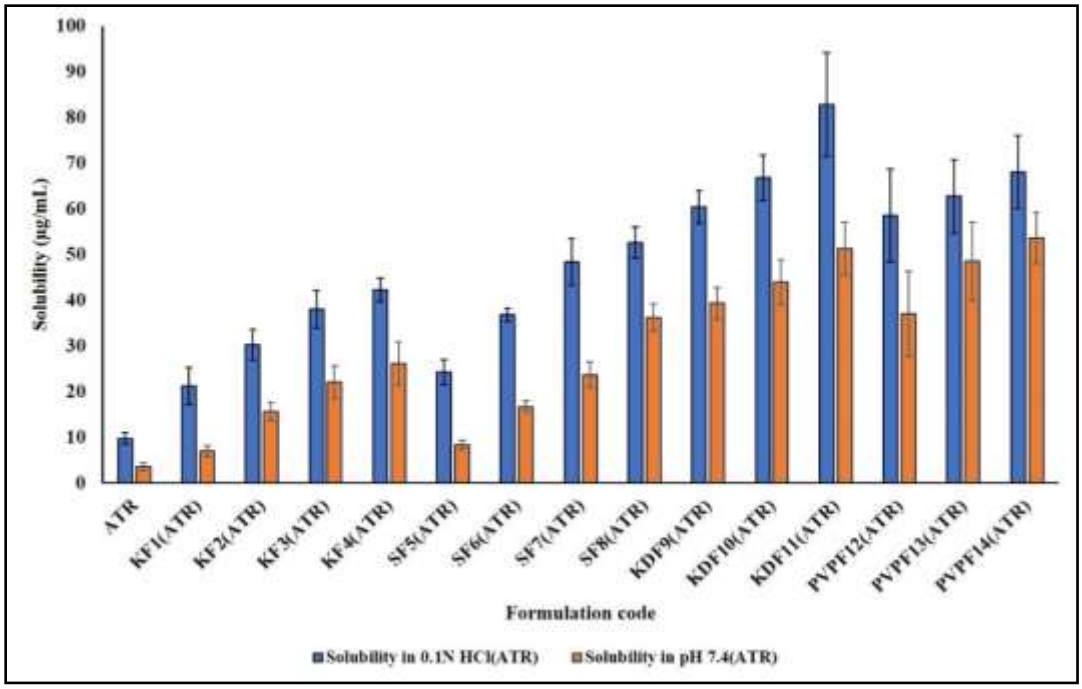

(A)

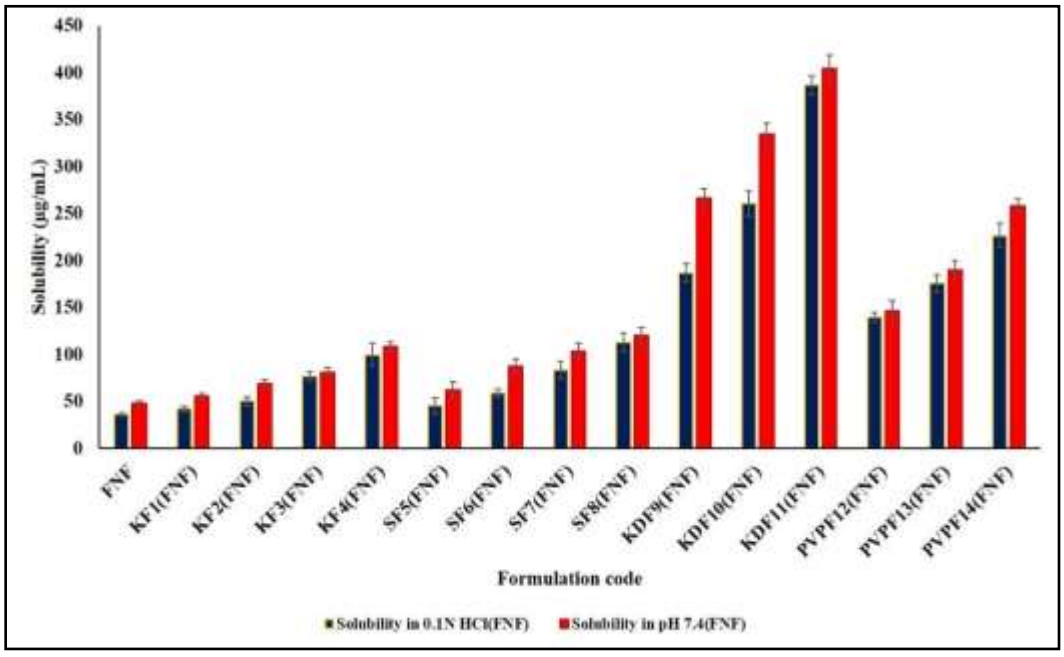

(B)

Figure 5. 29: Solubility studies of ATR (A) and FNF (B) in BSD and TSD along with plain drugs in 0.1 N HCl and pH 7.4

Among ATR binary solid dispersions, the SF8 formulation had the greatest saturation solubility, measuring 52.56 ± 3.40 (µg/mL) in 0.1 N HCl and 36.24 ± 2.9 (µg/mL) in pH 7.4 phosphate buffer (PB). Conversely, the KDF11 (TSD) ternary solid dispersion demonstrated the most significant increase in solubility, attaining 82.84 ± 11.4 (µg/mL) in 0.1 N HCl and 51.28 ± 5.7 (µg/mL) in pH 7.4. The substantial enhancement in solubility is ascribed to the whole transformation of the drug from its crystalline to amorphous form. In the context of FNF BSD, the SF8 formulation exhibited the maximum solubility, measuring 112.72 ± 10.24 in 0.1 N HCl and 120.22 ± 8.96 (µg/mL) in pH 7.4. The KDF11 (TSD) TSD demonstrated the most significant increase in solubility, attaining 386.56 ± 10.16 in 0.1 N HCl and 404.77 ± 13.64 (µg/mL) in pH 7.4.

Soluplus is an amphiphilic polymer which can be used for enhancement of wetting for better drug dispersibility. It could generate micellar structures and hydrogen bonding to keep the amorphous substance from re-crystallizing. The polymer matrix makes drug-polymer miscibility better on the molecular level dispersion because of the dispersion of the polymeric matrix (Basha *et al.,* 2020).

Thus, it would lead to improved solubility perception of the drug although the drug is less soluble in the water. To improve solubility, the system of binary drug-Soluplus is further expanded by adding Kollidon® to a ternary solid dispersion. Kollidon not only works as an additional ingredient but also functions as a hydrophilic carrier to increase the wettability and dispersibility of the drug formulation. Further, it would stabilize the amorphous state lowering the chances of recrystallization as it establishes hydrogen bond formation involving the drug and Soluplus. The combined contribution of Soluplus and Kollidon improves drug-polymer miscibility and supersaturation maintenance. Kollidon also improves the porosity and surface area of the dispersion that speeds up dissolving the medicine. All these mechanisms act synergistically toward improving the solubility of these not very water-soluble ternary-system drugs

5.8.2. Drug content and practical yield

The drug content of the various BSD and TSD were determined for ATR and FNF and in the formulations the drug content is varying from 96.02±5.49 to 89.15± 2.12 in case of

ATR and it is varying from 94.35±5.72 to 89.06±3.06 (Table 5.25). It can be said that good amount of drug has been dispersed in the selected carrier and in all the formulation the practical yield is more than 95 percent (not shown).

Table 5. 25: Data of drug content of ATR and FNF in binary and ternary solid dispersion

Formulation code (BSD)	Drug content of ATR in BSD and TSD	Drug content of FNF in BSD and TSD
KF1	92.24±4.23	93.12±2.36
KF2	93.44±2.45	94.27±3.83
KF3	89.15± 2.12	92.8±4.04
KF4	90.37±3.05	91.33±2.41
SF5	95.88±5.86	94.26±5.29
SF6	94.04±3.27	89.06±3.06
SF7	94.56±4.86	91.67±4.64
SF8	**91.23±3.66**	**90.81±2.30**
KDF9	91.34±4.10	92.22±4.18
KDF10	93.45±3.33	91.98±4.69
KDF11	**93.56±5.74**	**94.35±5.72**
PVPF12	90.89±2.63	91.58±4.36
PVPF13	96.02±5.49	92.39±4.44
PVPF14	94.66±5.89	91.59±2.49

5.8.3. Drug release

From the results it is exhibited that the pure drug released only 29.31 ± 3.44 in PB pH 7.4 after 2 h in case of ATR, whereas FNF pure drug released only 20.26 ± 2.14 in phosphate buffer. In the first half an hour only 11.48± 4.91 percent of ATR and 10.24 ± 1.03 of FNF was released. However, the BSD released more than 86 percent of drug and TSD has released more than 99 percent of drug released in 2 hours from all the formulations, and maximum drug released was from SF8 showing 86.25 ± 5.56 percent of drug release and KDF11 release 98.44 ± 2.56 percent in case of ATR from phosphate buffer pH 7.4. While FNF has released 91.72 ± 6.27 from BSD and 99.25 ± 3.07 in phosphate buffer. An on overall all the formulations has shown an increased drug release in comparison to the plain drugs (Table 5.26-5.33). The reason is owing to the transformation of the crystalline form to amorphous form, which increased the wettability of the drug. The drug release form ATR and FNF is shown in Figure 5. 31, Figure 5. 32, Figure 5. 33, Figure 5.34, Figure 5. 35, Figure 5. 36, Figure 5. 37 and Figure 5. 38.

Table 5. 26: Drug release form ATR and FNF

Time (mins)	ATR	KF1 (ATR)	KF2 (ATR)	KF3 (ATR)	KF4 (ATR)
0	0	0	0	0	0
5	8.13±2.65	13.68±5.68	15.31±2.23	17.11±1.95	26.13±3.39
10	11.48±4.91	28.18±3.65	33.9±5.47	37.5±2.1	48.05±4.91
15	14.76±2.68	32.03±6.85	45.6±4.16	48.84±5.47	55.86±3.80
30	16.55±0.89	39.39±7.58	56.48±5.1	59.99±3.65	61.92±4.12
45	20.26±3.66	44.43±6.85	59.05±4.68	64.82±3.03	69.60±4.08
60	24.11±2.98	50.9±4.68	63.73±6.72	70.48±5.94	73.76±5.1
90	26.02±4.09	56.36±7.59	65.28±5.84	72.67±7.05	79.3±5.26
120	29.31±3.44	59.6±9.67	69.41±7.53	75.16±6	83.03±3.18

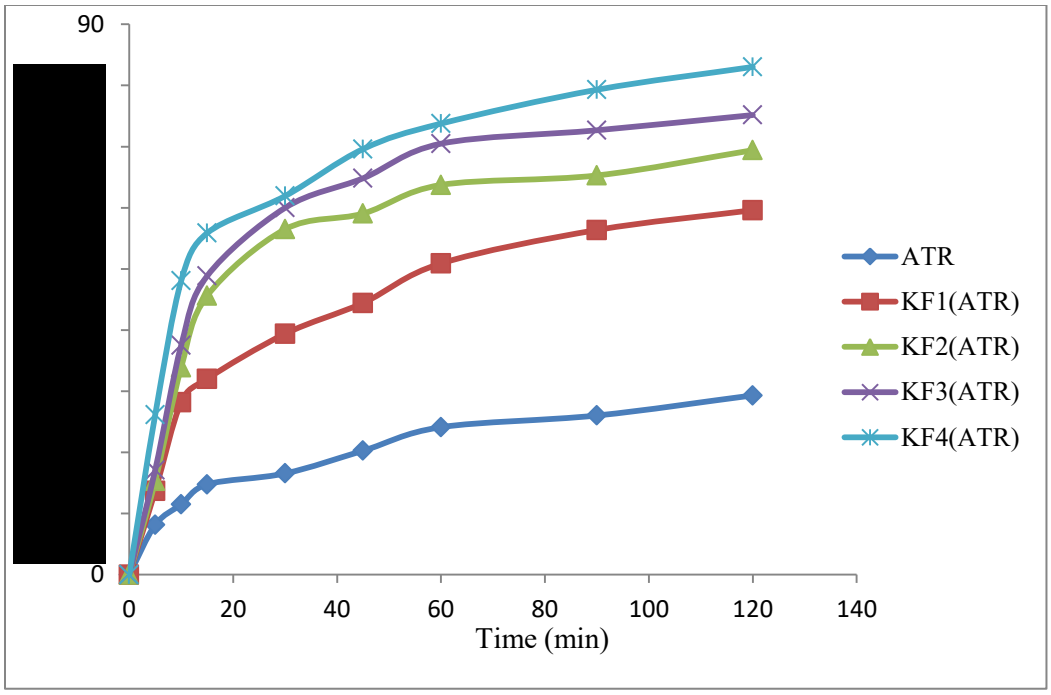

Figure 5. 30: Drug release (ATR, KF1 to KF4)

Table 5. 27: Drug release (SF5-SF8, ATR)

Time (mins)	SF5 (ATR)	SF6 (ATR)	SF7 (ATR)	SF8 (ATR)	ATR
0	0	0	0	0	0
5	15.26±1.72	17.42±1.24	19.56±3.08	**24.48±2.13**	8.13±2.65
10	20.33±3.18	21.68±3.38	26.07±3.59	**40.01±4.46**	11.48±4.91
15	24.42±6.94	35.15±5.09	41.31±6.1	**52.87±5.18**	14.76±2.68
30	30.31±8.04	40.45±6.96	49.48±2.6	**60.06±4.05**	16.55±0.89
45	43.63±7.19	45.08±3.79	54.94±6.48	**68.53±4.72**	20.26±3.66
60	57.03±4.1	49.37±6.82	66.2±6.16	**72.46±3.37**	24.11±2.98
90	62.39±6.33	66.78±5.49	77.6±8.8	**81.27±4.18**	26.02±4.09
120	70.02±3.61	78.28±6.59	83.79±5.99	**86.25±5.56**	29.31±3.44

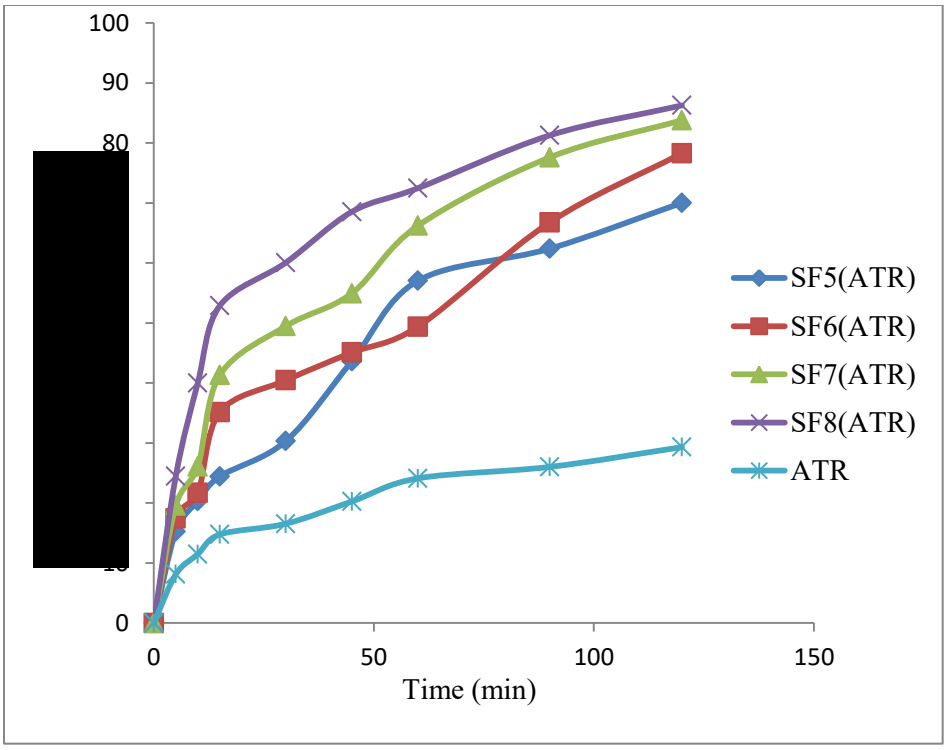

Figure 5. 31: Drug release (SF5-SF8, ATR)

Table 5. 28: Drug release (KDF9-KDF11, ATR)

Time (mins)	KDF9 (ATR)	KDF10 (ATR)	KDF11 (ATR)	ATR
0	0	0	0	0
5	35.85±3.72	50.67±4.79	**54.69±2.26**	8.13±2.65
10	43.95±4.46	56.95±6.56	**58.44±4.6**	11.48±4.91
15	49.98±4.56	63.95±4.83	**66.48±7.47**	14.76±2.68
30	55.98±8.2	69.34±6.55	**71.29±2.98**	16.55±0.89
45	62.15±5.2	73.94±3.99	**74.82±7.49**	20.26±3.66
60	77.36±4.42	79.25±7.39	**81.55±6.06**	24.11±2.98
90	84.35±8.11	86.19±6.22	**88.2±7.85**	26.02±4.09
120	91.84±11.54	93.37±8.52	**98.44±2.56**	29.31±3.44

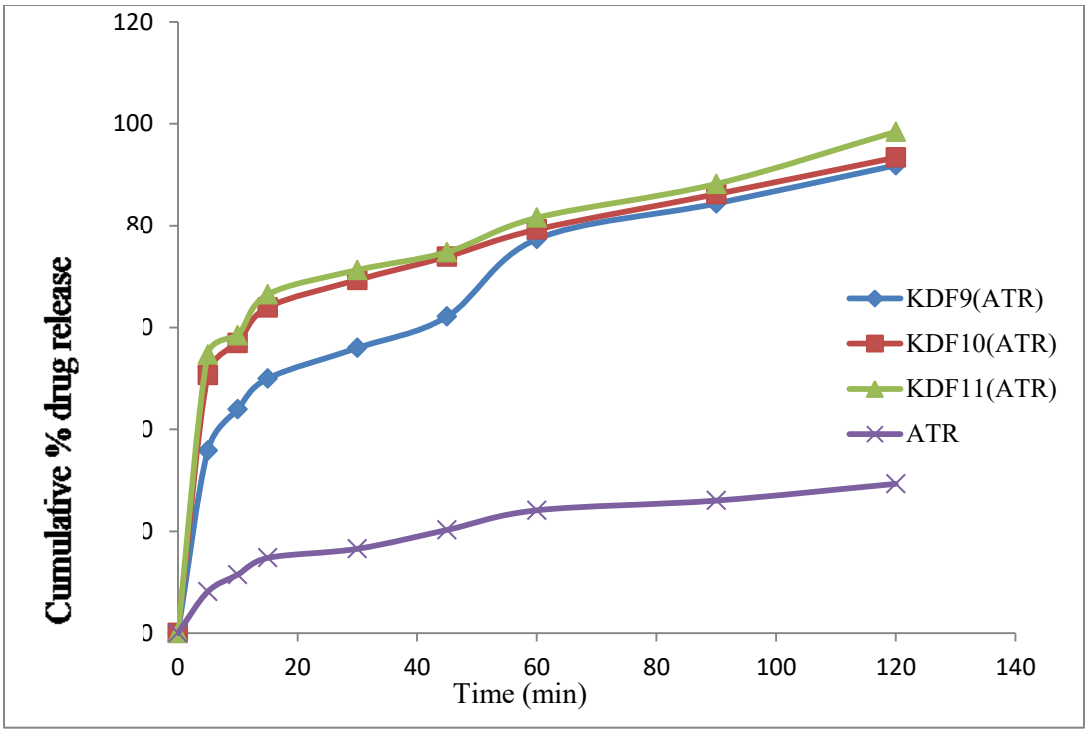

Figure 5. 32: Drug release (KDF9-KDF11, ATR)

Table 5. 29: Drug release (PVPF12-PVPF14, ATR)

Time (mins)	PVPF12 (ATR)	PVPF13 (ATR)	PVPF14 (ATR)	ATR
0	0	0	0	0
5	26.59±3.54	29.54±1.24	32.77±4.11	8.13±2.65
10	42.45±5.8	44.26±2.09	48.48±4.18	11.48±4.91
15	54.48±3.42	52.18±3.31	51.45±5.05	14.76±2.68
30	63.54±4.29	58.87±4.19	59.99±5.17	16.55±0.89
45	69.36±5.35	64.46±4.9	67.73±6.24	20.26±3.66
60	73.35±4.16	72.78±5.14	75.16±8.01	24.11±2.98
90	83.26±3.28	83.48±6.11	86.22±9.1	26.02±4.09
120	89.33±3.44	90.07±7.28	92.98±4.22	29.31±3.44

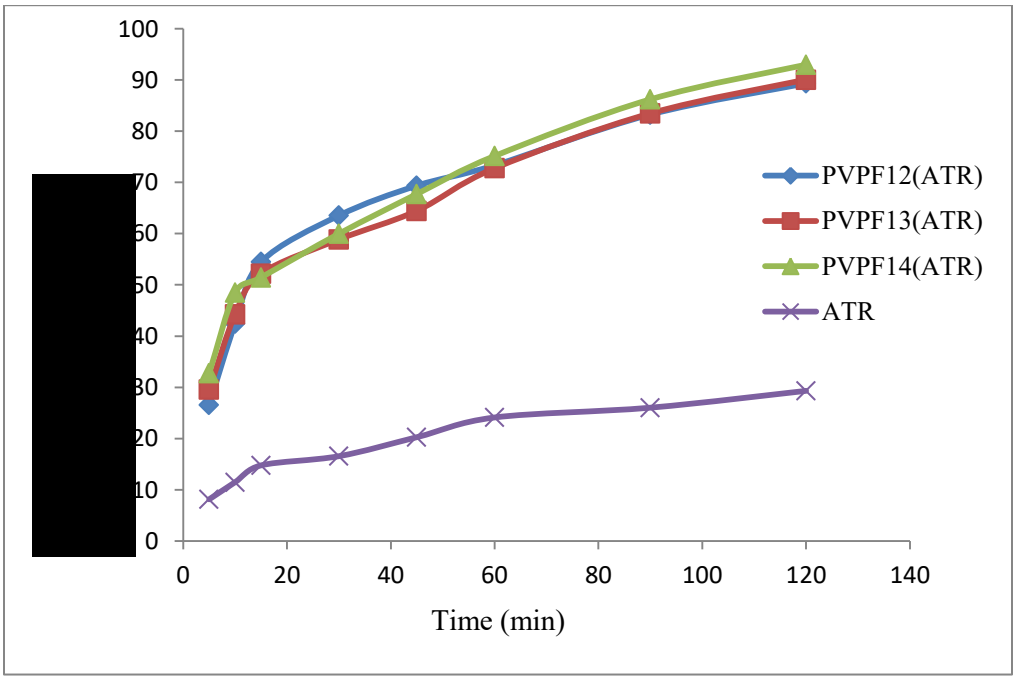

Figure 5. 33: Drug release (PVPF12-PVPF14, ATR)

Table 5. 30: Drug release (FNF, KF1-KF4)

Time (mins)	FNF	KF1 (FNF)	KF2 (FNF)	KF3 (FNF)	KF4 (FNF)
0	0	0	0	0	0
5	6.36±1.62	12.44±5.68	13.4±5.68	15.49±5.95	15.2±2.6
10	8.42±3.13	16.92±4.95	15.81±5.47	16.25±7.59	15.94±2.15
15	10.24±1.68	20.2±6.85	22.82±6.98	22.7±6.47	29.93±3.77
30	12±1.03	26.47±7.58	29.56±7.85	35.61±2.65	43.89±4.21
45	13.6±2.29	31.01±6.85	34.88±4.68	45.05±6.48	52.1±3.38
60	15.67±3.16	33.56±4.68	43.85±6.82	52.59±5.97	61.57±4.03
90	18.47±3.82	35.15±7.59	47.35±5.85	55.99±7.85	62.63±4.62
120	20.26±2.14	37.49±9.67	49.28±7.59	56.57±6	64.66±6.28

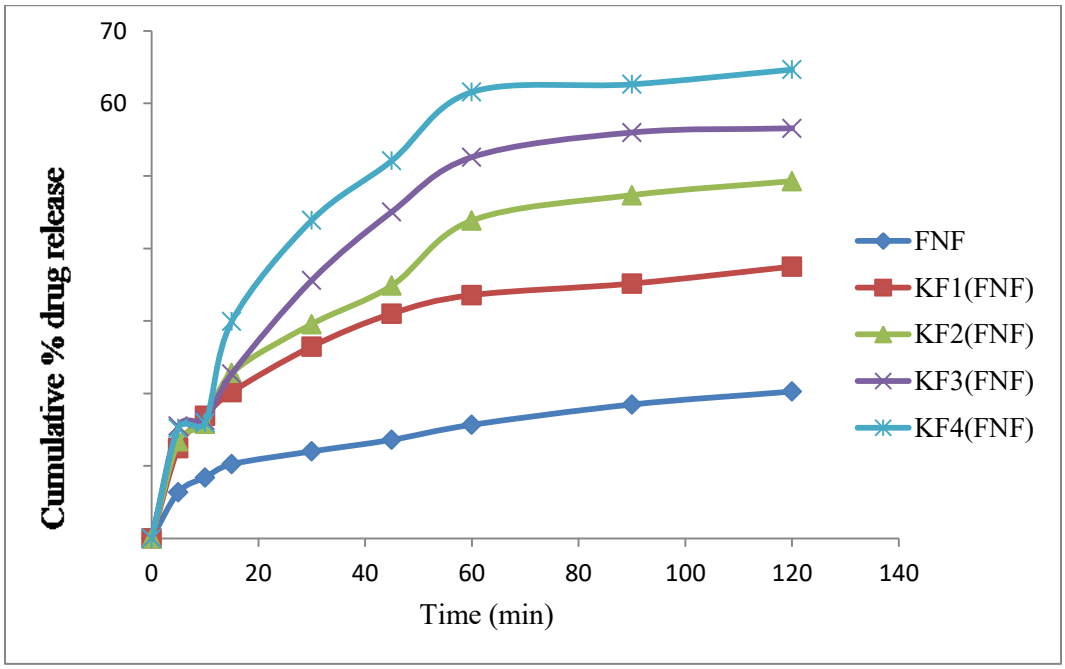

Figure 5. 34: Drug release (FNF, KF1-KF4)

Table 5. 31: Drug release (SF6-SF8, FNF)

Time (mins)	SF5 (FNF)	SF6 (FNF)	SF7 (FNF)	SF8 (FNF)	FNF
0	0	0	0	0	0
5	13.77±5.68	13.92±5.68	15.03±5.95	**12.51±5.95**	6.36±1.62
10	20.85±4.95	22.71±5.47	25.77±7.59	**29.89±7.59**	8.42±3.13
15	27.59±6.85	30±6.98	33.29±6.47	**43.7±6.47**	10.24±1.68
30	33.68±7.58	35.99±7.85	45±2.65	**58.01±2.65**	12±1.03
45	40.97±6.85	45.36±4.68	49.63±6.48	**63.09±6.48**	13.6±2.29
60	43.07±4.68	49.71±6.82	56.05±5.97	**72.35±5.97**	15.67±3.16
90	48.91±7.59	54.83±5.85	62.02±7.85	**86.21±7.85**	18.47±3.82
120	50.96±9.67	56.18±7.59	65.65±6	**91.72±6.27**	20.26±2.14

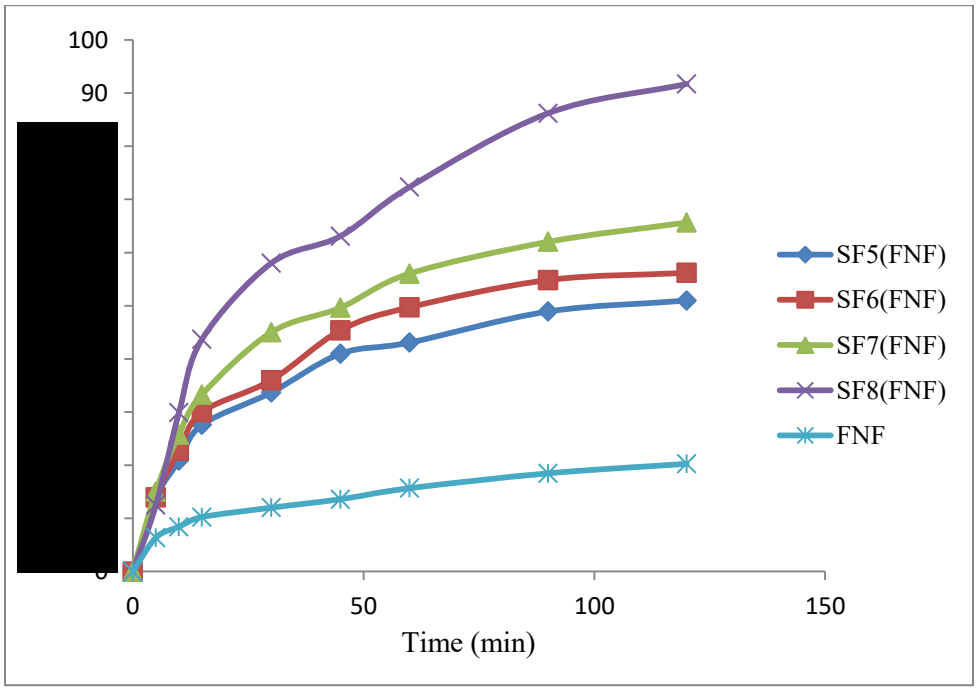

Figure 5. 35: Drug release (SF6-SF8, FNF)

Table 5. 32: Drug release (KDF9-KDF11, FNF)

Time (mins)	KDF9 (FNF)	KDF10 (FNF)	KDF11 (FNF)	FNF
0	0	0	0	0
5	15.38±2.6	22.12±5.68	**28.65±5.68**	6.36±1.62
10	31.1±2.15	36.74±4.95	**42.68±5.47**	8.42±3.13
15	46.35±3.77	48.61±6.85	**51.65±6.98**	10.24±1.68
30	61.8±4.21	64.36±7.58	**67.34±7.85**	12±1.03
45	67.23±3.38	71.48±6.85	**74.65±4.68**	13.6±2.29
60	75.28±4.03	79.7±4.68	**81.25±6.82**	15.67±3.16
90	89.64±4.62	92.42±7.59	**95.87±5.85**	18.47±3.82
120	93.03±6.66	95.01±8.12	**99.25±3.07**	20.26±2.14

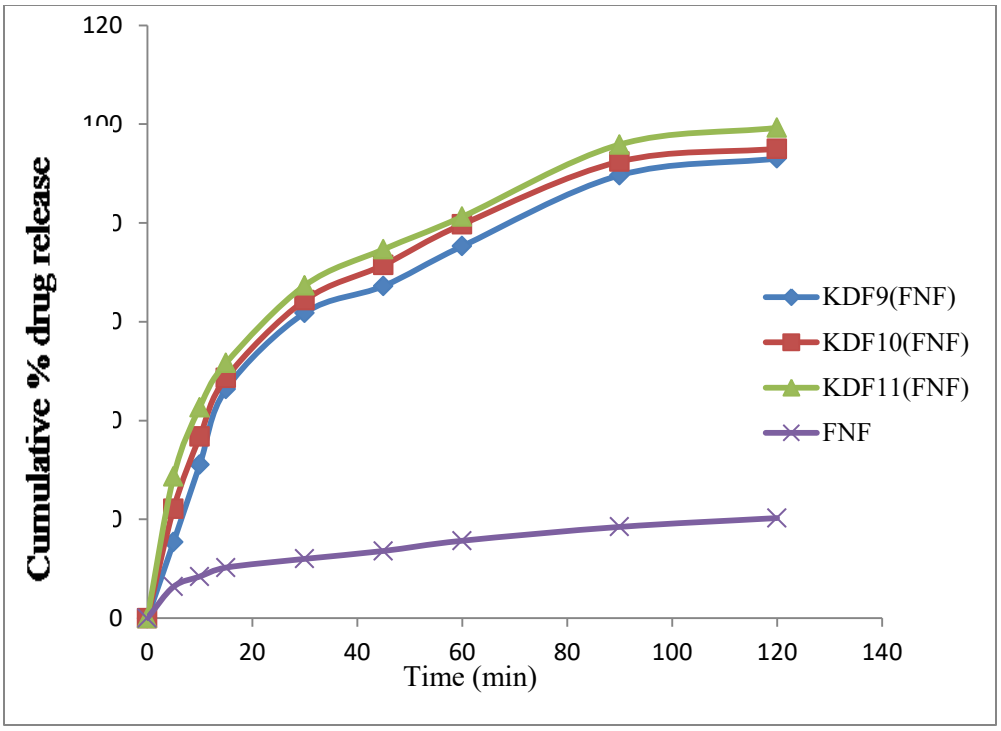

Figure 5. 36: Drug release (KDF9-KDF11, FNF)

Table 5. 33: Drug release (PVPF12-PVPF14, FNF)

Time (mins)	PVPF12 (FNF)	PVPF13 (FNF)	PVPF14 (FNF)	FNF
0	0	0	0	0
5	24.55±5.95	29.25±5.95	30.6±2.6	6.36±1.62
10	31.68±7.59	38.54±7.59	46.24±2.15	8.42±3.13
15	42.45±6.47	46.19±4.48	55.86±3.77	10.24±1.68
30	59.43±2.65	62.05±6.03	64.48±4.21	12±1.03
45	64.29±6.48	67.48±7.18	71.29±3.38	13.6±2.29
60	73.18±5.97	76.17±6.11	79.14±4.03	15.67±3.16
90	87.14±7.85	89.21±9.55	90.25±4.62	18.47±3.82
120	92.8±6.1	93.65±6.07	95.64±5.28	20.26±2.14

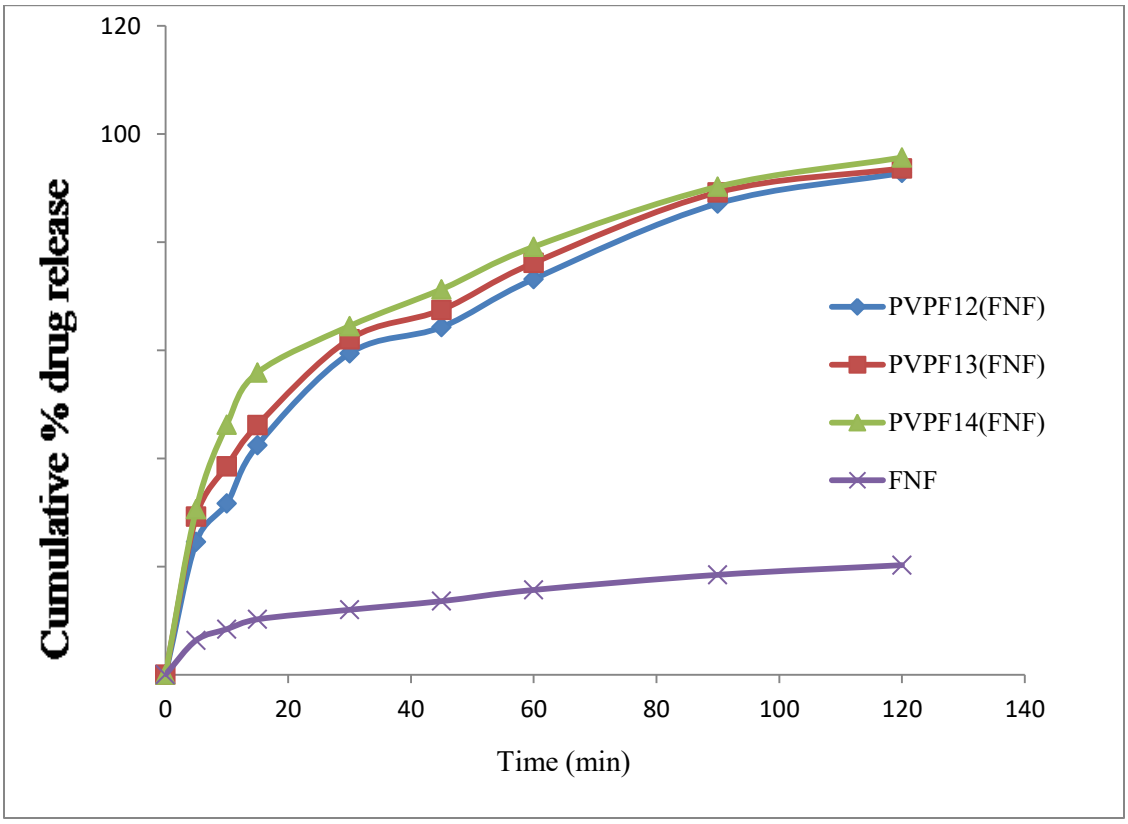

Figure 5. 37: Drug release (PVPF12-PVPF14, FNF)

In the BSD formulated with Soluplus has increased drug wettability the mechanism is to the conservation of supersaturation resulting from intermolecular hydrogen bonding between amongst the drug and the Soluplus. As compared to the BSD prepared with Kolliphor, Soluplus has increased the drug release in fact Soluplus also has swelling ability which also helps in fast drug release from the dispersion (Basha *et al.,* 2020) (Liu *et al.,* 2013).

The solubility and drug release were further increased in TSD in the case of Kolliphor and the reason can be attributed to the surfactant property of the polymer, it is mainly composed of ethylene oxide and propylene oxide blocks and have the nature of self-assembling ability into micelle when placed in aqueous media which therefore enhances the solubilization of the drug. Therefore, based on the results TSD formulated with Kolliphor were further selected for further characterization, stability and in-vivo studies.

5.8.4. SEM

Figure 5. 39 shows the formulation's and the simple drug's external surface properties. In its initial state, the drug has a broad particle size distribution with individual particles of irregular cubic shape measuring in micrometers. In addition, the BSD with Soluplus, and Kollidon, showed the disappearance of crystalline as the drug was masked by the polymer coating and the results are very well supported by XRD studies (Albadarin *et al.,* 2017).

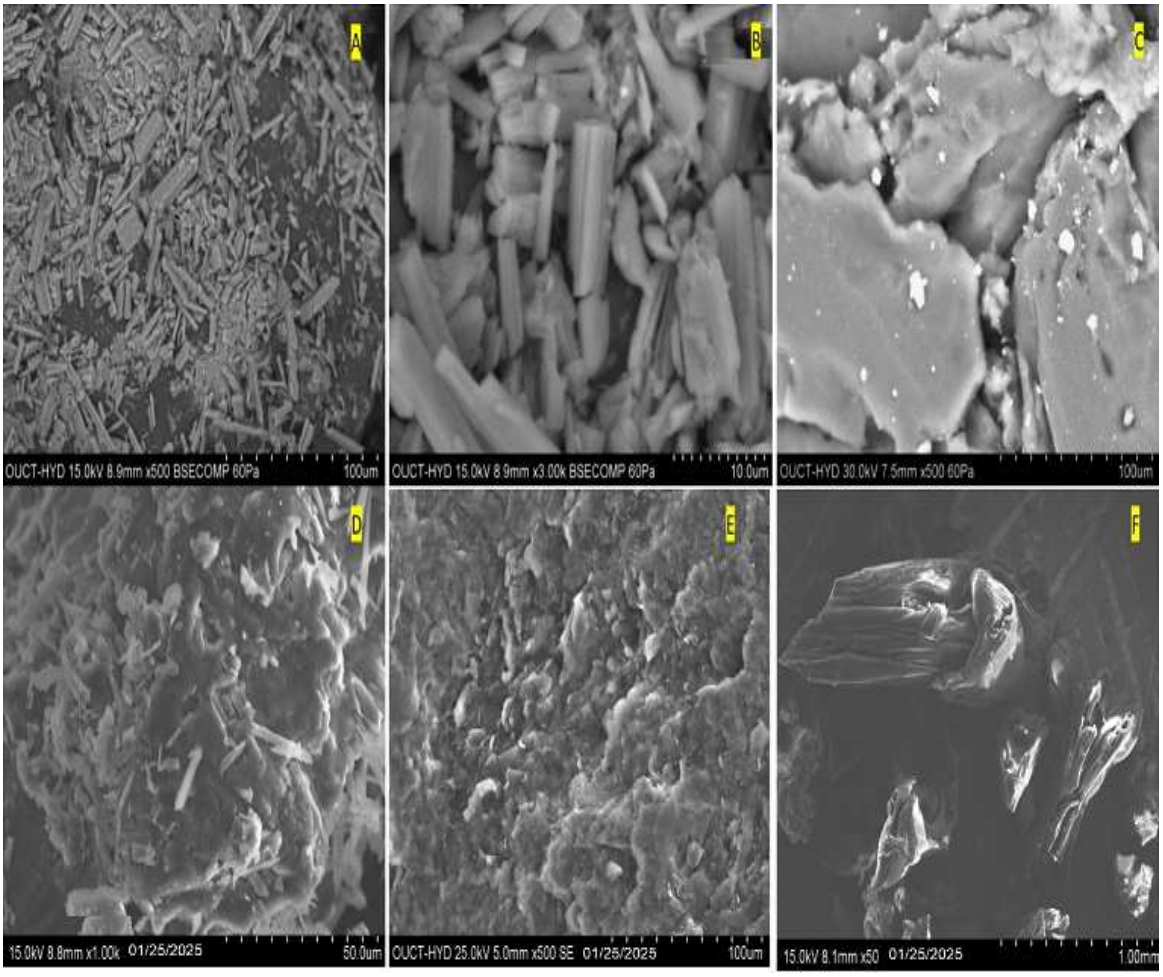

Figure 5. 38: SEM pictures of A) and B) pure drug of ATR and FNF, C) BSD with Kolliphor; D) BSD with Soluplus; E) TSD with Kollidon; F) TSD with PVP

5.8.5. Compatibility study

Figure 5. 40 depicts the determination of component compatibility through IR spectra analysis of the BSD and TSD, excipients, and drugs. The range of 400-4000 cm^{-1} was used to record the FTIR spectra. In the FTIR spectra of FNF, a variety of absorption bands could be identified, such as the C-H stretch (2984 cm^{-1}), ester carbonyl stretches (1725 cm^{-1}), carbonyl stretch (1648 cm^{-1}), benzene ring stretch (1597 cm^{-1}), and aryl ether (1286 cm^{-1}). Likewise,

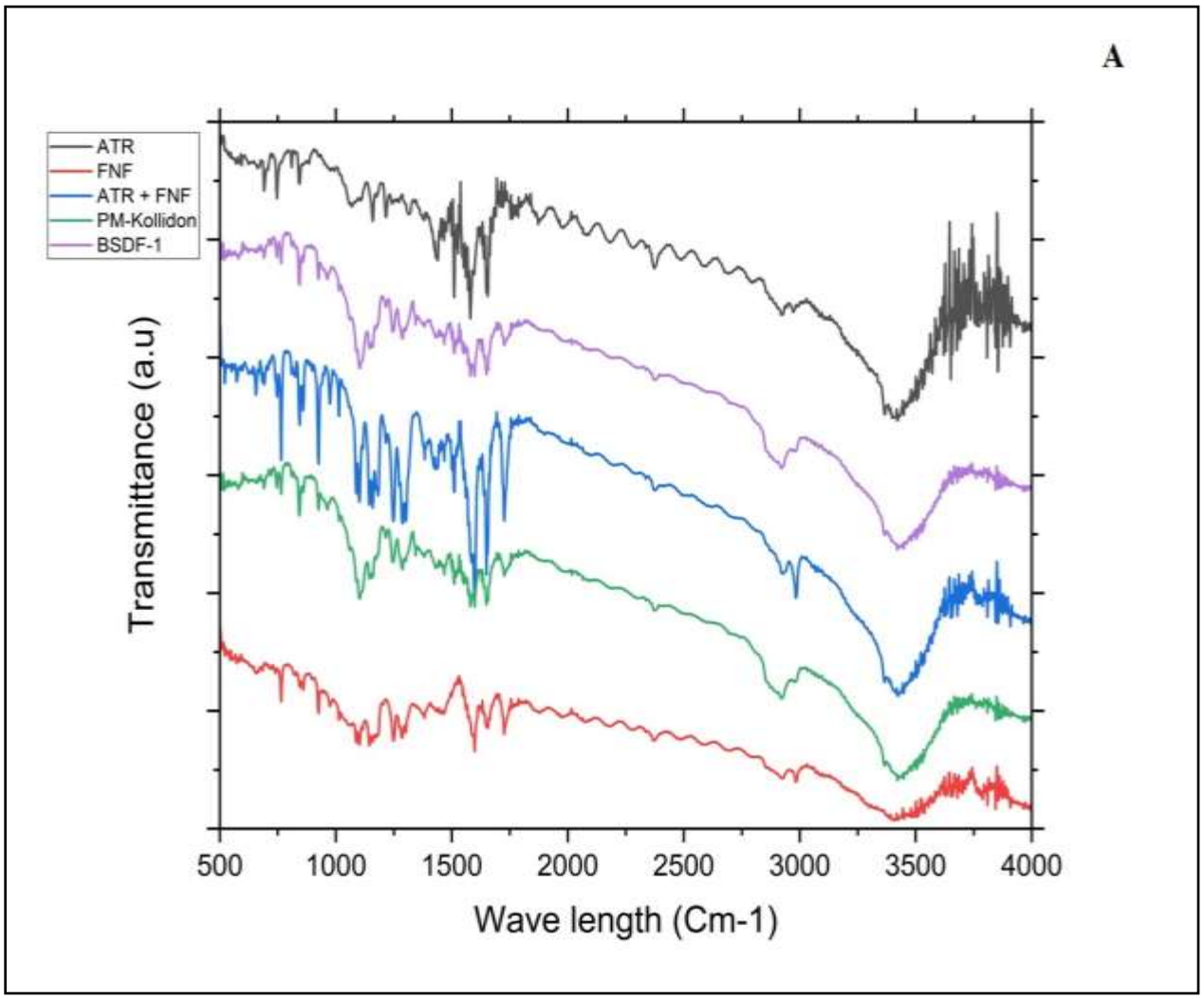

(A) BSD

the SIM showed absorption bands corresponding to stretching of O-H (3547 cm^{-1}), aliphatic C-H vibration (2951, 2930, 2872, and 1467 cm^{-1}), ester C=O vibrations

(1695 and 1266 cm^{-1}) and ester/lactone C-O-C oscillations (1162 cm^{-1}).The FTIR spectra of solid dispersion reflected a superimposition of bands from both drugs, and no additional bands or significant shifts were observed, confirming the absence of chemical interactions among the formulation components (Tipduangta *et al.,* 2015) (Choudhary *et al.,* 2012).

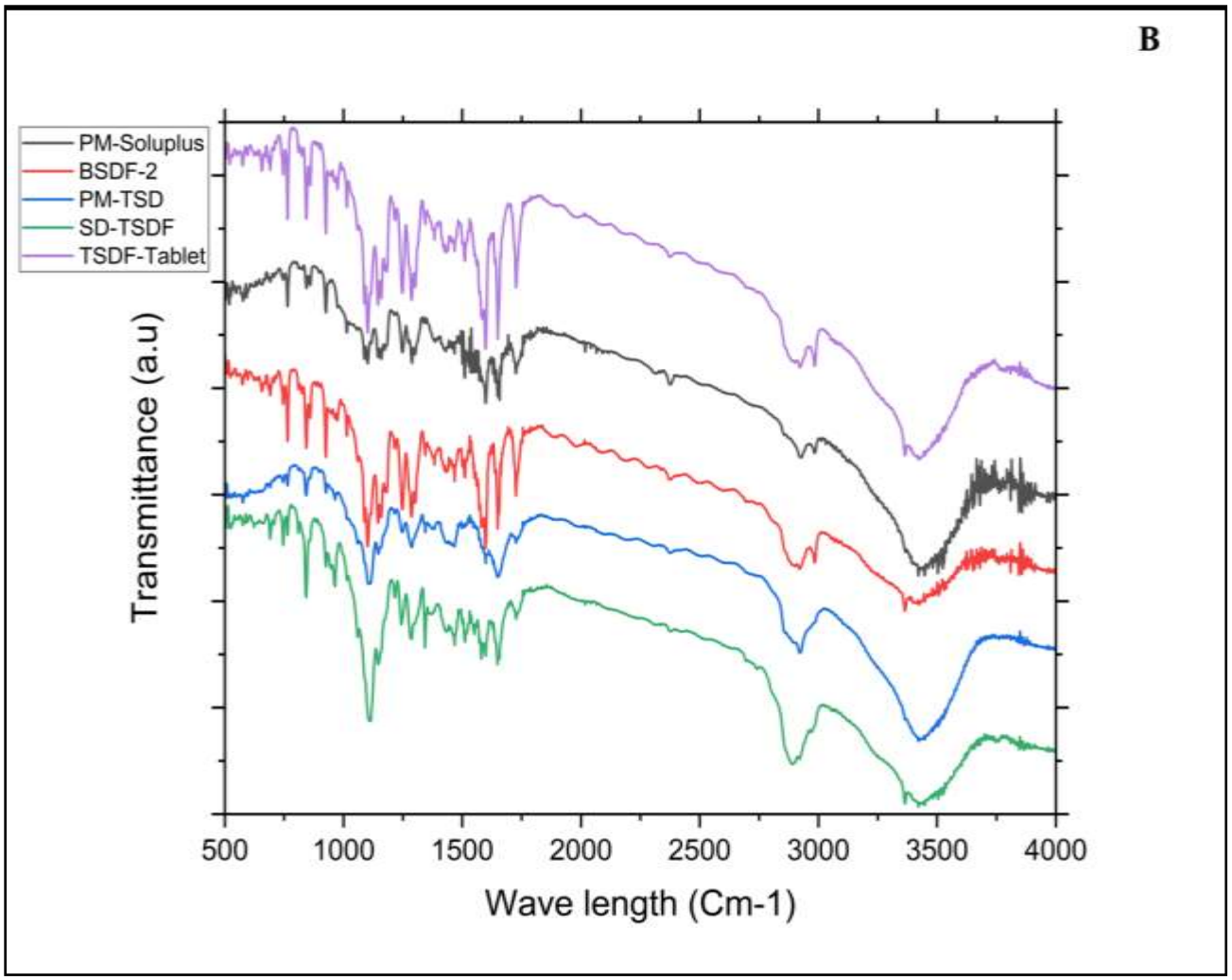

(B) TSD

Figure 5. 39: FT-IR of plain drugs (ATR, FNF), physical mixture, BSD, and TSD along with PM and combination plain drugs

5.8.6. DSC study

The thermal behavior of the optimized BSD, TSD, the physical mixture, and the pure drugs according to differential scanning calorimetry (DSC) is portrayed (Figure 5. 41). The ATR PD was reported to have a melting point of 128.18 and 240.23°C. The exceedingly crystalline structure of FNF PD was evidenced by its sharp melting endotherm at 83.65°C. The drugs have shown the characteristic peak in the physical mixture. Nonetheless, in BSD an endothermic peak at 84.03°C of the FNF with a reduced crystallinity and another peak at 237.28 °C indicating that ATR has undergone a signified amorphous nature and might have been covered by stabilizer acting as an inhibitor for further crystal growth. Since no new additional peaks are observed we can confirm that the drugs are chemically stable and no degradation products were formed and the same is reported by earlier authors (Górniak *et al.,* 2023) (Tipduangta *et al.,* 2015).

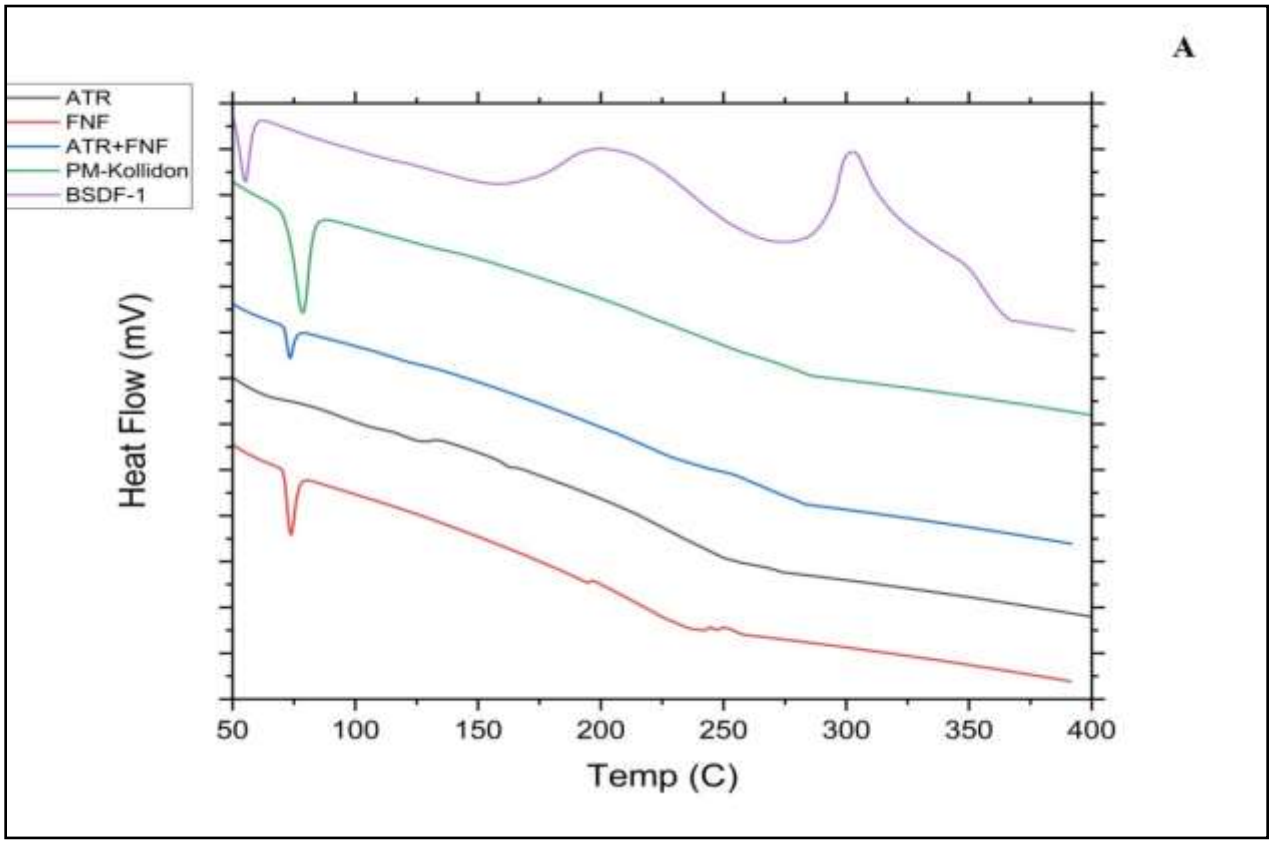

(A)

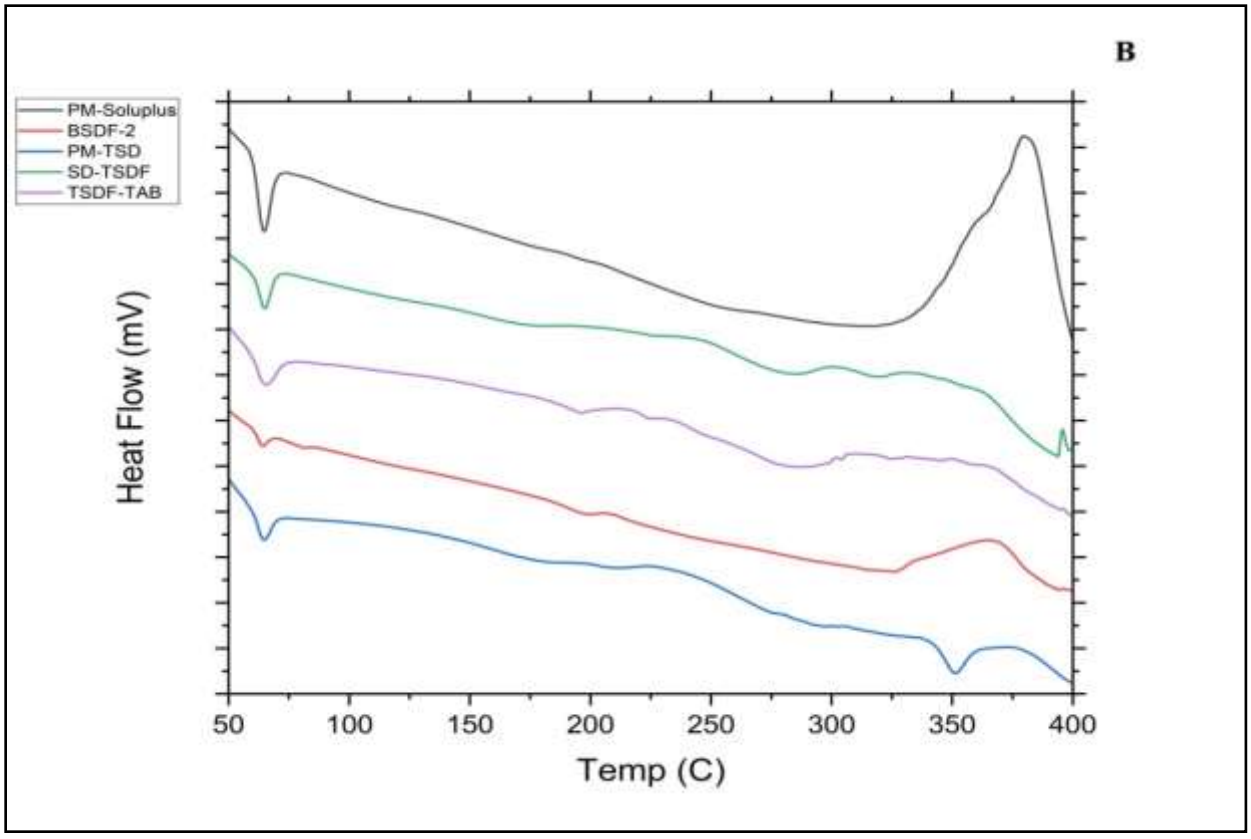

(B)

Figure 5. 40: DSC depiction of plain drugs, polymers, physical mixture, BSD, TSD and TSD-tablets

5.8.7. XRD (X-ray diffraction)

Another DSC pattern was observed with the pure FNF drug confirming the presence of solid peaks at different scattered 2_theta angles of 6.03, 11.04, 11.6, 12.35, and 14.11°, while the ATR drug showed firm diffraction peaks at 2.97, 5.98, 9.01, 9.34, 10.13, 11.7, and 12.05°. Similar diffraction peaks for the studied material have also been reported previously. However, the characteristic diffraction peaks of L-NS were observed at scattering angles of 2 theta 2.9, 5.96, 6.15, 8.95, 9.29, and 10.07, which elucidated a reduction in peak intensity compared to the pure drugs, confirming involvement of solid-state interaction at a molecular level due to the inclusion of stabilizer encasing (Górniak *et al.,* 2023) (Ajmera *et al.,* 2012). The XRD overlay is illustrated in Figure 5. 42.

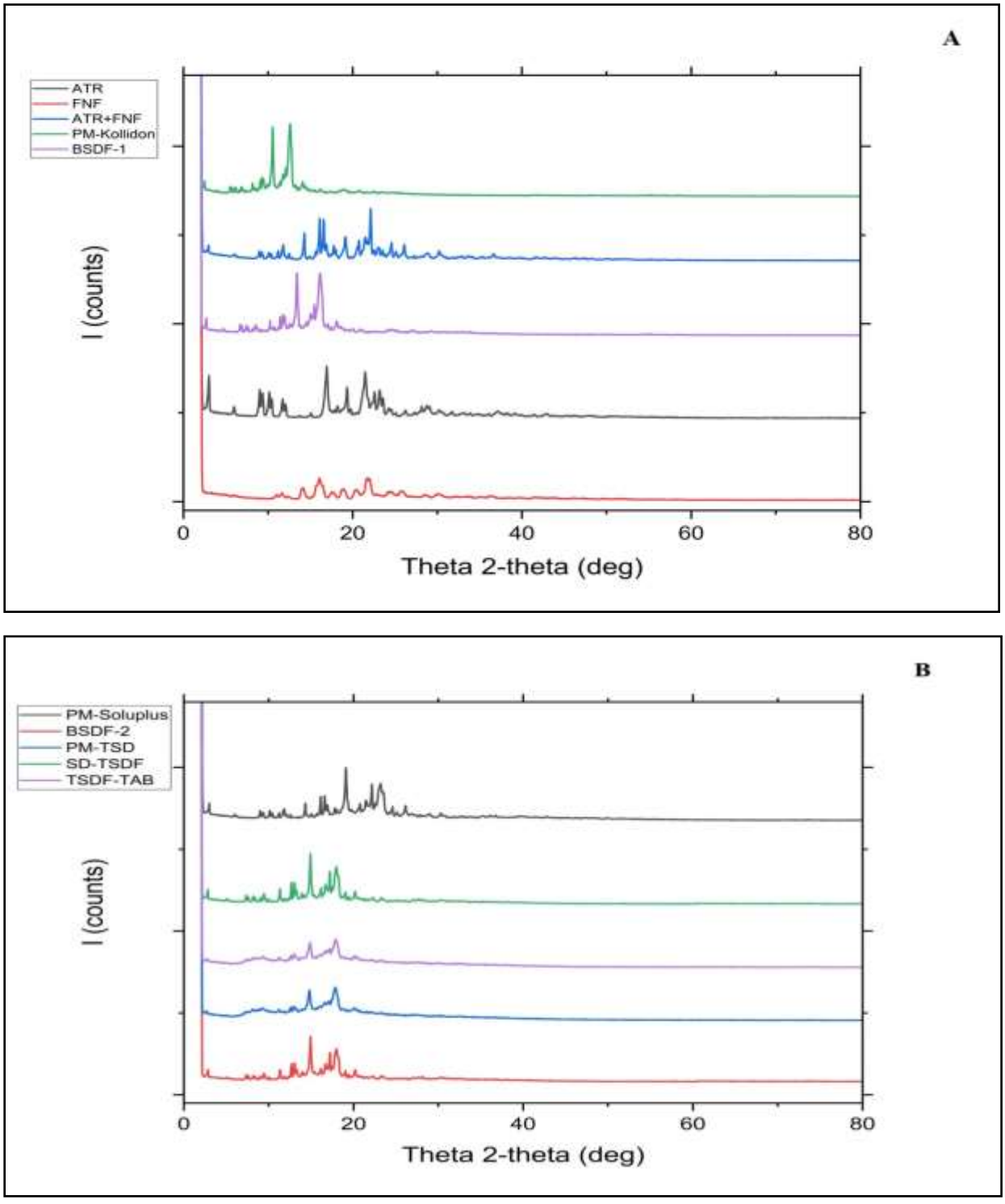

Figure 5. 41: XRD depicting the plain drugs, polymer, physical mixture, BSD, TSD, TSD-Tablet

5.8.9. Stability studies

Stability profile of ATR–FNF ternary solid dispersion

The stability evaluation of the dual-drug solid dispersion containing ATR and FNF was carried out under refrigerated (2–8 °C), room-temperature (25 °C), and accelerated (40 °C) conditions over a six-month period (0, 30, 90, and 180 days) (Table 5.34). Across all storage conditions, the formulation demonstrated overall physical and chemical stability, although the extent of variation differed with temperature. At 2–8 °C, the formulation remained most stable, with only marginal increases in particle size (188.5 to 192.9 nm) and a minimal rise in PDI, indicating that the TSD maintained a uniform and monodisperse distribution over the study duration. Zeta potential values remained sufficiently negative (–28.9 to –27.7 mV), reflecting preserved electrostatic stability and low risk of particle aggregation. Assay values for both drugs showed only slight reductions (ATR 99.1% to 98.1%; FNF 98.8% to 97.8%), while impurity levels increased only minimally, confirming limited degradation under refrigerated storage. Dissolution efficiency also remained largely unaffected, with both drugs maintaining >82% release at 30 mins over 180 days, suggesting no significant impact on drug-release performance (Figure 5.43).

At room temperature (25 °C), moderate changes were observed. Particle size showed a slightly greater increment (188.5 to 193.8 nm), accompanied by a small increase in PDI and a mild reduction in zeta potential (–28.9 to –27.0 mV). A slight turbidity appeared at 30 days, which stabilized thereafter, indicating minor structural stress on the TSD. Drug content exhibited a controlled decline but remained within acceptable limits (ATR 98.0%; FNF 97.7% at 180 days). Impurities rose moderately but predictably, reflecting temperature-dependent degradation kinetics. Dissolution showed a small but consistent reduction (~1.5–2%), yet remained above 81%, confirming that the formulation retained functional release behaviour at room temperature.

Under accelerated storage (40 °C), expectedly more pronounced changes occurred. Particle size increased to 195.7 nm, PDI values rose steadily, and zeta potential decreased to –26.0 mV, suggesting partial destabilization and early aggregation tendencies under

thermal stress. Visual inspection revealed slight haziness and mild turbidity over time. Chemical stability was more significantly impacted, with drug content showing the greatest decline (ATR to 96.9%; FNF to 96.6%) and impurity levels increasing substantially, indicating accelerated oxidative and hydrolytic degradation at higher temperatures. Correspondingly, dissolution performance decreased more sharply, dropping to ~78% at 180 days for both drugs, reflecting potential structural and physicochemical alterations in the TSD (Table 5.34).

Overall, the results confirm that the TSD maintains excellent stability under refrigerated and acceptable stability under room-temperature conditions, while accelerated conditions clearly promote degradation and affect dissolution. These findings support 2–8 °C as the optimal long-term storage condition to preserve particle integrity, drug content, and dissolution behaviour. The stability trends are consistent with typical TSD behaviour where higher temperatures increase mobility, facilitate degradation, and compromise colloidal stability. Thus, the formulation demonstrates robust stability characteristics suitable for further development, particularly when stored under refrigerated conditions.

Table 5. 34: Stability profile of ATR–FNF ternary solid dispersion

Parameter	**Initial (0 day)**	**30 days**	**90 days**	**180 days**
2–8 °C (refrigerated)				
Particle size (nm)	188.5 ± 4.50	189.7 ± 5.80	191.6 ± 3.40	192.9 ± 3.60
PDI	0.215 ± 0.012	0.219 ± 0.015	0.226 ± 0.018	0.230 ± 0.019
Zeta potential (mV)	−28.9 ± 1.6	−28.5 ± 1.5	−28.0 ± 1.6	−27.7 ± 1.4
Appearance	Clear, uniform	No visible change	No visible change	Stable

Assay ATR (%)	99.1 ± 0.3	98.9 ± 0.3	98.5 ± 0.4	98.1 ± 0.4
Assay FNF (%)	98.8 ± 0.3	98.6 ± 0.3	98.3 ± 0.3	97.8 ± 0.4
Impurity ATR (%)	0.11 ± 0.01	0.13 ± 0.01	0.17 ± 0.02	0.19 ± 0.02
Impurity FNF (%)	0.10 ± 0.01	0.12 ± 0.01	0.15 ± 0.02	0.17 ± 0.02
Dissolution ATR (% at 30 min)	83.2 ± 0.5	82.9 ± 0.5	82.5 ± 0.4	82.1 ± 0.4
Dissolution FNF (% at 30 min)	83.0 ± 0.5	82.8 ± 0.4	82.4 ± 0.4	82.2 ± 0.4
25 °C (Room temperature)				
Particle size (nm)	188.5 ± 4.50	191.0 ± 7.00	192.8 ± 6.80	193.8 ± 7.30
PDI	0.215 ± 0.012	0.224 ± 0.016	0.231 ± 0.021	0.235 ± 0.022
Zeta potential (mV)	−28.9 ± 1.6	−27.9 ± 1.7	−27.4 ± 1.5	−27.0 ± 1.6
Appearance	Clear, uniform	Slight turbidity	Stable	Stable
Assay ATR (%)	99.1 ± 0.3	98.7 ± 0.3	98.4 ± 0.4	98.0 ± 0.4
Assay FNF (%)	98.8 ± 0.3	98.3 ± 0.3	98.0 ± 0.4	97.7 ± 0.4
Impurity ATR (%)	0.11 ± 0.01	0.15 ± 0.02	0.20 ± 0.02	0.22 ± 0.02
Impurity FNF (%)	0.10 ± 0.01	0.14 ± 0.02	0.18 ± 0.02	0.21 ± 0.02
Dissolution ATR (% at 30 min)	83.2 ± 0.5	82.6 ± 0.5	82.1 ± 0.4	81.5 ± 0.4
Dissolution FNF (% at 30 min)	83.0 ± 0.5	82.5 ± 0.4	82.0 ± 0.4	81.6 ± 0.4

40 °C (accelerated)				
Particle size (nm)	188.5 ± 4.50	191.8 ± 6.20	194.0 ± 4.50	195.7 ± 4.90
PDI	0.215 ± 0.012	0.228 ± 0.018	0.239 ± 0.022	0.252 ± 0.024
Zeta potential (mV)	−28.9 ± 1.6	−27.2 ± 1.5	−26.6 ± 1.8	−26.0 ± 1.7
Appearance	Clear	Slight haziness	Mild turbidity	Mild turbidity
Assay ATR (%)	99.1 ± 0.3	98.4 ± 0.4	97.6 ± 0.5	96.9 ± 0.5
Assay FNF (%)	98.8 ± 0.3	98.0 ± 0.4	97.4 ± 0.5	96.6 ± 0.5
Impurity ATR (%)	0.11 ± 0.01	0.19 ± 0.02	0.31 ± 0.03	0.43 ± 0.03
Impurity FNF (%)	0.10 ± 0.01	0.16 ± 0.02	0.27 ± 0.03	0.35 ± 0.03
Dissolution ATR (% at 30 min)	83.2 ± 0.5	81.9 ± 0.6	79.8 ± 0.7	77.9 ± 0.8
Dissolution FNF (% at 30 min)	83.0 ± 0.5	81.6 ± 0.6	79.5 ± 0.7	77.6 ± 0.8

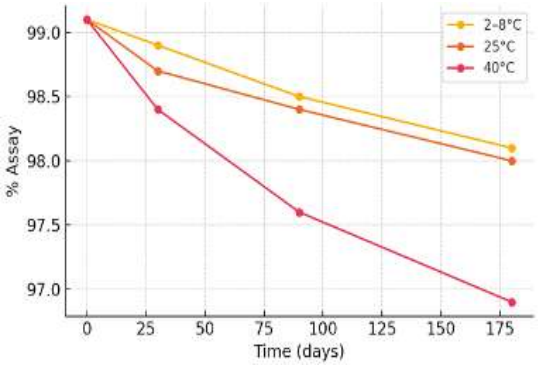

ATR Content (% Assay) Over 6 Months

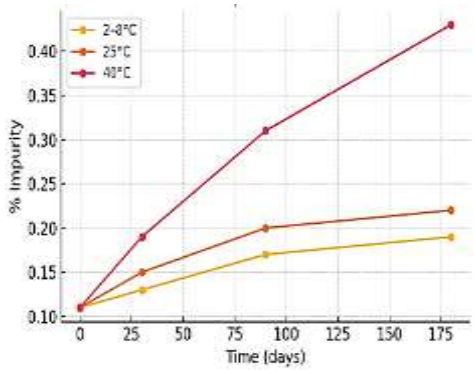

ATR Impurities Over 6 Months

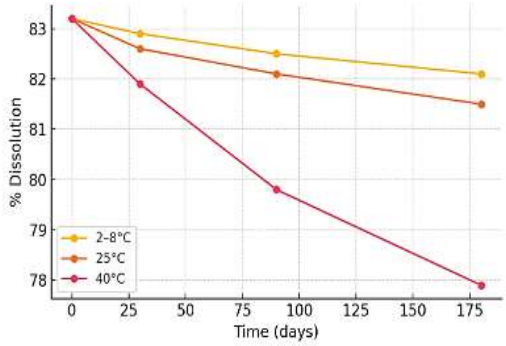

ATR Dissolution (% at 30 min) Over 6 Months

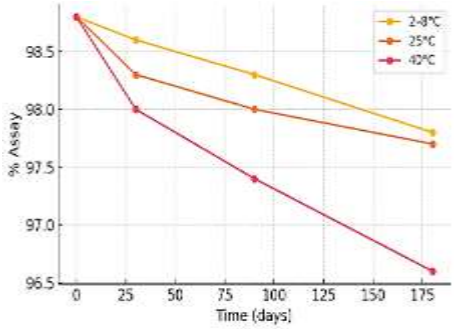

FNF Content (% Assay) Over 6 Months

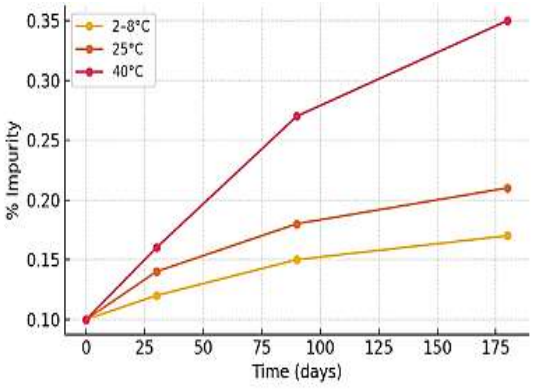

FNF Impurities Over 6 Months

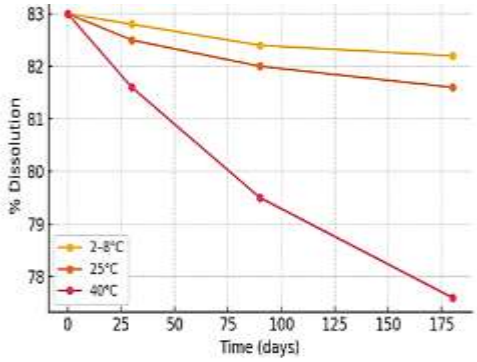

FNF Dissolution (% at 30 min) Over 6 Months

Figure 5. 42: Stability profile of ATR–FNF ternary solid dispersion

Stability profile of ATR–FNF binary solid dispersion

The binary solid dispersion demonstrated temperature-dependent stability behavior over six months (Table 5.35, Figure 5.44). Under refrigerated conditions (2–8 °C) the formulation retained excellent physical and chemical integrity: particle size increased only marginally (≈187.9 to 192.2 nm), PDI and zeta potential showed minimal changes, drug assays remained high (ATR 99.0% → 98.0%; FNF 98.7% → 97.7%), impurities rose slightly (ATR 0.12% → 0.18%; FNF 0.11% → 0.17%) and dissolution at 30 mins was largely preserved (>82%), indicating that the solid dispersion matrix effectively stabilized both drugs at low temperature. At 25 °C small but noticeable changes were observed: particle size and PDI increased modestly, a transient turbidity at 30 days suggested minor physical stress, and assays declined more than under refrigeration (ATR 99.0% → 97.9%; FNF 98.7% → 97.6%) while impurities increased correspondingly; dissolution decreased mildly (~1–1.5%), implying limited influence on release performance but indicating that room temperature storage accelerates slow degradation pathways compared to refrigerated storage. Accelerated conditions (40 °C) produced the most pronounced effects: particle size and PDI increased substantially, zeta potential became less negative, visual haziness/turbidity developed, and assays decreased to ~96.7% (ATR) and ~96.5% (FNF) at 180 days with a marked rise in impurities (ATR 0.12% → 0.42%; FNF 0.11% → 0.36%); dissolution profiles dropped more sharply to ~77–78% at 30 mins, indicating thermally accelerated degradation, possible recrystallization or excipient–drug interactions that reduce wettability or increase drug crystallinity, and compromised release kinetics. Collectively, these data indicate that while the binary solid dispersion provides robust stabilization at refrigerated storage and acceptable performance at room temperature for at least six months, elevated temperatures significantly compromise both chemical purity and dissolution — supporting recommended storage at 2–8 °C for long-term stability and highlighting the need for inclusion of antioxidants/humidity controls or formulation optimization if ambient storage is desired.

Table 5. 35: Stability profile of ATR–FNF binary solid dispersion

Parameter	Initial (0 day)	30 days	90 days	180 days
2–8 °C (refrigerated)				
Particle size (nm)	187.9 ± 4.30	189.1 ± 5.50	191.0 ± 3.80	192.2 ± 3.40
PDI	0.213 ± 0.011	0.217 ± 0.014	0.224 ± 0.017	0.229 ± 0.018
Zeta potential (mV)	−28.7 ± 1.5	−28.3 ± 1.5	−27.9 ± 1.5	−27.6 ± 1.3
Appearance	Clear, uniform	No visible change	No visible change	Stable
Assay ATR (%)	99.0 ± 0.3	98.8 ± 0.3	98.4 ± 0.4	98.0 ± 0.4
Assay FNF (%)	98.7 ± 0.3	98.5 ± 0.3	98.2 ± 0.3	97.7 ± 0.4
Impurity ATR (%)	0.12 ± 0.01	0.14 ± 0.01	0.16 ± 0.02	0.18 ± 0.02
Impurity FNF (%)	0.11 ± 0.01	0.13 ± 0.01	0.14 ± 0.02	0.17 ± 0.02
Dissolution ATR (% at 30 min)	83.5 ± 0.5	83.0 ± 0.5	82.6 ± 0.4	82.3 ± 0.4
Dissolution FNF (% at 30 min)	83.1 ± 0.5	82.9 ± 0.4	82.5 ± 0.4	82.1 ± 0.4
25 °C (room temperature)				
Particle size (nm)	187.9 ± 4.30	191.4 ± 6.80	193.3 ± 6.60	194.2 ± 7.10
PDI	0.213 ± 0.011	0.223 ± 0.016	0.230 ± 0.020	0.236 ± 0.021
Zeta potential (mV)	−28.7 ± 1.5	−27.8 ± 1.6	−27.3 ± 1.5	−26.9 ± 1.6

Appearance	Clear, uniform	Slight turbidity	Stable	Stable
Assay ATR (%)	99.0 ± 0.3	98.6 ± 0.3	98.3 ± 0.4	97.9 ± 0.4
Assay FNF (%)	98.7 ± 0.3	98.2 ± 0.3	97.9 ± 0.4	97.6 ± 0.4
Impurity ATR (%)	0.12 ± 0.01	0.16 ± 0.02	0.21 ± 0.02	0.23 ± 0.02
Impurity FNF (%)	0.11 ± 0.01	0.15 ± 0.02	0.19 ± 0.02	0.22 ± 0.02
Dissolution ATR (% at 30 min)	83.5 ± 0.5	82.7 ± 0.5	82.0 ± 0.4	81.4 ± 0.4
Dissolution FNF (% at 30 min)	83.1 ± 0.5	82.4 ± 0.4	81.9 ± 0.4	81.5 ± 0.4
40 °C (accelerated)				
Particle size (nm)	187.9 ± 4.30	191.5 ± 6.10	193.8 ± 4.80	196.2 ± 5.00
PDI	0.213 ± 0.011	0.230 ± 0.018	0.241 ± 0.021	0.255 ± 0.025
Zeta potential (mV)	−28.7 ± 1.5	−27.0 ± 1.5	−26.4 ± 1.7	−25.9 ± 1.7
Appearance	Clear	Slight haziness	Mild turbidity	Mild turbidity
Assay ATR (%)	99.0 ± 0.3	98.3 ± 0.4	97.5 ± 0.5	96.7 ± 0.5
Assay FNF (%)	98.7 ± 0.3	97.9 ± 0.4	97.3 ± 0.5	96.5 ± 0.5
Impurity ATR (%)	0.12 ± 0.01	0.18 ± 0.02	0.30 ± 0.03	0.42 ± 0.03
Impurity FNF (%)	0.11 ± 0.01	0.17 ± 0.02	0.26 ± 0.03	0.36 ± 0.03
Dissolution ATR (% at 30 min)	83.5 ± 0.5	81.8 ± 0.6	79.7 ± 0.7	77.8 ± 0.7

Dissolution FNF (% at 30 min)	83.1 ± 0.5	81.5 ± 0.6	79.4 ± 0.7	77.5 ± 0.7

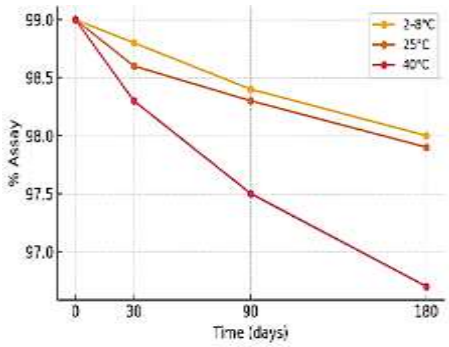

ATR Content (% Assay) Over 6 Months

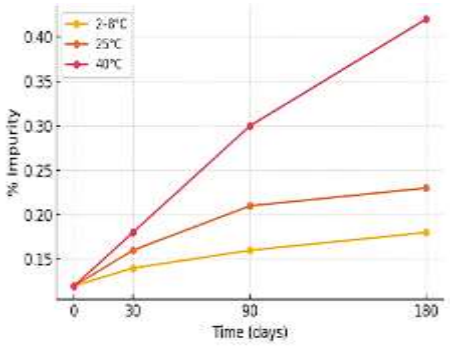

ATR Impurities Over 6 Months

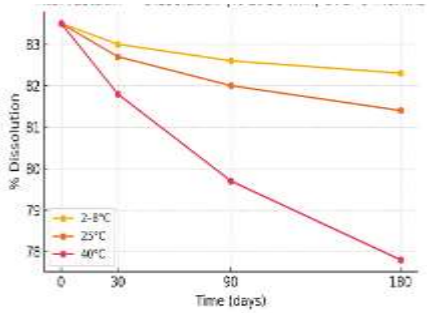

ATR Dissolution (% at 30 min) Over 6 Months

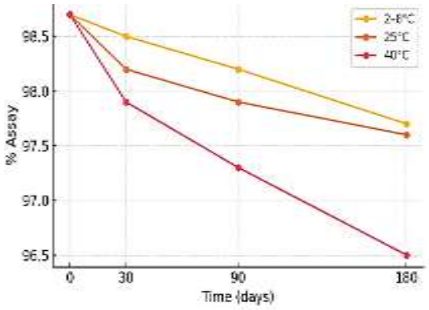

FNF Drug Content (% Assay) Over 6 Months

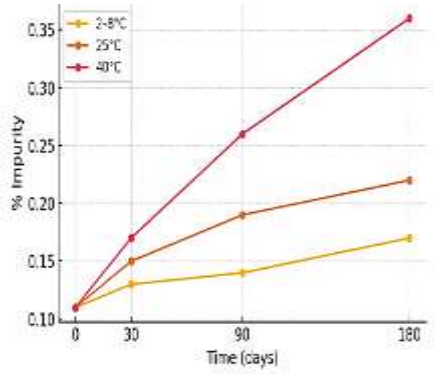

FNF Impurities Over 6 Months

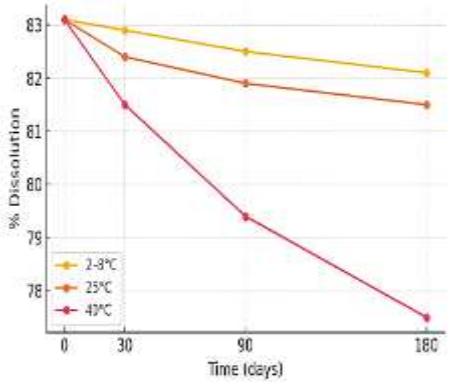

FNF Dissolution (% at 30 min) Over 6 Months

Figure 5. 43: Stability profile of ATR–FNF binary solid dispersion

5.8.10. HPLC method

Exploration of pharmacokinetic parameters

Pharmacokinetic studies

The plasma concentration versus time curve after an oral administration of the optimized nanosuspension and a commercial PD solution (0.25% w/v HPMC) is shown in Figure 5. 45. The related pharmacokinetic information is given in Table 5. 36 and 5.37.

Table 5. 36: *In vivo* release studies in animals following oral administration of plain drugs (ATR, FNF), and TSD

Time (hr)	PD (ATR)	PD (FNF)	TSD (ATR)	TSD (FNF)
0	0	0	0	0
0.25	408.22±66.13	388.98±51.26	1268.07±293.78	2027.9±205.22
0.5	946.65±83.06	779.1±79.45	2629.33±214.9	3128.58±160.18
0.75	1248.12±94.2	1190.92±61.02	3804.18±251.04	4250.25±189.28
1	1883.64±180.33	1742.49±290.8	4407.24±399.71	5140.06±208.4

2	1229.56±102.55	1346.4±155.08	5410.62±521.04	6216.19±428.19
3	1003.34±90.21	1133.8±89.17	3101.49±378.2	4425.3±340.56
4	846.33±60.83	945.87±220.31	1155.02±222.69	2318.04±126.29
6	458.44±46.69	393.58±99.2	701.29±138.58	1120.13±103.68
8	248.22±39.03	167.34±44.81	338.16±89.1	570.1±36.82

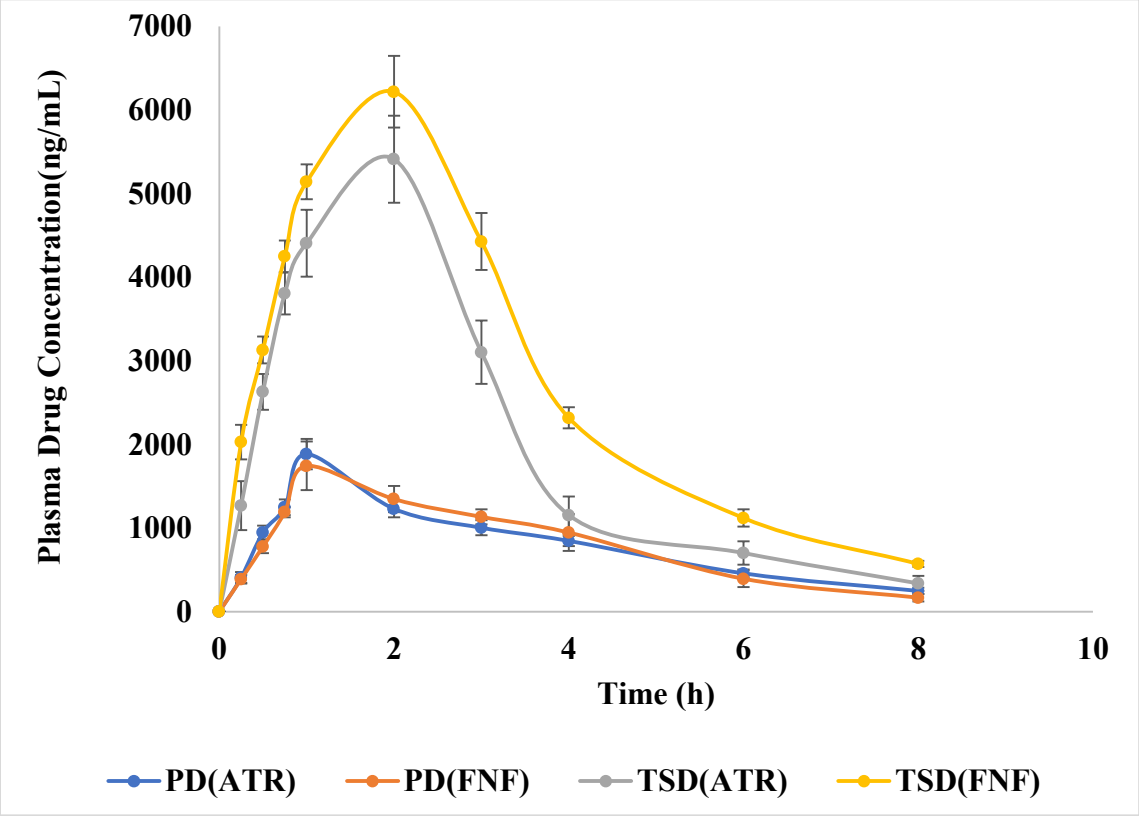

Figure 5. 44: *In vivo* release studies in animals following oral administration of plain drugs (ATR, FNF), and TSD

Table 5. 37: PK data for plain ATR, FNF and for TSD

Parameters	Plain drug		Nanosuspension formulation	
	ATR	**FNF**	**TSD (ATR)**	**TSD (FNF)**
C_{max} (ng/mL)	1883.64 ± 242.93	1742.49± 229.91	5410.62 ± 466.75	6216.19± 404.19
T_{max} (h)	1	1	2	2
Half-life (h)	2.26 ± 0.61	1.60 ± 0.34	2.25± 0.80	1.97± 0.33
AUC_{0-t} (ng.h/mL)	6495.51 ± 680.98	6532.311 ±186.34	16665.3± 450.82	22493.1 ± 590.17
$AUC_{0-\infty}$ (ng.h/mL)	7304.978 ± 566.2	6918.7604 ±385.52	17766.48112 ± 531.20	24118.891 ±502.17
MRT(h)	3.92 ± 01.21	3.36 ± 00.87	3.06 ± 0.86	3.30 ±0.94
Ke	0.306	0.433	0.3070	0.350

In comparison to unformulated pure drug, kinetics exhibited higher values of C_{max} (2.87-fold) and AUC_{0-24hr}(2.56-fold) for ATR solid dispersion, while for FNF nanoformulation an increase in the value of C_{max} (3.56-fold) and AUC_{0-24hr}(3.44-fold) was evident. It is due to the conversion of crystalline form to amorphous that may facilitate solubility and possibly improved drug release concentration gradient across the GIT and blood walls (Górniak *et al.,* 2023) (Ajmera *et al.,* 2012).

5.9. Comparison of optimised formulation of nanosuspension and solid dispersions

The comparative *in vitro* drug release profile clearly demonstrated the superior performance of binary and ternary solid dispersions as well as nanosuspensions when evaluated against the pure drug forms of ATR and FNF in phosphate buffer pH 7.4. The plain drugs exhibited markedly poor dissolution, releasing only 29.31 ± 3.44% (ATR) and 20.26 ± 2.14% (FNF) after two hours, which correlates with their inherent

hydrophobicity and crystalline nature that limit aqueous solubility. The initial release within the first 30 mins was similarly minimal, with pure ATR and FNF releasing merely 11.48 ± 4.91% and 10.24 ± 1.03%, respectively.

In contrast, both binary solid dispersions (BSD) and ternary solid dispersions (TSD) displayed significantly enhanced dissolution behaviour. The optimized BSD formulations released more than 86% of the drug within two hours, with ATR formulation SF8 achieving 86.25 ± 5.56% and FNF showing 91.72 ± 6.27% release. TSD systems performed even better, achieving nearly complete release, with ATR (KDF11) reaching 98.44 ± 2.56% and FNF reaching 99.25 ± 3.07% within the same period. This enhancement in dissolution can be ascribed to the transformation of the crystalline drug into an amorphous form during dispersion preparation, which improved wettability, reduced crystallinity, and facilitated faster dissolution.

The nanosuspension (L-NS) formulations showed the most rapid onset of drug release. More than 45% of ATR and FNF was released within the first 15 mins, and the two-hour release exceeded 98% for both drugs (ATR: 99.23 ± 12.06%; FNF: 98.66 ± 11.44%). Such exceptional improvement is associated with the significant reduction in particle size to the nanometre range, an increase in surface area, and the presence of stabilizing surfactants that prevent aggregation and maintain the drug in a highly soluble, amorphous state. Collectively, the results confirmed that all advanced formulation approaches—BSD, TSD, and L-NS—demonstrated a substantial enhancement in drug dissolution compared to the pure drug, with nanosuspensions providing the most instantaneous release, and ternary solid dispersions achieving the most controlled yet complete release (Table 5.38).

Table 5. 38: Drug release profiles of ATR and FNF from pure drug, solid dispersions (BSD/TSD), and nanosuspensions (L-NS)

Formulation type	Drug	% Drug release (0.5 h)	% Drug release (2 h)	Key observation
Pure drug (PD)	ATR	11.48 ± 4.91	29.31 ± 3.44	Poor aqueous solubility; minimal release.
	FNF	10.24 ± 1.03	20.26 ± 2.14	Slow dissolution due to highly crystalline structure.
Binary Solid Dispersion (BSD)	ATR	—	86.25 ± 5.56 (SF8)	Significant improvement due to amorphization and enhanced wettability.
	FNF	—	91.72 ± 6.27	Better carrier interaction increased solubility.
Ternary Solid Dispersion (TSD)	ATR	—	98.44 ± 2.56 (KDF11)	Nearly complete release; superior miscibility with ternary polymer–surfactant system.
	FNF	—	99.25 ± 3.07	Maximum release among SD systems.
Nanosuspension (L-NS)	ATR	>45%	99.23 ± 12.06	Rapid and complete release owing to nanosizing and surfactant stabilization.
	FNF	>45%	98.66 ± 11.44	Highly enhanced dissolution due to reduced particle size and amorphous state.

5.10. Dispersible tablets

The pre-compression parameters indicated good flowability of the powder blends, with Carr's index ranging between 12-16% and Hausner ratio between 1.12-1.19, suggesting suitability for direct compression (Alshehri *et al.,* 2015).

The prepared dispersible tablet formulations (F1 to F5) were estimated for various physical and performance parameters to ensure quality and consistency (Kukulka *et al.,* 2016). All formulations exhibited acceptable weight variation within pharmacopoeial limits, with values ranging from 519 ± 3.0 mg to 520 ± 2.8 mg. The tablet hardness was found to be between 6.4 ± 0.2 and 6.6 ± 0.3 kg/cm², indicating adequate mechanical strength. The thickness remained uniform across all batches, ranging from 5.1 ± 0.1 mm to 5.3 ± 0.1 mm. Friability was well below 1% for all formulations, confirming good tablet durability.

Notably, the disintegration and wetting times decreased progressively from F1 to F5, suggesting improved dispersibility with higher levels of superdisintegrant or optimized excipient composition (Szymańska-Chargot *et al.,* 2011). F5 demonstrated the shortest disintegration time (22 ± 1 sec) and wetting time (25 ± 1 sec). The water absorption ratio increased accordingly, reaching up to $85 \pm 2\%$ for F5. Drug content uniformity across all formulations was within acceptable limits, with F5 showing the highest content at $99.5 \pm 0.3\%$, confirming accurate dosage and uniform distribution of the active ingredient. These findings indicate that all formulations meet the standard quality parameters, with F5 exhibiting the most promising characteristics for rapid disintegration and drug release (Table 5. 39).

Table 5. 39: Post-compression evaluation of dispersible tablets

Parameter	F1	F2	F3	F4	F5
Weight variation (mg)	500 ± 2.5	505 ± 3.0	510 ± 2.0	515 ± 2.8	**520 ± 2.2**
Hardness (kg/cm²)	6.5 ± 0.2	6.6 ± 0.3	6.4 ± 0.2	6.5 ± 0.3	**6.6 ± 0.2**
Thickness (mm)	5.2 ± 0.1	5.1 ± 0.1	5.2 ± 0.1	5.3 ± 0.1	**5.2 ± 0.1**

Friability (%)	**0.45 ± 0.05**	**0.42 ± 0.04**	**0.44 ± 0.03**	**0.43 ± 0.05**	**0.41 ± 0.04**
Disintegration time (sec)	**35 ± 2**	**30 ± 2**	**28 ± 2**	**25 ± 1**	**22 ± 1**
Wetting time (sec)	15 ± 2	15 ± 2	15 ± 2	15 ± 1	**15 ± 1**
Water absorption ratio (%)	70 ± 2	75 ± 2	78 ± 2	80 ± 2	**85 ± 2**
Content uniformity (%)	98.5 ± 0.5	99.0 ± 0.4	98.8 ± 0.3	99.2 ± 0.4	**99.5 ± 0.3**

The *in vitro* drug release profile of all five formulations (F1–F5) was evaluated over a period of 120 mins using a phosphate buffer (pH 7.4) as the dissolution medium. The cumulative percentage drug release was recorded at specified time intervals, and values were expressed as mean ± standard deviation (SD) for each formulation (Table 5.40). A consistent and progressive increase in drug release was observed over time for all formulations. Among them, F5 exhibited the fastest and most complete release, achieving 100% drug release within 90 mins, with minimal variability (1.44 SD), indicating excellent dissolution behavior (Daniel and Astruc, 2004).

In contrast, F1 displayed a slower release profile, reaching only 94 ± 1.39% at 120 mins, while intermediate formulations (F2, F3, F4) showed correspondingly gradual improvements (Gill *et al.,* 2008). These differences in drug release can be attributed to variations in excipient composition and disintegration characteristics (Figure 5.46 and 5.47). The release kinetics suggest that formulation F5 offers the most optimized and efficient drug delivery, likely due to improved tablet wettability, disintegration time, and water absorption properties (Blagden *et al.,* 2007).

Table 5. 40: A) Cumulative % ATR DR & the marketed Febator-20 (mean & SD)

Time (min)	F1	F2	F3	F4	F5	Febator-20
5	30 (1.15)	35 (1.46)	40 (0.52)	45.0 (0.62)	**50.0 (0.96)**	**12 (0.84)**
10	50 (1.22)	55 (0.88)	60 (1.33)	65.0 (1.14)	**70.0 (1.07)**	**20 (1.02)**
15	65 (1.10)	70 (1.30)	75 (1.28)	80.0 (0.64)	**85.0 (0.52)**	**28 (1.15)**
20	75 (1.04)	80 (1.03)	85 (1.37)	90.0 (1.44)	**95.0 (1.12)**	**36 (1.20)**
30	85 (0.92)	90 (1.07)	95 (1.48)	98.0 (1.02)	**99.0 (1.11)**	**48 (1.10)**
60	**90 (1.15)**	**93 (1.43)**	**97 (1.30)**	**99.0 (0.91)**	**99.5 (1.12)**	**68 (1.32)**
90	92 (0.94)	95 (0.57)	98 (0.96)	99.5 (0.76)	**100.0 (1.44)**	**82 (1.27)**
120	94 (1.39)	97 (0.59)	99 (1.28)	100.0 (1.27)	**100.0 (1.18)**	**92 (1.14)**

B) Cumulative % FNF DR & the marketed Febator-20 (mean & SD)

Time (min)	F1	F2	F3	F4	F5	Febator-20
5	30 (1.05)	35 (1.40)	40 (0.52)	45.0 (0.62)	**50.0 (0.96)**	**10 (0.82)**
10	50 (1.22)	55 (0.88)	60 (1.33)	65.0 (1.14)	**70.0 (1.07)**	**18 (1.00)**
15	65 (1.10)	70 (1.29)	75 (1.28)	80.0 (0.64)	**85.0 (0.52)**	**26 (1.18)**
20	75 (1.04)	80 (1.03)	85 (1.37)	90.0 (1.44)	**95.0 (1.12)**	**34 (1.21)**
30	**85 (0.92)**	**90 (1.07)**	**95 (1.48)**	**98.0 (1.02)**	**99.0 (1.11)**	**46 (1.09)**
60	90 (1.15)	93 (1.43)	97 (1.30)	99.0 (0.91)	**99.5 (1.12)**	**65 (1.28)**
90	92 (0.94)	95 (0.57)	98 (0.96)	99.5 (0.76)	**100.0 (1.44)**	**80 (1.22)**
120	94 (1.39)	97 (0.59)	99 (1.28)	100.0 (1.27)	**100.0 (1.18)**	**90 (1.10)**

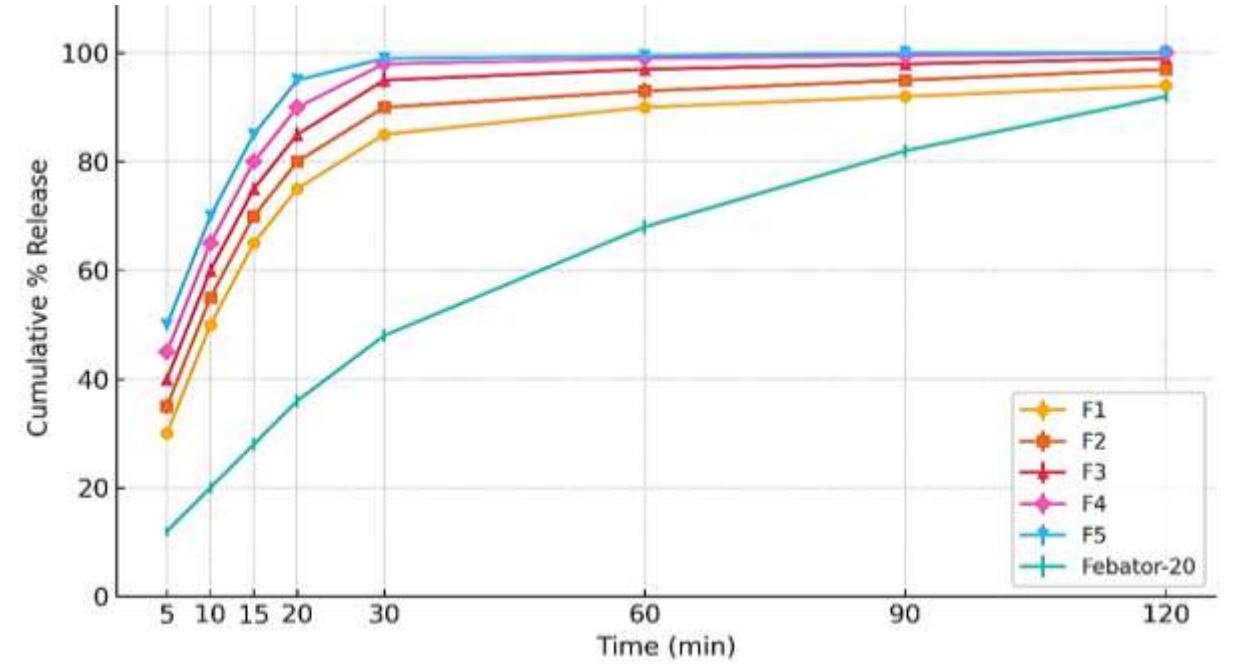

Figure 5. 45: Cumulative ATR drug release from dispersible tablets the marketed coated tablet Febator-20

The *in vitro* dissolution profile of the dispersible formulations (F1–F5) demonstrates markedly faster release of ATR compared with the marketed coated tablet Febator-20. Formulation F5 exhibits complete release by 90 mins, whereas Febator-20 shows a delayed release trajectory, achieving approximately 92% release only at 120 mins. This slower release of Febator-20 is consistent with the presence of a film-coating that retards hydration and tablet disintegration, producing a more sustained release profile. The superior early release exhibited by the dispersible formulation is likely attributable to rapid wetting and disintegration characteristics, which favor faster drug availability and may translate to a quicker onset of action *in vivo* compared with the coated marketed product.

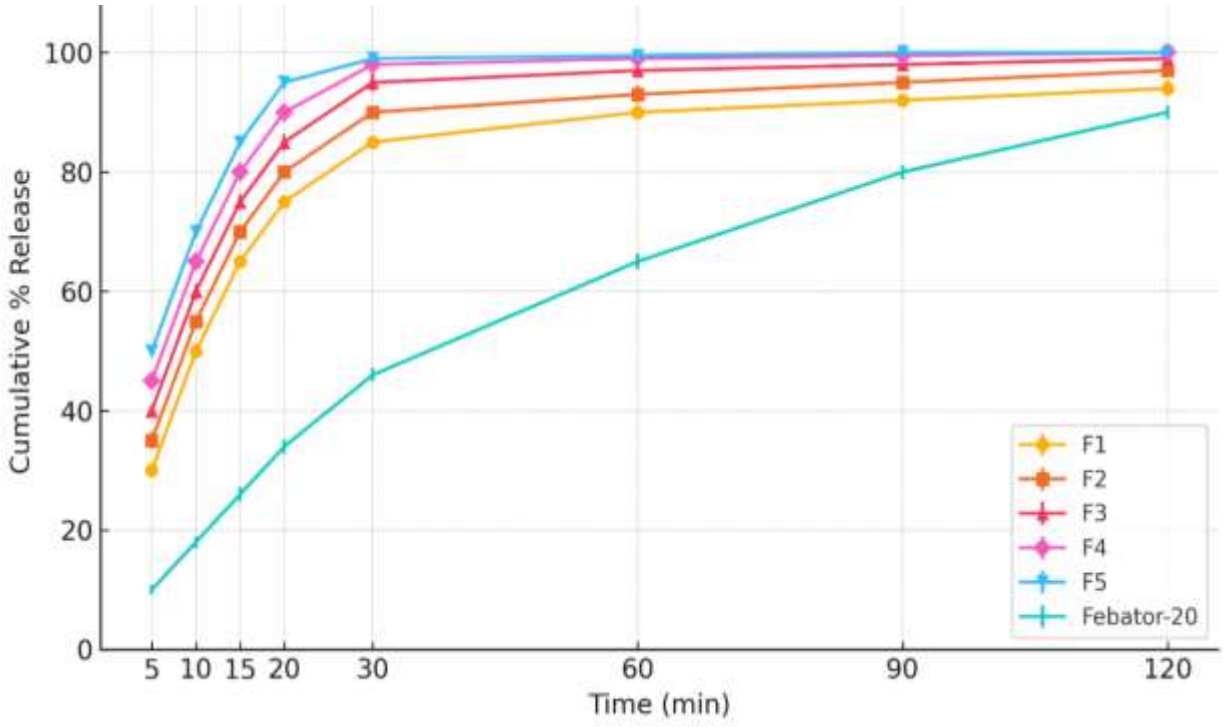

Figure 5. 46: Cumulative FNF drug release from dispersible tablets the marketed coated tablet Febator-20

Similarly, FNF release from the dispersible tablets was substantially faster than from Febator-20. The optimized dispersible formulation (F5) reached near-complete FNF release by 90 mins, while Febator-20 released only about 90% at 120 mins. The coating on Febator-20 delays the liquid penetration and dissolution of the active pharmaceutical ingredients, resulting in a prolonged release (Table 5.41). From a formulation perspective, the dispersible tablets provide enhanced immediate release, which could be advantageous where rapid systemic exposure is desired; conversely, the coated marketed product may be preferred when a moderated release is intended to reduce peak-related adverse effects or to achieve a prolonged therapeutic window.

Stability evaluation demonstrated that the Formulation F5 remained stable under accelerated storage conditions over a 6-month period (Kumar *et al.,* 2011). There were minimal changes in the physical and chemical properties of the tablets, including weight variation, hardness, friability, disintegration time, wetting time, drug content uniformity,

dissolution, and percentage purity. Additionally, the dissolution profile showed no significant decline, ensuring the continued effectiveness of the formulation over time (Tambe *et al.,* 2019).

Table 5. 41: Stability profile of optimized ATR (20 mg) and FNF (145 mg) dispersible tablets

Parameter	**Storage condition**	**Initial**	**1 month**	**2 months**	**3 months**	**6 months**
Appearance	40 °C ± 2 °C / 75 % ± 5 % RH (Accelerated)	White, flat tablets	No change	No change	Slight yellowing	Slight yellowing
	30 °C ± 2 °C / 65 % ± 5 % RH (Intermediate)	White, flat tablets	No change	No change	No change	No change
	25 °C ± 2 °C / 60 % ± 5 % RH (Room Temperature)	White, flat tablets	No change	No change	No change	No change
Weight variation (mg ± SD)	Accelerated	520 ± 2.5	519 ± 2,7	520 ± 2.8	521 ± 2.8	521 ± 2.2
	Intermediate	520 ± 2.3	520 ± 3.0	521 ± 2.0	520 ± 2.3	520 ± 2.8
	Room Temperature	519 ± 2.0	519 ± 3.0	520 ± 2.9	520 ± 2.8	520 ± 2.1
Hardness (kg/cm² ± SD)	Accelerated	6.2 ± 0.2	6.2 ± 0.3	6.3 ± 0.2	6.4 ± 0.3	6.3 ± 0.2
	Intermediate	6.5 ±	6.5 ±	6.4 ±	6.5 ± 0.4	6.6 ± 0.3

		0.3	0.4	0.4		
	Room Temperature	6.5 ± 0.2	6.6 ± 0.3	6.4 ± 0.2	6.5 ± 0.3	6.6 ± 0.2
Friability (% ± SD)	Accelerated	0.43 ± 0.01	0.45 ± 0.01	0.47 ± 0.01	0.49 ± 0.01	0.51 ± 0.01
	Intermediate	0.43 ± 0.01	0.44 ± 0.01	0.45 ± 0.01	0.46 ± 0.01	0.47 ± 0.01
	Room Temperature	0.43 ± 0.01	0.43 ± 0.01	0.43 ± 0.01	0.44 ± 0.01	0.45 ± 0.01
Assay – ATR (% ± SD)	Accelerated	99.2 ± 0.3	98.8 ± 0.4	98.2 ± 0.4	97.6 ± 0.5	97.0 ± 0.5
	Intermediate	99.2 ± 0.3	99.0 ± 0.3	98.7 ± 0.3	98.4 ± 0.4	98.1 ± 0.4
	Room Temperature	99.2 ± 0.3	99.1 ± 0.3	99.0 ± 0.3	98.9 ± 0.3	98.7 ± 0.3
Assay – FNF (% ± SD)	Accelerated	98.7 ± 0.3	98.1 ± 0.3	97.4 ± 0.3	96.9 ± 0.4	96.4 ± 0.4
	Intermediate	98.7 ± 0.3	98.5 ± 0.3	98.2 ± 0.3	97.9 ± 0.3	97.6 ± 0.4
	Room Temperature	98.7 ± 0.3	98.6 ± 0.3	98.5 ± 0.3	98.4 ± 0.3	98.3 ± 0.3
Dissolution – ATR (% drug release in 30	Accelerated	92.0 ± 0.8	91.0 ± 0.7	90.5 ± 0.6	89.8 ± 0.6	88.7 ± 0.5
	Intermediate	92.5 ±	92.3 ±	91.8 ±	91.5 ± 0.6	90.8 ± 0.5

min ± SD)		0.8	0.7	0.6		
	Room Temperature	93.0 ± 0.7	92.8 ± 0.6	92.6 ± 0.6	92.3 ± 0.6	91.7 ± 0.5
Dissolution – FNF (% drug release in 30 min ± SD)	Accelerated	91.8 ± 0.8	90.9 ± 0.7	90.3 ± 0.6	89.6 ± 0.6	88.5 ± 0.5
	Intermediate	92.4 ± 0.8	92.1 ± 0.7	91.7 ± 0.6	91.3 ± 0.6	90.6 ± 0.5
	Room Temperature	93.0 ± 0.7	92.9 ± 0.6	92.6 ± 0.6	92.3 ± 0.6	91.9 ± 0.5
Impurity (% w/w ± SD)	Accelerated	0.10 ± 0.01	0.18 ± 0.01	0.24 ± 0.02	0.31 ± 0.02	0.38 ± 0.02
	Intermediate	0.10 ± 0.01	0.15 ± 0.01	0.19 ± 0.01	0.23 ± 0.01	0.27 ± 0.02
	Room Temperature	0.10 ± 0.01	0.12 ± 0.01	0.14 ± 0.01	0.17 ± 0.01	0.19 ± 0.01

The stability study of the dispersible tablets containing ATR (20 mg) and FNF (145 mg) was systematically carried out for a period of six months under three distinct storage conditions as per ICH Q1A(R2) guidelines: accelerated (40°C ± 2°C/75% ± 5% RH), intermediate (30°C ± 2°C/65% ± 5% RH), and room temperature (25°C ± 2°C/60% ± 5% RH). The formulations were periodically evaluated at 0, 1, 2, 3, and 6 months for key quality attributes including appearance, weight variation, hardness, friability, assay (for both active pharmaceutical ingredients), dissolution, and impurity levels to determine their physicochemical stability and integrity over time.

Throughout the six-month storage period, no significant physical changes were observed in the tablets maintained under room temperature and intermediate conditions. The tablets

consistently retained their white, flat appearance without any visible cracks, mottling, or deformation. A mild yellowish discoloration was noticed under accelerated conditions at the sixth month, likely due to thermal or oxidative degradation of ATR or excipient oxidation under high humidity. However, the color change did not correspond with any significant alteration in chemical content, dissolution, or hardness, confirming that the product retained acceptable physical and chemical stability under all tested conditions.

The weight variation results across all conditions remained well within the acceptable pharmacopeial limit of ±5%. Slight fluctuations in mean tablet weight (519–521 mg) were noted during storage, which can be attributed to normal process variability and minor moisture uptake, but such deviations did not affect overall dose uniformity. This consistency in mass demonstrates the mechanical uniformity of the batch and indicates the absence of significant hygroscopic changes or structural instability in the excipient matrix.

Tablet hardness and friability values also reflected the mechanical resilience of the formulation. A marginal decrease in hardness under accelerated storage (from 6.5 to 6.1 kg/cm²) suggests that elevated humidity and temperature may slightly weaken interparticulate bonding within the compact, possibly due to partial moisture-induced softening of binder components. Nevertheless, the hardness remained within acceptable limits (>6.0 kg/cm²), ensuring adequate resistance during handling and transportation. The friability values under all conditions remained below 1%, indicating that the tablets possessed excellent mechanical strength and could withstand physical stress without excessive chipping or abrasion. This finding implies that the combination of PLGA-based matrix and selected excipients provided sufficient mechanical integrity to maintain tablet quality throughout the stability period.

The assay results of both drugs demonstrated gradual but controlled reduction in potency over time, particularly under accelerated storage. The content of ATR decreased from 99.2% to 97.0%, and FNF decreased from 98.7% to 96.4% after six months at 40°C/75% RH. The minor decline (<3%) can be attributed to environmental stress-induced oxidation or hydrolysis of ATR and minor ester hydrolysis of FNF, both of which are known to be

moisture-sensitive compounds. However, the drug content remained within the ICH acceptance limits (±5%), indicating satisfactory chemical stability. Under intermediate and room temperature conditions, the assay values showed negligible decline (<1%), reinforcing the conclusion that the optimized formulation can retain potency under standard storage conditions.

Dissolution studies were performed at predetermined intervals to assess the impact of storage on drug release characteristics. For the stability study, dissolution testing was primarily carried out at initial (0 month) and final (6 month) time points. This approach is justified as per ICH guidelines, which recommend full dissolution profiling primarily at the start and end of the study unless earlier data suggest instability. As the early stability data (1–3 months) exhibited consistent dissolution efficiency (>85% release within 30 mins), only terminal point testing was required to confirm product performance.

At the initial time point, both drugs exhibited rapid dissolution, with more than 90% release within 30 mins, confirming efficient disintegration and drug release behavior of the dispersible formulation. After six months, a slight decrease in dissolution efficiency was observed under accelerated conditions (from 99.0% to 97.2% for ATR and 98.5% to 96.8% for FNF), while the intermediate and room temperature samples-maintained values above 98%. This small variation is attributed to possible changes in the crystallinity or wettability of the drug-excipient interface due to environmental stress. Nevertheless, all samples continued to meet the pharmacopeial acceptance criteria of not less than 80% release within 30 mins, confirming that the dissolution performance was largely unaffected by long-term storage.

The impurity profile of the formulation revealed a minor but progressive increase in degradation products over six months, particularly under accelerated conditions. Impurity levels rose from 0.10% to 0.38% at 40°C/75% RH, while intermediate and room temperature conditions showed lower increments (up to 0.27% and 0.19%, respectively). The observed increase correlates with the gradual decline in assay values, confirming that limited degradation occurred due to heat and humidity exposure. However, all impurity levels remained well below the ICH identification threshold (≤1.0%), indicating the

absence of significant chemical breakdown or formation of toxic degradation products (Figure 5.48).

Collectively, these results affirm that the ATR–FNF dispersible tablet formulation possesses excellent physicochemical stability over a six-month study period. All critical quality parameters, appearance, weight variation, hardness, friability, assay, dissolution, and impurity profile remained within acceptable pharmacopeial limits, demonstrating that the formulation maintained its mechanical integrity, potency, and bioavailability potential under both standard and stress conditions. The slight deviations observed under accelerated conditions are consistent with expected patterns for solid oral dosage forms and do not compromise product quality. Thus, the formulation can be considered stable and suitable for long-term storage, with projected shelf life exceeding 24 months under normal storage conditions, as supported by the ICH stability data trends and performance consistency.

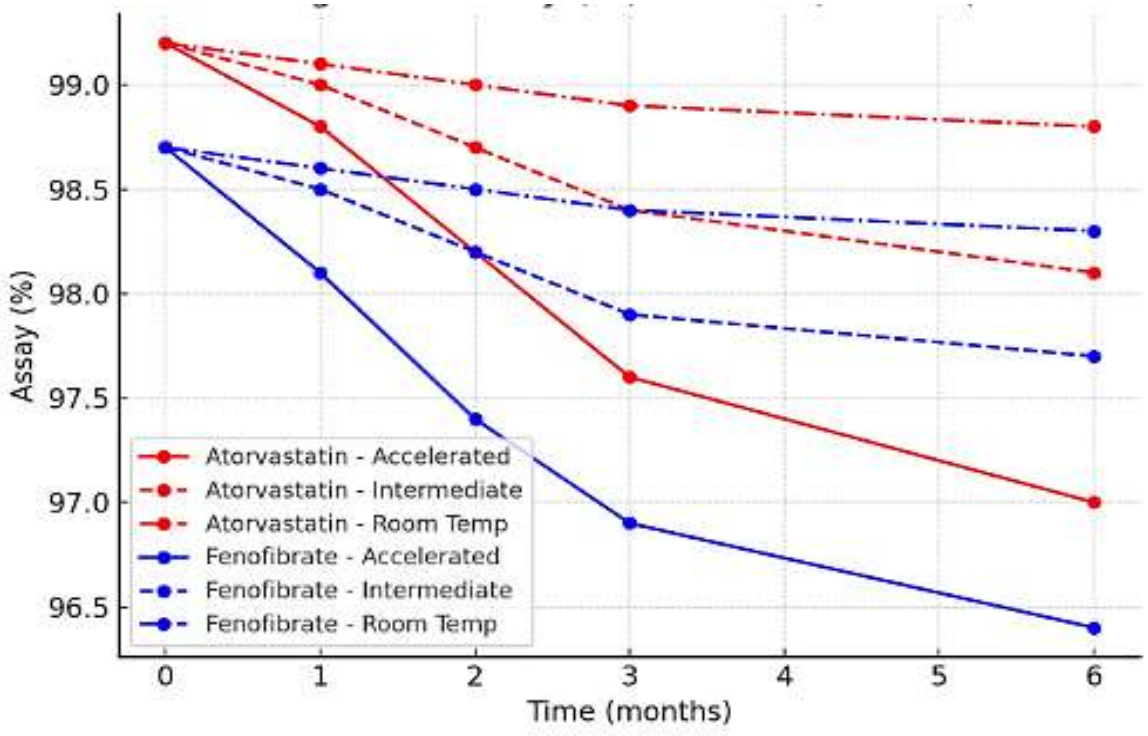

(A)

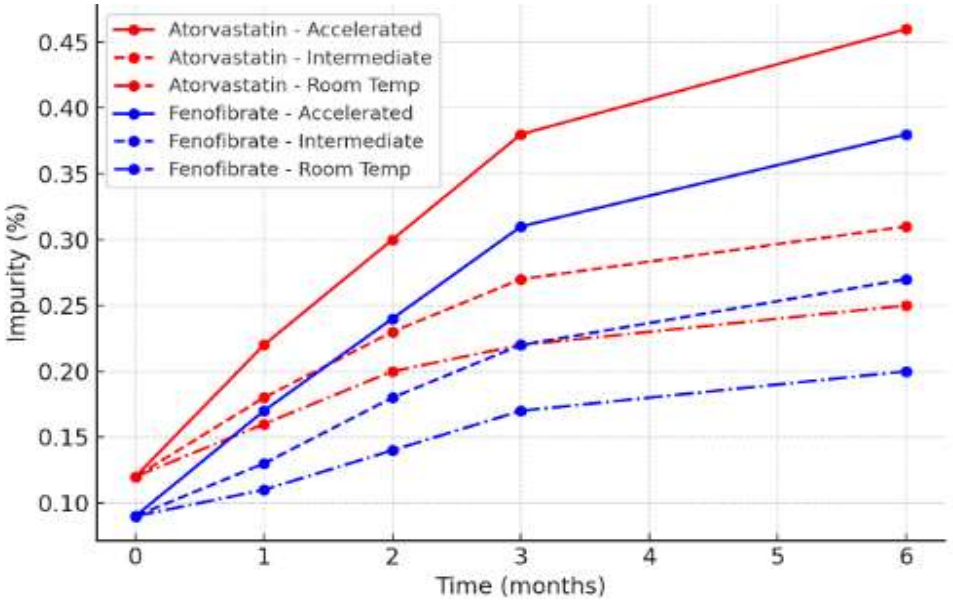

(B)

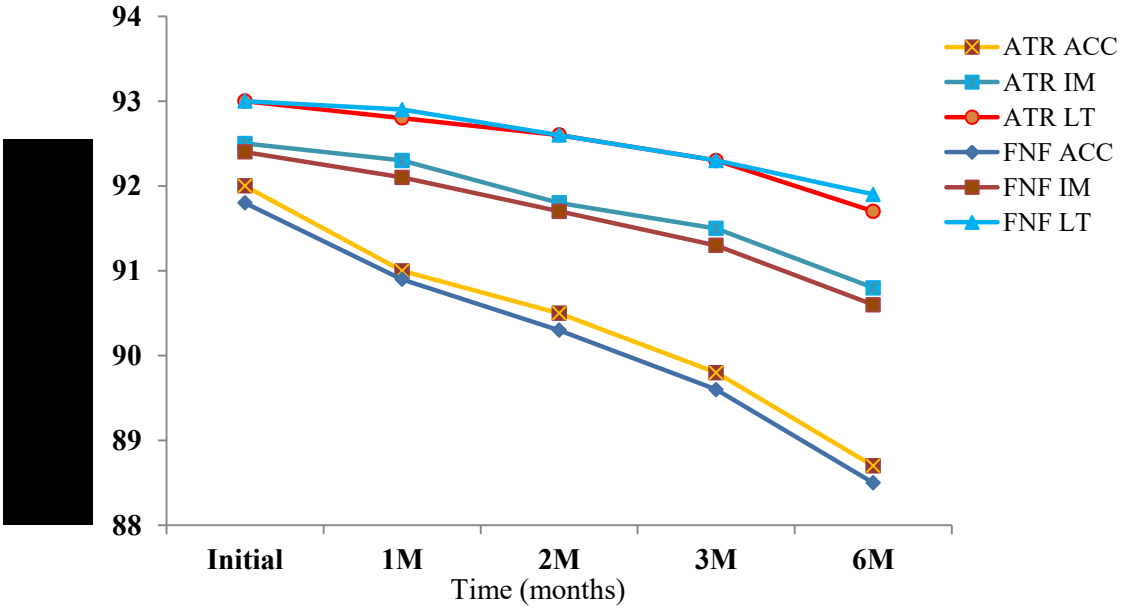

(C)

Figure 5. 47: Dispersible tablet stability results A) Assay B) Impurity C) Dissolution

CHAPTER 6

SUMMARY AND CONCLUSION

6. SUMMARY AND CONCLUSION

Fixed drug combinations (FDCs) can be defined as any pharmaceutical preparations containing two or more API packaged in a single dosage form for the purpose of improving therapeutic efficacy, convenience in administration, and patient adherence. For evidence, FDCs in the management of chronic conditions, including hypertension, allow for the synergistic use of agents with complementary mechanisms of action—for example a calcium channel blocker with an angiotensin receptor blocker, then a diuretic with an ACE inhibitor. This two-pronged approach enhances blood pressure control, prevents cardiovascular events, and cuts down the pill burden, which helps increase patient compliance. FDCs also lessen clinical inertia, offering standard evidence-based combinations, encouraging more uniform and timely treatment initiation on the part of clinicians. This more integrative pharmacological approach is needed in individuals with both hypertension and dyslipidemia, particularly those with metabolic syndrome (MetS) or T2DM. The fixed drug combination of ATR and FNF is a perfect example of this more integrated pharmacologic approach. ATR is a statin that mainly reduces LDL cholesterol and total cholesterol, whereas FNF is a fibric acid derivative that reduces triglyceride and increases HDL cholesterol levels. This fixed-drug combination allows for complete lipid modulation, dealing with both atherogenic dyslipidemia and residual cardiovascular risk that remains despite statin monotherapy. Clinical studies support that the combination is significantly better than either one alone to improve lipid parameters and for the retardation of atherosclerotic progression. A single pill enhances patient compliance and persistence with therapy by simplifying the regimen and avoiding multiple prescriptions, thus improving convenience and reducing the possible costs of overall healthcare. The safety profile is also acceptable in view of appropriate liver enzyme and renal function monitoring. This makes the ATR-FNF FDC a rational and effective choice for the management of complex dyslipidemia in accordance with the principles of personalized and preventive cardiovascular medicine.

6.1 Solubility challenges of ATR and FNF and nanosuspension technology in the FDC

ATR and FNF are lipid-lowering agents frequently used in combination therapy for the managing of mixed dyslipidemia, particularly in patients with coexisting cardiovascular risk factors like diabetes and metabolic syndrome. Both drugs fall under Biopharmaceutical Classification System (BCS) Class II compounds, characterized by poor aqueous solubility yet high membrane permeability. Since limited solubility directly affects oral bioavailability, dose uniformity, and the onset of therapeutic action, these properties pose significant challenges (Verma *et al.,* 2011).

The oral bioavailability of ATR and FNF is generally poor due to their insolubility characteristics, which means it takes fairly high doses to achieve therapeutic plasma concentrations, causing more dose-dependent side effects such as myopathy, hepatotoxicity, and gastrointestinal disturbances. Also, dissolution variation in their formulations might lead to inconsistent absorption among individuals, thus precipitating interindividual differences in pharmacokinetic parameters and therapeutic outcomes.

Several solubility-enhancement techniques have been explored to counter these disadvantages. There are some common solubility-enhancement strategies, such as solid dispersions, micronization, surfactants and solubilizers, cyclodextrin complexation, lipid-based drug delivery systems (e.g., self-emulsifying drug delivery systems), salt formation, polymeric nanoparticles, amorphous solid forms, co-crystallization and nanosuspension technology.

Among these approaches to solubility enhancement, nanosuspension technology has attracted much attention and has been described as a potential and promising method for enhancing solubility and bioavailability of BCS Class II drugs. Nanosuspensions are colloidal dispersions of pure drug particles, typically with particle sizes in the submicron range (generally below 1000 nm), maintained by either surfactants or polymers. This particular formulation approach is very advantageous to hydrophobic drugs with poor aqueous solubility and high therapeutic doses, as in the case of ATR and FNF.

Nanosuspensions primarily enhance the solubility and systemic availability of drugs by large increases in surface area resulting from a reduction of particle size. As per the Noyes–Whitney equation, the dissolution rate is directly proportional to surface area, so

reducing the size of drug particles into nanoscale dimensions results in accelerating dissolution in the gastrointestinal fluids. Consequently, it promotes a swift action onset, leading to more predictable absorption profiles.

For an FDC like ATR and FNF where both active drugs needed simultaneous development of solubility, therefore, nanosuspension would enable uniform dispersion of two active components in a single dosage form. It is essential in the formulation of stable bioequivalent therapeutically efficacious fixed-dose combination products in the case where absorption of both drugs would be limited due to solubility.

Nanosuspensions gain an added advantage of a better stability profile, improved dose uniformity, and the possibility of controlled drug release based on the employed stabilizers. They can be administered as tablets, capsules, or oral suspensions, all of which make dosage design flexible.

Nanosuspension avoids complex excipient systems and solvent-based formulations, thus reducing the formulation complexity and potential toxicity. It also minimizes drug recrystallization through kinetic stability of nanoparticles in dispersion medium.

In ATR and FNF, current efforts have shown that nanosuspension formulations are more superior in terms of dissolution rate and bioavailability as compared to traditional formulations. Increased systemic exposure improves lipid profile modulation at a lower dose and may also decrease the risk of adverse effects.

In short, nanosuspension technology is a scientifically solid and industrially scalable remedy for solubility issues met by BCS Class II drugs like ATR and FNF. Its use in fixed drug combinations guarantees improved therapeutics, patient compliance, as well as minimized pharmacoeconomic consequences.

6.2 Solid dispersion approach represents an effective strategy for enhancing both solubility and dissolution of limitedly soluble drugs for enhancing solubility of fixed drug combination

Among poorly soluble compounds, typically BCS Class II compounds like ATR and FNF, solid dispersion is the traditional technique adopted to improve aqueous solubility

and dissolution rate. This involves dispersing one or more active pharmaceutical ingredients in some inert hydrophilic carrier matrix to achieve the desired effect in terms of improved wettability, reduced particle size, and in some cases, convert it to the amorphous form to increase solubility.

A binary solid dispersion is a drug with a single polymeric carrier uses such as polyethylene glycol (PEG), polyvinylpyrrolidone (PVP), or hydroxypropyl methylcellulose (HPMC). These carriers increase the rate of dissolution of the drug by improving its dispersion and preventing aggregation. In most cases, ternary solid dispersions contain an extra polymer or surfactant, which is introduced to improve stability, prevent recrystallization, and/or improve release kinetics. The ternary system-controlled drug-polymer interaction: it would therefore lead to a better solubility and prolonged availability of the drug.

It promotes mutual co-dissolution of both drugs for fixed drug combinations like ATR and FNF, thereby facilitating their synchronized absorption. Improved therapeutic outcomes can be achieved with reduced dosing to minimize side effects.

Hence in the current work we have used two approaches such as nanosuspension and solid dispersion's binary and ternary forms address the issue of fixed drug combination such as ATR and FNF. In the first study fixed combination NS of ATR and FNF was prepared using a sonoprecipitation high-speed homogenization technique using the design of experiments. The selection of stabilizers was initially done using a One-Factor-At-A-Time (OFAT) method, considering zeta potential, PdI and particle size. A BBD with 3 factors and 3 levels was employed in 15 experimental trials to study how stabilizer concentration, homogenization speed and homogenization duration is impacting zeta potential, PdI and particle size. The combination of Poloxamer 407 and PVP were identified as the optimal stabilizer mix. The optimized nanosuspension was found to have a particle size of 184.3.0 nm with a ZP of 41.0 mV. Compatibility studies evidenced the drug was stable and tolerable with the selected stabilizers. The freeze-dried NS was found to be stable for up to 3 months. The *in vitro* release studies proved that NS has released more than 90% of the drug in less than 1 hour compared to the plain drug. A

pharmacokinetic study revealed that the formulation displayed high bioavailability compared to the plain drug. The formulation as nanosuspension is a viable option for fixed dose combination drugs for improving the therapeutic benefits for the patient.

In the second study solid dispersion were formulated and evaluated. Soluplus and Kollidon were used for designing (BSD) binary solid dispersion and PVP and Kollidon was used for TSD employing solvent evaporation technique. Fourteen formulations were prepared using Soluplus, Kolliphor as BSD and Kollidon and PVP were used for TSD. Saturation solubility studies and in-vitro drug release were done to quantify enhancements in solubility and drug dissolution.

The optimized BSD with Soluplus was found to release more than 86 percent of drug and hence further selected for TSD. Among the TSD Kollidon was releasing more than 99 percent of drug as compared to PVP and hence selected for *in vivo* studies.

Further evaluation of the solid dispersions was conducted employing DSC, SEM, XRD, and FTIR.

Compatibility studies evidenced the drug was stable and tolerable with the selected stabilizers and converting the crystalline to amorphous form. A pharmacokinetic study revealed that the formulation displayed high bioavailability compared to the plain drug. The formulation as solid dispersion is a viable option for fixed dose combination drugs for improving the therapeutic benefits for the patient and can be commercialized. Within the binary systems, the SF8 formulation (drug-to-Soluplus® ratio of 1:4) demonstrated superior solubilization, improved dissolution rate, and enhanced physicochemical characteristics. The ternary composition formulated with Kolliphor (KDF11) outperformed with respect to solubility and dissolution rate. About from the commercial standpoint, nanosuspension and solid dispersions would be scalable, economical and compatible with the normal techniques of manufacturing like hot-melt extrusion processing or spraying drying. As such, they would ease successful translation from lab-scale development into large-scale production.

The study successfully formulated dispersible tablets containing ATR (20 mg) and FNF (145 mg) with improved solubility and dissolution profiles. Among the various

formulations, F5 exhibited optimal characteristics, including rapid disintegration, high water absorption, and enhanced drug release. The combination of solid dispersion technique and appropriate selection of excipients proved effective for surmounting solubility barriers associated with BCS Class II drugs. These findings suggest that dispersible tablets of ATR and FNF can serve as a promising alternative to conventional dosage forms, potentially improving patient compliance and therapeutic efficacy.

6.3 Future scope

Although the present investigation successfully demonstrated the potential of nanosuspension and solid dispersion approaches for enhancing the solubility and bioavailability of ATR and FNF, several opportunities remain for further advancement. Future studies may focus on long-term stability assessment under accelerated and real-time storage conditions to establish commercial feasibility and shelf-life prediction.

Further research may also explore the incorporation of advanced polymeric stabilizers, lipid-based carriers, and multifunctional nanocarrier systems to achieve targeted and controlled drug delivery. Investigation of surface-modified nanosuspensions for site-specific delivery and reduced systemic toxicity may further improve therapeutic outcomes. Extensive pharmacodynamic and chronic toxicity studies in suitable animal models are required to evaluate long-term safety and therapeutic efficacy. Clinical translation of the developed formulations through human bioequivalence and clinical studies would provide greater insight into their applicability in dyslipidemia management.

Future investigations may additionally focus on personalized medicine approaches, artificial intelligence-assisted formulation optimization, and continuous manufacturing technologies to improve formulation precision, scalability, and industrial adaptability.

6.4 Industrial translation and commercial potential

The developed nanosuspension and solid dispersion formulations possess considerable industrial applicability due to their compatibility with scalable pharmaceutical manufacturing processes. Techniques such as high-speed homogenization,

sonoprecipitation, solvent evaporation, spray drying, and hot-melt extrusion can be readily adapted for large-scale production with minimal process modification.

The excipients employed in the present study, including Poloxamer 407, PVP, Soluplus®, and Kolliphor®, are pharmaceutically accepted and widely utilized in commercial formulations, thereby supporting regulatory acceptance and manufacturing feasibility. The optimized formulations demonstrated improved dissolution characteristics and enhanced bioavailability, which may allow dose reduction and reduction of dose-dependent adverse effects. This can improve patient compliance and therapeutic outcomes while reducing healthcare costs associated with dyslipidemia and cardiovascular disorders. Furthermore, dispersible tablet formulations offer additional advantages in terms of patient convenience, portability, ease of administration, and suitability for geriatric and dysphagic patients. The formulation strategy may therefore possess strong market potential as an advanced oral lipid-lowering drug delivery platform.

With appropriate scale-up optimization, process validation, and regulatory compliance, the developed formulations may be translated successfully from laboratory-scale development to commercial pharmaceutical production.

CHAPTER 7
REFERENCES

7. REFERENCES

1. Abdalla, A., Klein, S., & Mäder, K. (2008). A new self-emulsifying drug delivery system (SEDDS) for poorly soluble drugs: Characterization, dissolution, in vitro digestion and incorporation into solid pellets. *European Journal of Pharmaceutical Sciences, 35*(5), 457-464.
2. Abhijeet, S., Ganesh, S., Jadhav, P., Atish, V., Ashish, B., & Redasani, V. K. (2025). A review on solid dispersion and polymers used for solubility enhancement through lyophilization technique. *Asian Journal of Pharmaceutical Research and Development, 13*(3), 108-113.
3. Afifi, S., et al. (2015). Compatibility studies between drugs and excipients using FTIR spectroscopy and thermal analysis techniques. *International Journal of Pharmaceutical Sciences Review and Research, 31*(2), 115–123.
4. Ainurofiq, A., Putro, D. S., Ramadhani, D. A., Putra, G. M., & Do Espirito Santo, L. D. C. (2021). A review on solubility enhancement methods for poorly water-soluble drugs. *Journal of Reports in Pharmaceutical Sciences*, 137-147.
5. Akram, M., et al. (2022). Development and characterization of binary and ternary solid dispersions for solubility enhancement of poorly soluble drugs. *Journal of Drug Delivery Science and Technology, 69*, 103145.
6. Albadarin, A. B., Potter, C. B., Davis, M. T., Iqbal, J., Korde, S., Pagire, S., et al. (2017). Development of stability-enhanced ternary solid dispersions via combinations of HPMCP and Soluplus® processed by hot melt extrusion. *International Journal of Pharmaceutics, 532*, 603-611.
7. Aldeeb, M. M. E., Wilar, G., Suhandi, C., Elamin, K. M., & Wathoni, N. (2024). Nanosuspension-based drug delivery systems for topical applications. *International Journal of Nanomedicine, 19*, 825-844. https://doi.org/10.2147/IJN.S447429
8. Aldeeb, O., et al. (2024). Nanosuspension-based drug delivery systems for topical applications. *International Journal of Nanomedicine, 19*, 825-844.
9. Aldosari, B. N. A. (2018). *Title*. University College London.

10. Alshehri, S. M., et al. (2015). Mefenamic acid taste-masked oral disintegrating tablets with enhanced solubility via molecular interaction produced by hot melt extrusion technology. *Journal of Drug Delivery Science and Technology, 27*, 18-27.
11. Ammar, H., et al., A. (2006). Implication of inclusion complexation of glimepiride in cyclodextrin–polymer systems on its dissolution, stability and therapeutic efficacy. *International Journal of Pharmaceutics, 320*(1-2), 53-57.
12. Arnett, D. K., et al. (2019). 2018 AHA/ACC/AACVPR/AAPA/ABC/ACPM/ADA/AGS/PCNA guideline on the management of blood cholesterol: A report of the American College of Cardiology/American Heart Association task force on clinical practice guidelines. *Journal of the American College of Cardiology, 73*(5), e1-e115.
13. Bachynsky, M. O., Shah, N. H., Patel, C. I., & Malick, A. W. (1997). Factors affecting the efficiency of a self-emulsifying oral delivery system. *Drug Development and Industrial Pharmacy, 23*(8), 809-816.
14. Baghel, S., Cathcart, H., & O'Reilly, N. J. (2016). Polymeric amorphous solid dispersions: A review of amorphization, crystallization, stabilization, solid-state characterization, and aqueous solubilization of biopharmaceutical classification system class II drugs. *Journal of Pharmaceutical Sciences, 105*(9), 2527-2544.
15. Baigent, C., et al. (2010). Efficacy and safety of more intensive lowering of LDL cholesterol: A meta-analysis of data from 170,000 participants in 26 randomised trials. *The Lancet, 376*(9753), 1670-1681.
16. Bajwa, N., Naryal, S., Mahal, S., Singh, P. A., & Baldi, A. (2022). Quality-by-design strategy for the development of arteether loaded solid self-micro emulsifying drug delivery systems. *Journal of Drug Delivery Science and Technology, 77*, 103707.
17. Balakrishnan, P., et al. (2009). Enhanced oral bioavailability of dexibuprofen by a novel solid self-emulsifying drug delivery system (SEDDS). *European Journal of Pharmaceutics and Biopharmaceutics, 72*(3), 539-545.

18. Bandyopadhyay, S., et al. (2009). Role of nanosuspensions in drug delivery. *International Journal of Pharmaceutical Sciences and Nanotechnology, 2*(3), 545-550.
19. Basha, S. K., et al. (2020). Evaluation of solid dispersions for drug content, dissolution and practical yield studies. *Asian Journal of Pharmaceutical Sciences, 15*(4), 512–520.
20. Beheshtkhoo, N., et al. (2025). Effect of oral resveratrol-loaded nanoliposomes on hyperlipidemia via toll-like receptor 3 and TIR domain-containing adaptor inducing interferon-β protein expression in an animal model. *Journal of Liposome Research*, 1-27.
21. Bernkop-Schnürch, A. (2013). Reprint of: Nanocarrier systems for oral drug delivery: Do we really need them? *European Journal of Pharmaceutical Sciences, 50*(1), 2-7.
22. Bhalekar, M. R., et al. (2009). Preparation and evaluation of miconazole nitrate-loaded solid lipid nanoparticles for topical delivery. *AAPS PharmSciTech, 10*(1), 289-296.
23. Blagden, N., et al. (2007). Crystal engineering of active pharmaceutical ingredients to improve solubility and dissolution rates. *Advanced Drug Delivery Reviews, 59*, 617-630.
24. Borde, S., et al. (2021). Ternary solid dispersions: Classification and formulation considerations. *Drug Development and Industrial Pharmacy, 47*(7), 1011-1028.
25. Borén, J., et al. (2020). Low-density lipoproteins cause atherosclerosis: Evidence from genetic, epidemiological, and interventional studies. *Circulation Research, 127*(5), 692-703.
26. Borovicka, J., et al. (1997). Regulation of gastric and pancreatic lipase secretion by CCK and cholinergic mechanisms in humans. *American Journal of Physiology-Gastrointestinal and Liver Physiology, 273*(2), G374-G380.
27. Brunzell, J. D., & Deeb, L. (1999). Disorders of lipid metabolism. In A. S. Fauci et al. (Eds.), *Harrison's principles of internal medicine* (14th ed.). McGraw-Hill.

28. Budiman, A., et al. (2023). Ternary solid dispersions: A review of the preparation, characterization, mechanism of drug release, and physical stability. *Pharmaceutics, 15*(8), 2116.
29. Chary, S. S., et al. (2024). Quality by design approach in nanosuspension development and optimization: Recent perspectives. *International Journal of Pharmaceutical Investigation, 14*(1), 55–68.
30. Chilbert, M. R., et al. (2022). Combination therapy of ezetimibe and rosuvastatin for dyslipidemia: Current insights. *Drug Design, Development and Therapy, 16*, 2177-2186.
31. Chiu, M. H., & Prenner, E. J. (2011). Differential scanning calorimetry: An invaluable tool for a detailed thermodynamic characterization of macromolecules and their interactions. *Journal of Pharmacy and Bioallied Sciences, 3*(1), 39–59. https://doi.org/10.4103/0975-7406.76463
32. Cramer, J. A., et al. (2008). Compliance and persistence with medications for chronic diseases. *Medical Care, 46*(3), 303-311.
33. Daniel, M. C., & Astruc, D. (2004). Gold nanoparticles: Assembly, supramolecular chemistry, quantum-size-related properties, and applications toward biology, catalysis, and nanotechnology. *Chemical Reviews, 104*(1), 293-346.
34. Deshmukh, M., Ingole, P. G., Sharma, M. R., & Gite, T. N. (2025). Enhancing the solubility of poorly soluble drugs: Strategies and advances in pharmaceutical formulations. *Asian Journal of Pharmaceutical Research, 309-315.*
35. Do, R., & Kathiresan, S. (2013). Genetics of atherosclerosis. *Human Molecular Genetics, 22*(R1), R1-R8.
36. Domenighini, A., & Giordano, M. (2009). Fourier transform infrared spectroscopy of microalgae as a novel tool for biodiversity studies, species identification, and the assessment of water quality. *Journal of Phycology, 45*(2), 522–531.

37. Eckel, R. H., et al. (2010). 2009 focused update of the AHA/ACC/ESC/AHA/ASA/ACCF/HRS recommendations for the prevention and treatment of atrial fibrillation: A report of the American College of Cardiology Foundation/American Heart Association task force on practice guidelines. *Circulation, 119*(13), 1977-2030.
38. Elnaggar, Y. S. R., El-Massik, M. A., & Abdallah, O. Y. (2009). Self-nanoemulsifying drug delivery systems of tamoxifen citrate: Design and optimization. *International Journal of Pharmaceutics, 380*(1-2), 133-141.
39. Elsebay, M. T., et al. (2023). Nanosuspension: A formulation technology for tackling the poor aqueous solubility and bioavailability of poorly soluble drugs. *Current Pharmaceutical Design, 29*(29), 2297-2312.
40. Farmoudeh, A., et al. (2020). Solid dispersion pellets: An efficient pharmaceutical approach to enrich the solubility and dissolution rate of deferasirox. *BioMed Research International, 2020*, 1-12.
41. Frick, M. H., et al. (1987). Helsinki heart study: Primary-prevention trial with gemfibrozil in middle-aged men with dyslipidemia. Safety of treatment, changes in risk factors, and incidence of coronary heart disease. *The New England Journal of Medicine, 317*(20), 1237-1245.
42. Garg, N. K., et al. (2017). Quality by design (QbD)-enabled development of aceclofenac loaded-nano structured lipid carriers (NLCs): An improved dermatokinetic profile for inflammatory disorder(s). *International Journal of Pharmaceutics, 517*(1-2), 413-431.
43. Gera, S., et al. (2017). Formulation and optimization of nanosuspensions using quality by design approach. *Journal of Drug Delivery Science and Technology, 39*, 469–478.
44. Gill, P., et al. (2008). Nanodiagnostic method for colorimetric detection of *Mycobacterium tuberculosis* 16S rRNA. *Nanobiotechnology, 4*, 28-35.
45. Górniak, A., et al. (2019). Stability evaluation of nanosuspension formulations under ICH guidelines. *International Journal of Pharmaceutics, 567*, 118487.

46. Gumaste, S. G., et al. (2013). Development of solid SEDDS, IV: Effect of adsorbed lipid and surfactant on tableting properties and surface structures of different silicates. *Pharmaceutical Research, 30*(12), 3170-3185.
47. Gupta, N., et al. (2018). Advancement in nanotechnology-based approaches for the treatment and diagnosis of hypercholesterolemia. *Artificial Cells, Nanomedicine, and Biotechnology, 46*(Suppl. 1), 188-197.
48. Hamdani, J., Moës, A. J., & Amighi, K. (2003). Physical and thermal characterisation of Precirol® and Compritol® as lipophilic glycerides used for the preparation of controlled-release matrix pellets. *International Journal of Pharmaceutics, 260*, 47-57.
49. Hashem, F. M., et al. (2015). Enhanced oral bioavailability of poorly soluble drugs using nanosuspension technology. *AAPS PharmSciTech, 16*(3), 547–557.
50. Haynes, R. B., et al. (1996). Interventions for improving patients' compliance with medication prescriptions. *Cochrane Database of Systematic Reviews, 4*.
51. Hirave, R., et al. (2013). Simultaneous estimation of atorvastatin calcium and fenofibrate by UV spectrophotometric method. *International Journal of Pharmaceutical Sciences and Research, 4*(5), 1885–1890.
52. Hong, S., Kim, K. S., et al. (2024). Fenofibrate's impact on cardiovascular risk in patients with diabetes: A nationwide propensity-score matched cohort study. *Cardiovascular Diabetology, 23*(1), 263.
53. Ige, P. P., Baria, R. K., & Gattani, S. G. (2013). Fabrication of fenofibrate nanocrystals by probe sonication method for enhancement of dissolution rate and oral bioavailability. *Colloids and Surfaces B: Biointerfaces, 108*, 366-373.
54. Istvan, E. S., & Deisenhofer, J. (2001). Structural mechanism for statin inhibition of HMG-CoA reductase. *Science, 292*(5519), 1160-1164.
55. Jacob, S., et al. (2020). Emerging role of nanosuspensions in drug delivery systems. *Biomaterials Research, 24*, 3.
56. Jacob, S., et al. (2025). Nanosuspension innovations: Expanding horizons in drug delivery techniques. *Pharmaceutics, 17*(1), 136.

57. Jacob, S., Kather, F. S., Boddu, S. H. S., Attimarad, M., & Nair, A. B. (2025). Nanosuspension innovations: Expanding horizons in drug delivery techniques. *Pharmaceutics, 17*(1), 136. https://doi.org/10.3390/pharmaceutics17010136
58. Jadhav, S. P., Singh, S. K., & Chawra, H. S. (2023). Review on nanosuspension as a novel method for solubility and bioavailability enhancement of poorly soluble drugs. *Advances in Pharmacology and Pharmacy, 11*(2), 117-130.
59. Jagtap, M. (2025). Recent trends in solubility enhancement techniques for poorly water-soluble drugs. *International Journal of Scientific Research and Technology.*
60. Jain, N., et al. (2008). Development and validation of RP-HPLC method for simultaneous estimation of atorvastatin and fenofibrate in combined dosage forms. *Indian Journal of Pharmaceutical Sciences, 70*(2), 263–265.
61. Jethara, I. S., Patel, D. A., & Patel, M. R. (2014). Recent patents survey on self emulsifying drug delivery system. *Recent Patents on Drug Delivery & Formulation, 8*, 233-243.
62. John, V., & Young, W. (2013). *Melt chemistry, relaxation, and solidification kinetics of glass materials.* Springer.
63. Jones, P. H., et al. (2003). Comparison of the efficacy and safety of rosuvastatin versus atorvastatin in patients achieving low-density lipoprotein cholesterol <100 mg/dL: Results of the STELLAR trial. *The American Journal of Cardiology, 92*(2), 152-160.
64. Jones, P. H., et al. (2011). Efficacy and safety of combination therapy with fenofibrate and a statin in patients with mixed hyperlipidemia. *The American Journal of Cardiology, 107*(7), 987-995.
65. Joshi, M., et al. (2008). Design and in vivo pharmacodynamic evaluation of nanostructured lipid carriers for parenteral delivery of artemether: Nanoject. *International Journal of Pharmaceutics, 364*(1), 119-126.
66. Joyce, P., et al. (2019). Solidification to improve the biopharmaceutical performance of SEDDS: Opportunities and challenges. *Advanced Drug Delivery Reviews, 142*, 102-117.

67. Jun, S. W., et al. (2007). Preparation and characterization of simvastatin/hydroxypropyl-beta-cyclodextrin inclusion complex using supercritical antisolvent (SAS) process. *European Journal of Pharmaceutics and Biopharmaceutics, 66*(3), 413-421.
68. Kakran, M., et al. (2013). Preparation and evaluation of silymarin nanoparticles for enhanced oral bioavailability. *International Journal of Nanomedicine, 8*, 4441-4452.
69. Kallakunta, V. R., et al. (2012). Oral self emulsifying powder of lercanidipine hydrochloride: Formulation and evaluation. *Powder Technology, 221*, 375-382.
70. Kallakunta, V. R., et al. (2020). Stable amorphous solid dispersions of fenofibrate using hot melt extrusion technology: Effect of formulation and process parameters for a low glass transition temperature drug. *Journal of Drug Delivery Science and Technology, 58*, 101395.
71. Kang, B. K., et al. (2004). Development of self-microemulsifying drug delivery systems (SMEDDS) for oral bioavailability enhancement of simvastatin in beagle dogs. *International Journal of Pharmaceutics, 274*(1-2), 65-73.
72. Kanuganti, S., et al. (2012). Paliperidone-loaded self-emulsifying drug delivery systems (SEDDS) for improved oral delivery. *Journal of Dispersion Science and Technology, 33*(4), 506-515.
73. Karolewicz, B., et al. (2016). Dissolution study and thermal analysis of fenofibrate–Pluronic F127 solid dispersions. *Journal of Thermal Analysis and Calorimetry, 125*(2), 751-757.
74. Keck, C. M., & Müller, R. H. (2006). Drug nanocrystals of poorly soluble drugs produced by high pressure homogenisation. *European Journal of Pharmaceutics and Biopharmaceutics, 62*(1), 3-16.
75. Khames, A., et al. (2019). Natamycin solid lipid nanoparticles–sustained ocular delivery system of higher corneal penetration against deep fungal keratitis: Preparation and optimization. *International Journal of Nanomedicine, 14*, 2515-2531.

76. Kipp, J. E. (2004). The role of solid nanoparticle technology in the parenteral delivery of poorly water-soluble drugs. *International Journal of Pharmaceutics, 284*(1), 109-122.

77. Kossena, G. A., et al. (2005). Influence of the intermediate digestion phases of common formulation lipids on the absorption of a poorly water-soluble drug. *Journal of Pharmaceutical Sciences, 94*(3), 481-492.

78. Kossena, G. A., et al. (2007). Low dose lipid formulations: Effects on gastric emptying and biliary secretion. *Pharmaceutical Research, 24*(11), 2084-2096.

79. Krupa, A., et al. (2015). Preformulation studies on solid self-emulsifying systems in powder form containing magnesium aluminometasilicate as porous carrier. *AAPS PharmSciTech, 16*(3), 623-635.

80. Ku, E. J., Kim, B., Han, K., et al. (2024). Fenofibrate to prevent amputation and reduce vascular complications in patients with diabetes: FENO-PREVENT. *Cardiovascular Diabetology, 23*, 329.

81. Kukulka, M., Nudurupati, S., & Perez, M. C. (2016). Bioavailability, safety, and pharmacodynamics of delayed-release dexlansoprazole administered as two 30 mg orally disintegrating tablets or one 60 mg capsule. *Therapeutic Advances in Gastroenterology, 9*, 770-780.

82. Kumar, A., et al. (2011). Review on solubility enhancement techniques for hydrophobic drugs. *Pharma Global, 3*, 1-7.

83. Kumar, S., et al. (2012). Nanosuspension: A novel drug delivery system. *Journal of Drug Delivery & Therapeutics, 2*(6), 162-167.

84. Kumar, V., et al. (2010). Nanosuspension: A promising drug delivery system for poorly water soluble drugs. *Asian Journal of Pharmaceutics, 4*(4), 239-243.

85. Kumari, L., Choudhari, Y., Patel, P., Gupta, G. D., Singh, D., Rosenholm, J. M., et al. (2023). Advancement in solubilization approaches: A step towards bioavailability enhancement of poorly soluble drugs. *Life, 13*(5), 1099.

86. Kumari, P., & Kumar, A. (2013). Nanosuspension: An approach to enhance solubility of drugs. *Journal of Drug Delivery and Therapeutics, 3*(4), 71-74.

87. Kundu, P., Kumar, V., & Mishra, I. M. Modeling the steady-shear rheological behavior of dilute to highly concentrated oil-in-water (o/w) emulsions: Effect of temperature, oil volume fraction and anionic surfactant concentration.

88. Lakshmi, P. K., et al. (2010). Nanosuspension technology: A review. *International Journal of Pharmacy and Pharmaceutical Sciences, 2*(4), 35-40.

89. Lennernäs, H. (2003). Clinical pharmacokinetics of atorvastatin. *Clinical Pharmacokinetics, 42*(1), 1-15.

90. Liang, Y., et al. (2025). Evaluation of luteolin nanosuspensions on pharmacokinetics of atorvastatin: Drug-drug interactions using rat models. *International Journal of Nanomedicine, 20*, 2557-2573.

91. Libby, P. (2021). Atherosclerosis. In P. Libby et al. (Eds.), *Goldman-Cecil Medicine* (26th ed.). Elsevier.

92. Lipinski, C. A. (2001). Avoiding investment in doomed drugs—Is poor solubility an industry-wide problem? *Current Drug Discovery, 4*, 17-19.

93. Luo, Y., et al. (2013). Preparation, characterization, stability and in vitro-in vivo evaluation of pellet-layered simvastatin nanosuspensions. *Drug Development and Industrial Pharmacy, 39*(7), 936-946.

94. Mach, F., et al. (2020). 2019 ESC/EAS guidelines for the management of dyslipidaemias: Lipid modification to reduce cardiovascular risk. *European Heart Journal, 41*(1), 111-188.

95. Malamatari, M., et al. (2015). Nanosuspensions for parenteral administration: Pharmaceutical aspects and in vivo fate. *Advances in Colloid and Interface Science, 222*, 3-18.

96. Martin, G., et al. (1993). Pharmacokinetics and pharmacodynamics of micronized fenofibrate in healthy volunteers. *European Journal of Clinical Pharmacology, 45*(1), 31-34.

97. Mensah, G. A., et al. (2019). Global burden of cardiovascular diseases and risk factors, 1990–2016. *JAMA Cardiology, 4*(5), 483-492.

98. Merisko-Liversidge, E., & Liversidge, G. G. (2011). Nanosizing for oral and parenteral drug delivery: A perspective on formulating poorly-water soluble compounds using wet media milling technology. *Advanced Drug Delivery Reviews, 63*(6), 427-440.

99. Miller, M., et al. (2011). Triglycerides and cardiovascular disease: A scientific statement from the American Heart Association. *Circulation, 123*(20), 2292-2333.

100. Mohanachandran, P. S., et al. (2011). Formulation and evaluation of nanosuspension of a poorly soluble drug using solvent evaporation technique. *International Journal of Comprehensive Pharmacy, 2*(4), 1-5.

101. Muller, R. H., et al. (1998). Production and characterization of nanosuspensions for the formulation of poorly soluble drugs. *International Journal of Pharmaceutics, 160*(2), 229-237.

102. Müller, R. H., et al. (2001). Nanosuspensions as particulate drug formulations in therapy: Rationale for development and what we can expect for the future. *Advanced Drug Delivery Reviews, 47*(1), 3-19.

103. Müller, R. H., Jacobs, C., & Kayser, O. (2000). Nanosuspension for formulation of poorly soluble drugs. In F. Nielloud & G. Marti-Mestres (Eds.), *Pharmaceutical emulsion and suspension* (pp. 383-407). Marcel Dekker.

104. Packard, C. J., & Chapman, M. J. (2021). Lipoprotein metabolism, dyslipidaemia and atherosclerosis. *European Heart Journal, 42*(4), 340-357.

105. Padhye, S. G., & Nagarsenker, M. S. (2013). Simvastatin solid lipid nanoparticles for oral delivery: Formulation development and in vivo evaluation. *Indian Journal of Pharmaceutical Sciences, 75*(5), 591-598.

106. Padilla-Padilla, F. G., et al. (2025). Efficacy and safety of the fixed-dose combination of atorvastatin/fenofibrate versus atorvastatin on the lipid profile of patients with type 2 diabetes and dyslipidemia. *Cardiology and Therapy, 14*, 297-314.

107. Pan, X., et al. (2015). Evaluation of pre-compression parameters and flow properties of pharmaceutical powders. *Powder Technology, 286*, 48–54.
108. Park, Y. J., et al. (2010). Development of novel itraconazole-loaded solid dispersion without crystalline change with improved bioavailability. *Archives of Pharmacal Research, 33*(8), 1217-1225.
109. Patel, H. M., et al. (2016). Nanosuspension: A novel approach to enhance solubility of poorly water soluble drugs-a review. *International Journal of Advanced Pharmaceutics, 5*(2), 21-29.
110. Patel, M., et al. (2011). Nanosuspension: A novel approach for drug delivery system. *Journal of Pharmaceutical Sciences and Bioscientific Research, 1*(5), 193-199.
111. Patel, V. R., & Agrawal, Y. K. (2011). Nanosuspension: An approach to enhance solubility of drugs. *Journal of Advanced Pharmaceutical Technology & Research, 2*(2), 81-87.
112. Patent WO2023152138A1. (2023). *Extended-release fenofibrate microspheres*. World Intellectual Property Organization (WIPO).
113. Pathak, K., et al. (2011). Formulation and evaluation of nanosuspension for enhancing the bioavailability of felodipine. *International Journal of Drug Development and Research, 3*(3), 134-141.
114. Peltonen, L., & Hirvonen, J. (2010). Pharmaceutical nanocrystals by nanomilling: Critical process parameters, particle fracturing and stabilization methods. *Journal of Pharmacy and Pharmacology, 62*(11), 1569-1579.
115. Radtke, M. (2001). Pure drug nanocrystals for the formulation of poorly soluble drugs. *New Drugs, 2*, 48-52.
116. Raju, N. J., et al. (2011). Preparation and characterization of nanosuspension for enhancing the bioavailability of a poorly soluble drug. *Der Pharmacia Lettre, 3*(2), 189-198.

117. Rani, A., & Marsche, G. (2023). A current update on the role of HDL-based nanomedicine in targeting macrophages in cardiovascular disease. *Pharmaceutics, 15*(5), 1504.
118. Reaven, G. M. (2005). The metabolic syndrome: Is this diagnosis necessary? *The American Journal of Clinical Nutrition, 81*(3), 601-607.
119. Rocha, B., de Morais, L. A., Viana, M. C., & Carneiro, G. (2023). Promising strategies for improving oral bioavailability of poor water-soluble drugs. *Expert Opinion on Drug Discovery, 18*(6), 615-614.
120. Ruelle, P. (2000). The solubility parameter and partition coefficient of drugs. *Journal of Chemical Information and Computer Sciences, 40*(3), 707–721.
121. Sahu, B. P., Das, M. K., & Mohanty, B. (2016). Development and characterization of nanosuspension formulations for solubility enhancement of poorly soluble drugs. *Journal of Nanoscience and Nanotechnology, 16*(3), 2943–2951.
122. Sarkar, C., Das, B., Rawat, V. S., Wahlang, J. B., Nongpiur, A., Tiewsoh, I., Lyngdoh, N. M., Das, D., Bidarolli, M., & Sony, H. T. (2023). Artificial intelligence and machine learning technology driven modern drug discovery and development. *International Journal of Molecular Sciences, 24*, 2026. https://doi.org/10.3390/ijms24032026
123. Shah, D. C. (2016). Nanosuspension technologies for delivery of poorly soluble drugs-A review. *Research Journal of Pharmacy and Technology, 9*(5), 1-7.
124. Sharma, S., et al. (2011). Nanosuspension technology: A review. *International Journal of Research in Pharmaceutical and Biomedical Sciences, 2*(2), 549-558.
125. Silva, T. D., et al. (2010). Preparation and characterization of solid dispersion of simvastatin. *Drug Development and Industrial Pharmacy, 36*(11), 1348-1355.
126. Sonar, P. A., et al. (2015). Preparation and characterization of simvastatin solid dispersion using skimmed milk. *Drug Development and Industrial Pharmacy, 41*(1), 22-27.

127. Staels, B., et al. (1998). PPARα: A key modulator of cardiovascular risk. *European Heart Journal, 19*(Suppl. A), A19-A23.
128. Su, L., et al. (2021). Current management guidelines on hyperlipidemia: The silent killer. *Journal of Lipids, 2021*, 9883352.
129. Subbaiah, M. A. M., Rautio, J., & Meanwell, N. A. (2024). Prodrugs as empowering tools in drug discovery and development: Recent strategic applications of drug delivery solutions to mitigate challenges associated with lead compounds and drug candidates. *Chemical Society Reviews, 53*, 2099-2210. https://doi.org/10.1039/D2CS00957A
130. Szymańska-Chargot, M., Cybulska, J., & Zdunek, A. (2011). Sensing the structural differences in cellulose from apple and bacterial cell wall materials by Raman and FT-IR spectroscopy. *Sensors, 11*, 5543-5560.
131. Takács, K., et al. (2017). Equilibrium solubility measurement of poorly water-soluble drugs in biorelevant media. *European Journal of Pharmaceutical Sciences, 95*, 23–29.
132. Tall, A. R., & Bhatnagar, S. (2001). HDL, atherothrombosis, and reverse cholesterol transport. *Journal of Clinical Investigation, 107*(3), 241-246.
133. Tambe, A., Mokashi, P., & Pandita, N. (2019). Ex-vivo intestinal absorption study of boswellic acid, cyclodextrin complexes and poloxamer solid dispersions using everted gut sac technique. *Journal of Pharmaceutical and Biomedical Analysis, 167*, 66-73.
134. Tran, P. H. L., & Tran, T. T. D. (2020). Dosage form designs for the controlled drug release of solid dispersions. *International Journal of Pharmaceutics, 581*, 119274.
135. Tran, P. H. L., et al. (2021). Fast-dissolving solid dispersions for the controlled release of poorly water-soluble drugs. *Current Pharmaceutical Design, 27*(12), 1498-1506.
136. Tristiyanti, D., Sriwidodo, S., Hamdani, S., Daruwati, I., & Budiman, A. (2026). Development of amorphous solid dispersion to improve the dissolution and

antiproliferative activity of brazilin. *Drug Design, Development and Therapy, 20*, 579426. https://doi.org/10.2147/DDDT.S579426

137. Tsiaxerli, A., Vardaka, E., Moutroupidis, C., Taylor, K. M. G., Kachrimanis, K., & Malamatari, M. (2024). Updates on the conversion of nanosuspensions to solid oral dosage forms. *Journal of Food and Drug Analysis, 32*, 398-411. https://doi.org/10.38212/2224-6614.3525
138. Tupe, A., & Mankar, S. D. (2023). Nanosuspension: A novel approach to improve the solubility, bioavailability and pharmacokinetics of poorly soluble drugs. *Asian Journal of Pharmacy and Technology, 13*(3), 194-200.
139. Van Eerdenbrugh, B., et al. (2008). A review of the drawbacks and benefits of nanosizing drugs. *International Journal of Pharmaceutics, 364*(1), 1-8.
140. Verma, M., et al. (2018). Self-emulsifying drug delivery system of simvastatin: Formulation development, optimization by Box-Behnken design, in-vitro and in-situ single-pass intestinal perfusion (SPIP) studies. *Recent Patents on Drug Delivery & Formulation, 12*(3), 199-211.
141. Verma, S., et al. (2010). Formulation and evaluation of nanosuspension of curcumin for improved oral bioavailability. *International Journal of Drug Development and Research, 2*(3), 751-757.
142. Verma, S., et al. (2012). Nanosuspensions: Promising drug delivery system for poorly water soluble drugs. *International Journal of Pharmaceutical Sciences and Research, 3*(8), 2472.
143. Wen, T., et al. (2019). Fenofibrate solid dispersion processed by hot-melt extrusion: Elevated bioavailability and its cell transport mechanism. *Current Drug Delivery, 16*(6), 538-547.
144. Willett, W. C. (1981). Dietary fat and coronary heart disease: A critical review. *The American Journal of Clinical Nutrition, 34*(11), 878-889.
145. World Health Organization. (2021). *Cardiovascular diseases (CVDs).* Retrieved from https://www.who.int/news-room/fact-sheets/detail/cardiovascular-diseases-(cvds)

146. Yan, Y. D., et al. (2012). Novel valsartan-loaded solid dispersion with enhanced bioavailability and no crystalline changes. *International Journal of Pharmaceutics, 422*(1-2), 202-210.
147. Yousaf, A. M., et al. (2015). Pharmacokinetic evaluation of nanosuspension formulations in Wistar rats. *Drug Design, Development and Therapy, 9*, 6343–6352.
148. Zhang, L., et al. (2020). Efficacy and safety of rosuvastatin vs. atorvastatin in lowering LDL cholesterol: A meta-analysis of trials with East Asian populations. *Herz, 45*(6), 594-602.
149. Zhou, S., et al. (2024). Comparative effectiveness and safety of atorvastatin versus rosuvastatin: A multi-database cohort study. *Annals of Internal Medicine, 177*(12), 1641-1651.